THE STRUCTURE OF METALLIC OXIDE AEROSOLS PRODUCED BY ELECTRIC ARCS IN GASES AT PRESSURES UP TO 35 ATMOSPHERES

by

J. R. RUSHTON, B.Sc.,A.R.C.S.

A thesis submitted for the Degree of Doctor of Philosophy in the University of London.

Department of Chemical Engineering and Chemical Technology,
Imperial College of Science and Technology,
London, S.W.7.

December 1965.

A B S T R A C T

The mode of generation of aerosols from electric arcs of magnesium, aluminium, magnox (Mg 99.1 - 99.3%, Al 0.7 - 0.9%, Be 0.005 - 0.03%), zirconium, stainless steel, (Fe 73%, Cr 18%, Ni 8%), uranium dioxide and gold in air and in CO_2 at pressures from atmospheric up to 500 p.s.i. is described. Using the techniques of electron microscopy and electron diffraction the crystal structure, particle size distribution, mean particle size and particle shape of the aerosols are determined.

From these data, together with measurements of the arc-flame structure, the rate of evaporation of material from the arc, and the temperature gradient in the vicinity of the arc, a model for the formation of aerosol particles in arc-flames is suggested. The conditions of formation (vapour pressure at the start of growth, temperature, nucleation rate, particle growth rate and particle concentration) are then approximately determined.

With increase in the gas pressure at which the aerosol is generated, the mean particle size of an aerosol of a particular substance is found to increase, and in general the particle shape is found to become more nearly spherical. These results are interpreted in terms of changes in the conditions of formation, notably the diffusion coefficient of the vapour and the nucleation rate.

The particle sizes of the aerosols are found to follow the Log-Normal distribution; from this result some inferences are drawn concerning the mode of growth of the aerosol particles.

C O N T E N T S

Page

Abstract

1. Introduction 11

1.1 General Introduction. 11

1.2 Processes occurring during growth from the vapour. 14

1.2.1 Self-nucleation of droplets from the vapour. 15

1.2.2 Self-nucleation of a vapour in a gas at high pressure. 18

1.2.3 Heterogeneous nucleation of droplets on gaseous ions. 19

1.2.4 A survey of previous work on nucleation from the vapour. 20

1.2.5 The growth of aerosol particles. 27

(i) The "stationary" growth of aerosol particles. 27

(ii) The "non-stationary" growth of aerosol particles. 29

1.2.6 A survey of previous work on the growth and evaporation of aerosol particles. 33

(i) "Stationary" growth and evaporation of aerosols. 33

(ii) "Non-stationary" growth and evaporation of aerosols. 36

1.2.7 The coagulation of aerosol particles. 39

(i) The coagulation of uncharged particles. 39

Page

(ii) The coagulation of electrically charged particles. 40

(iii) Coagulation in an electric field. 41

1.3 A survey of previous related work on the combustion of metals, and the temperature and structure of the reaction zone. 43

1.4 A survey of previous work on the structure of aerosols. 47

1.5 The distribution of particle sizes. 54

1.5.1 The form of the distribution law. 55

(i) The Normal Law. 55

(ii) The Log-Normal Law. 56

1.5.2 The correlation between the particle size distribution and the particle growth mechanism. 57

2. Experimental details. 61

2.1 Materials. 61

2.2 The preparation of specimens. 62

2.2.1 The preparation of support films. 62

2.2.2 The apparatus for the generation of aerosols. 63

(i) The high-pressure vessel. 63

(ii) The gas supply. 64

(iii) The high-pressure system. 65

(iv) The electric arc. 66

(v) Operation of the electromagnetically-drawn arc. 68

		Page
2.2.3	The generation and collection of aerosols.	68
	(i) The scope of the experiments.	69
	(ii) Experimental procedure.	70
2.3	The examination of specimens.	72
2.3.1	The electron diffraction technique.	72
2.3.2	A brief account of the interpretation of electron diffraction patterns obtained from randomly orientated polycrystalline specimens.	73
2.3.3	The electron microscopy technique.	75
	(i) Resolution.	76
	(ii) Focusing.	77
	(iii) Magnification.	78
	(iv) Image formation.	79
	(v) Selected-area diffraction.	79
	(vi) Contamination.	80
	(vii) Photography,	80
2.4	Particle size analysis.	81
2.4.1	The technique of size analysis.	81
2.4.2	Graphical representation of the size distribution.	82
2.5	The investigation of the structure of the arc flame.	82
2.6	The determination of the temperature distribution in the vicinity of the arc.	83
2.7	The determination of the rate of evaporation of material from the arc.	84

Page

3. Results 85

3.1 The size, shape, and structure of the aerosol particles. 85

3.1.1 Aerosols formed by the combustion of magnesium. 86

(i) General observations. 86

(ii) Aerosols from the combustion of magnesium in air. 86

(a) The composition and crystal structure of the particles. 86

(b) The particle shape. 88

(c) The particle size distributions. 90

(d) The effect of air pressure on the mean particle size. 91

(iii) Aerosols from the combustion of magnesium in CO_2. 92

(a) The effect of CO_2 pressure on the mean particle size. 93

(iv) Summary of the results for aerosols formed by the combustion of magnesium in air and CO_2. 93

3.1.2 Aerosols formed from the aluminium arc. 95

(i) General observations. 95

(ii) Aerosols formed from the aluminium arc in air. 95

(a) The composition and crystal structure of the aerosols. 95

(b) The particle shape. 96

(c) The particle size distributions. 97

Page

(d) The effect of air pressure on the mean particle size. 97

(iii) Aerosols from the aluminium arc in CO_2. 98

(a) The particle shape, structure, amd size distributions. 98

(b) The effect of CO_2 pressure on mean particle size. 100

(iv) Summary of the results for aerosols formed from the aluminium arc in air and CO_2. 101

3.1.3 Aerosols from the magnox arc. 102

(i) General observations. 102

(ii) Aerosols formed by the combustion of magnox in air. 102

(a) The composition and crystal structure of the particles. 102

(b) The particle shape. 104

(c) The particle size distributions. 105

(d) The effect of air pressure on the mean particle size. 106

(iii) Aerosols from the magnox arc in CO_2. 106

(a) The particle shape, structure and size distributions. 106

(b) The effect of CO_2 pressure on the mean particle size. 107

(iv) Summary of the results for aerosols formed by the combustion of magnox in air, and the magnox arc in CO_2. 108

		Page
3.1.4	Aerosols from the stainless steel arc.	109
	(i) General observations.	109
	(ii) Aerosols from the stainless steel arc in air.	109
	(a) The composition and crystal structure of the particles.	109
	(b) The particle shape.	111
	(c) The particle size distributions.	112
	(d) The effect of air pressure on the mean particle size.	112
	(iii) Aerosols from the stainless steel arc in CO_2.	113
	(a) The particle shape, structure, and size distributions.	113
	(b) The effect of CO_2 pressure on the mean particle size.	114
	(iv) Summary of the results for aerosols formed from the stainless steel arc in air and CO_2.	115
3.1.5	Aerosols from the UO_2/carbon arc.	116
	(i) General observations.	116
	(ii) Aerosols from the UO_2/carbon arc in air.	116
	(a) The composition and crystal structure of the aerosols.	116
	(b) The particle shape.	120
	(c) The particle size distributions.	120
	(d) The effect of air pressure on the mean particle size.	121

Page

(iii) Aerosols from the UO_2/carbon arc in CO_2. 122

(a) The particle shape, structure, and size distributions. 122

(b) The effect of CO_2 pressure on mean particle size. 123

(iv) Summary of the results for aerosols formed from the UO_2/carbon arc in air and CO_2. 123

3.1.6 Aerosols from the zirconium arc. 124

(i) General observations. 124

(ii) Aerosols from the zirconium arc in air. 124

(iii) Aerosols from the zirconium/carbon arc in CO_2. 124

(a) The composition and crystal structure of the aerosols. 124

(b) The particle shape. 126

(c) The particle size distributions. 127

(d) The effect of CO_2 pressure on the mean particle size. 128

(iv) Summary of the results for aerosols formed from the zirconium arc in air and CO_2. 128

3.1.7 Aerosols from the gold/carbon arc. 130

(i) General observations. 130

(ii) Aerosols from the gold/carbon arc in air. 130

(a) The composition and crystal structure of the aerosols. 130

(b) The particle shape. 130

Page

(c) The particle size distributions. 132

(d) The effect of air pressure on the mean particle size. 132

(iii) Aerosols from the gold/carbon arc in CO_2. 133

(a) The composition, crystal structure and size distributions of the aerosols. 133

(b) The effect of CO_2 pressure on the mean particle size. 133

(iv) Summary of the results for aerosols from the gold/carbon arc. 134

3.2 The structure of the arc flames. 135

3.3 The temperature distribution in the vicinity of the arc. 136

3.4 The rate of evaporation of material from the arc. 137

4. Discussion 139

4.1 The generation of the aerosols. 139

4.1.1 The time available for particle growth, and the average growth rate. 141

4.1.2 The particle concentration in the growth zone. 144

4.1.3 Coagulation of the aerosol particles. 145

4.1.4 The nucleation rate, supersaturation and vapour pressure at the start of growth. 147

4.1.5 Summary of the measured and calculated conditions for the formation of the gold aerosol at atmospheric pressure. 149

Page

4.2 The crystal structure and temperature of formation of the aerosols. 150

4.3 The particle shape. 153

4.3.1 The characteristic particle shapes observed in aerosols formed at atmospheric pressure. 153

4.3.2 The change in particle shape with increase in gas pressure. 160

4.4 The particle size. 168

4.4.1 The mean particle size of aerosols formed at atmospheric pressure. 168

4.4.2 The correlation between the mean particle size and shape in aerosols formed at atmospheric pressure. 172

4.4.3 The effect of increased gas pressure on the mean particle size. 174

4.4.4 The particle size distributions. 178

5. Conclusion. 181

Acknowledgements. 184

References. 185

1. INTRODUCTION

1.1. GENERAL INTRODUCTION.

An aerosol may be defined as a suspension in a gas of fine particles or droplets, of diameter not exceeding about 100μ. As a class of aerosols, smokes are disperse systems consisting of particles of low vapour pressure, which settle slowly under gravity. The size of the particles in smokes ranges from about 5μ diameter down to the "submicroscopic" region, less than 0.1μ diameter.

Aerosols have been the subject of considerable interest in recent years. This interest has been stimulated mainly by problems in meteorology : the formation of rain and snow in clouds, the formation and persistence of fog and mist, atmospheric pollution, etc. Most experimental investigations of aerosols have concentrated on substances, such as water, which have a high vapour pressure at moderate temperatures, and whose properties are well known. Also a technique for producing aerosols of these substances under controlled conditions, the Wilson cloud chamber, has long been available. Thus, although the condensation process is as yet far from being fully understood, a considerable body of data related to the condensation of water vapour has been accumulated. The same cannot be said, however, of aerosols produced by the condensation of other

substances, particularly metals and metal oxides. A very limited number of investigations of metal and metal oxide aerosols have been carried out, and have been concerned almost exclusively with the coagulation process. Experimental studies of condensation and growth in metal and metal oxide aerosols seem to be totally lacking. No determinations of size distributions in these aerosols have been carried out, only rough estimates of particle size being given in the literature.

The present work forms a continuation of investigations of metal arc smokes begun in 1960 by Harvey, Matthews, and Wilman (cf. also Finch, Quarrell and Wilman, 1935) at the Applied Physics and Chemistry of Surfaces Laboratory, Department of Chemical Engineering and Chemical Technology, Imperial College. During these investigations, they observed that the particle size and state of aggregation of the aerosols appeared to depend on the pressure of the surrounding gas, and also that the size, external form, and crystalline nature of the particles was dependent on the recrystallisation temperature of the particular oxide. It was in connection with these observations that the present further work on metal arc smokes was undertaken, to investigate in particular the effect of the nature and pressure of the surrounding gas on the structure of the aerosols.

The present work is described in four sections, the first of which includes brief accounts of the theories of nucleation and growth of aerosols formed by condensation from the vapour, and a survey of previous related work on the structure of aerosols and the combustion of metals. The other sections refer to the author's own investigations into the structure of metal and metal-oxide aerosols, the results of which are discussed with reference to those of other workers in the field.

1.2. Processes occurring during growth from the vapour.

When a vapour condenses to a liquid or solid, the phase change is believed to take place through a process of nucleation. This is indicated by the well-known Thomson-Gibbs equation (Thomson, 1928) which gives the condition for a liquid drop to be in equilibrium with its vapour :

$$\ln(p/p_{\infty}) = 2\sigma M/ RT\rho r \qquad ...(1)$$

(r = radius of a drop, of molecular weight M, densityρ, and surface tension σ. R = gas constant, T = absolute temperature. p = vapour pressure, p_{∞} = equilibrium vapour pressure at temp. T) p/p_{∞} is called the "supersaturation". The equation indicates that for every supersaturation there must be a critical droplet size. Drops smaller than this will evaporate, while those larger will continue to grow. The equation predicts that, for the growth of a droplet from a single molecule, a very high supersaturation, of the order of several hundred, would be required. But in practice it has been found that condensation occurs at much lower values of the supersaturation. It has therefore been postulated that condensation occurs on nuclei consisting of clusters of molecules produced by random density fluctuations in the vapour phase. This process (which is, of course, a hypothetical one) is known as self-nucleation. When nuclei of

the critical size for any supersaturation are present in the vapour, growth of these nuclei can continue until the vapour is exhausted, producing a cloud of particles. In any such aerosol cloud, collisions between the individual particles will result in them sticking together; if the particles are solid, numbers of such collisions will result in the production of large aggregates. This process is known as coagulation. If the aerosol particles are liquid, coagulation will result in the production of larger droplets. This coagulation process will be going on continuously after condensation has begun.

It is convenient to consider the condensation of a vapour in three stages :

a) Nucleation i.e. the production of nuclei of the critical size;

b) Growth of aerosol particles by condensation on nuclei;

c) Coagulation of the aerosol cloud.

In reality, these three processes will be going on simultaneously after the onset of condensation.

1.2.1. Self-nucleation of droplets from the vapour.

The theory of self-nucleation of a vapour was first proposed by Volmer and Weber in 1926, and subsequently modified by various workers, notably Becker

and Doring (1935), and Frenkel (1946). The growth of clusters from a supersaturated vapour of single molecules is considered to take place by a series of bimolecular reactions in which clusters grow by the addition of one molecule per reaction. They develop initially with an increase in free energy until a critical size is reached, above which growth continues with a decrease in free energy.

The total Gibbs free energy change involved in the formation of a cluster is given by :

$$\Delta G = 4\pi r^2 \sigma + 4\pi r^3 \Delta G_v / 3 \qquad \ldots(2)$$

where r = radius of cluster, σ = surface tension, and

$\Delta G_v = - \frac{kT}{v} \ln \left(\frac{p}{p_\infty} \right)$, v = molecular volume.

This free energy of formation increases with r to a maximum ΔG^* at r^*, the radius of the critical nucleus, as shown in

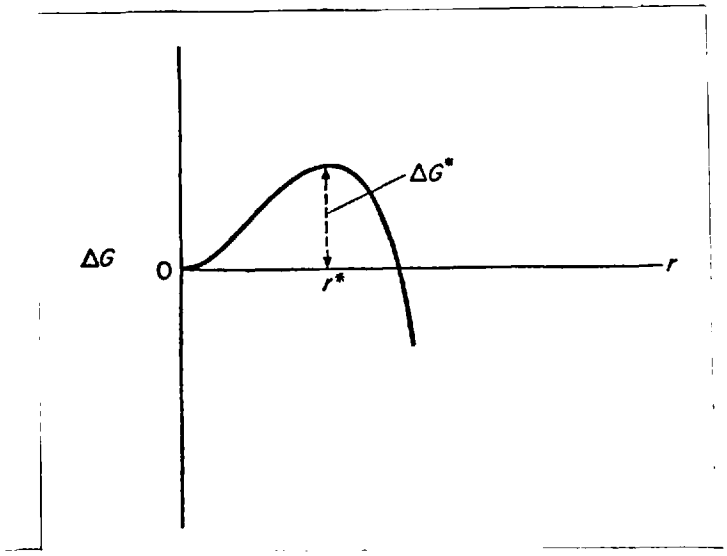

Fig. 1 The Gibbs free energy of formation of a particle of radius r.

fig. (1). Maximising equation (2) with respect to r, we

obtain $r^{*} = 2\sigma/\Delta G_v$, the Thomson-Gibbs equation, and :

$$\Delta G^{*} = 16\pi\sigma^3 / 3\Delta G_v^{\,2}$$

If n is the concentration of vapour, and n^{*} is the concentration of critical nuclei, it can be shown that

$$n^{*} = n \exp(-\Delta G^{*} / kT)$$

The Becker and Doring equation for the homogeneous nucleation rate is :

$$J = 4\pi r^{*2} w n^{*} \qquad \ldots(3)$$

Where w = molecular collision rate = $\alpha p / (2\pi m k T)^{\frac{1}{2}}$, and α = condensation coefficient.

The nucleation rate J is simply the product of the total surface area of the critical nuclei and the rate at which molecules collide with that surface. Thus

$$J = \alpha(4\pi r^{*2}) \left[p / (2\pi m k T)^{\frac{1}{2}} \right] n \exp(-\Delta G^{*} / kT) \qquad \ldots(4)$$

In equation (4), it is the exponential term which is the controlling one; hence the nucleation rate is very sensitive to the supersaturation p/p_∞. This is shown in fig. (2).

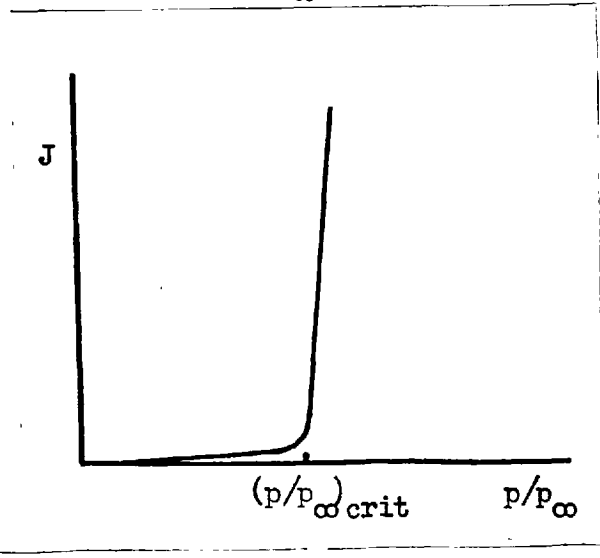

Fig. 2 The dependence of the nucleation rate on the supersaturation.

1.2.2. Self-nucleation of a vapour in a gas at high pressure.

The effect of high pressure of the surrounding gas on the rate of nucleation of a vapour has been examined theoretically by Bradley (1960), using the Becker and Doring theory.

For a vapour of a substance X at pressure p, in the presence of an inert gas Y at pressure P, (P>>p), the Gibbs free energy of nucleus formation is :

$$\Delta G = 4\pi r^2\sigma(P) - 4/3\pi r^3 \frac{\rho(P)}{M} RT \ln(p/p_\infty(P))$$

where $\rho(P)$, $\sigma(P)$ and $p_\infty(P)$ are the density, surface tension and saturated vapour pressure of the drop at pressure P. The value of p(P) is given by the Poynting equation :

$$\ln\left[p_\infty(P) \,/\, p_\infty(0)\right] = Pv(P) \,/\, RT$$

where v is the molar volume of the liquid at pressure P. Hence

$$\Delta G = 4\pi r^2\sigma(P) - 4/3\pi r^3 \frac{\rho(P)}{M} \quad RT\left[\ln(p/p_\infty) - Pv(P)\right]$$

and the radius of the critical nucleus is given by :

$$r^*(P) = 2\sigma(P)M \,/\, \rho(P) \quad RT\left[\ln(p/p_\infty) - Pv(P)\right]$$

If P is kept constant, there will be a limiting gas pressure given by $P_c = RT \ln(p/p_\infty) \,/\, v(P)$, above which there can be no critical nucleus. It would therefore be expected that the rate of nucleation would gradually decrease to zero with increase in pressure, since the controlling term in the

nucleation rate is $\exp(-\Delta G^{*}/ kT)$.

Bradley has pointed out that the effects of pressure on v and σ are small.

1.2.3. Heterogeneous nucleation of droplets on gaseous ions.

If foreign nuclei such as dust particles are present in the gas, the nucleation process may be changed considerably. A particle, if insoluble, may absorb a thin film of vapour, then acting as a ready-made nucleus for condensation; or, if soluble in the condensed liquid, lower its vapour pressure, reducing the supersaturation necessary for condensation.

It is well known from experiments with the Wilson cloud chamber that condensation takes place at lower supersaturations in the presence of ions, and it has therefore been concluded that ions can act as condensation nuclei. This important case was first investigated by J.J. Thomson (1928), who showed that vapour molecules form stable clusters about all gaseous ions. For such a charged cluster, the Thomson-Gibbs equation becomes :

$$\frac{RT}{M} \ln(p/p_{\infty}) = \frac{2\sigma}{r} - q^2/ 8\pi\varepsilon r^4 \qquad \ldots(5)$$

where q = charge on the cluster. ε = dielectric constant of gas. This function exhibits a maximum at a certain value of r , as shown in fig.(3). This value is given by:

$$r_{crit} = (q^2 / 4\pi\varepsilon\sigma)^{1/3} \qquad \ldots(6)$$

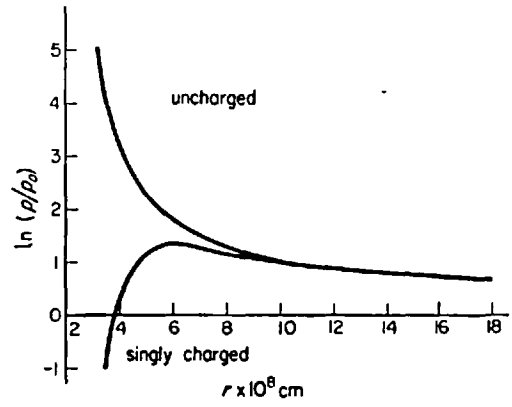

Fig. 3 The radius of a droplet in equilibrium with vapour of supersaturation p/p_∞

1.2.4. Survey of previous work on nucleation from the vapour.

To initiate nucleation and growth in a vapour it is necessary to produce a given critical supersaturation. The supersaturation must be produced in such a way that there is no opportunity for its relief by diffusion to the chamber walls; usually, this means that the cooling of the vapour must be done rapidly. Wilson (1897) invented the cloud chamber for this purpose.

Most of the data on nucleation kinetics have been obtained with the Wilson cloud chamber. A variety of vapours and carrier gases have been used, and most of the results have been expressed as the critical supersaturation necessary to initiate condensation and produce an aerosol

cloud. These results have been used to test the predictions of the Becker and Doring theory.

With water vapour, experiments have been carried out by Wilson (1899), Powell (1928), Volmer and Flood (1934), and others, in which very clean water-saturated air was rapidly expanded in a cloud chamber, and the minimum supersaturation required to produce a detectable aerosol cloud determined. Volmer and Flood (1934) found reasonable agreement with the theoretical value of the critical supersaturation necessary for homogeneous nucleation of water vapour; they also found reasonable agreement for a number of organic liquids, methyl alcohol alone exhibiting serious discrepancy. Some of the values obtained are listed in Table (1).

Vapour	p/p_∞ (theory)	p/p_∞ (expt.)
Water	4.85	4.85
Methyl alcohol	1.84	3.20
Ethyl alcohol	2.30	2.34
Propyl alcohol	3.20	3.05

Table (1). Observed and theoretical values of the critical supersaturation for various vapours (Volmer and Flood, 1934).

The data of Powell (1928) for water vapour, however, indicated that neither the critical supersaturation nor its temperature dependance were in good agreement with the theory.

The most recent cloud chamber work was carried out by Pound et al. (1955), who used water vapour, with purified and filtered nitrogen as the carrier gas, and an electric field to remove ions. At $0^{\circ}C$, good agreement with the theory was obtained, but at lower temperatures, large deviations from the theory occurred.

The production of aerosols by the mixing of a vapour jet with cooler air was studied by Amelin (1948). He calculated from experiment the critical supersaturation for condensation when a jet of steam was mixed with cold air. O'Konski and Higuchi (1956) used the vapour jet technique to find the critical supersaturation and nucleation rate for a number of vapours. With dibutyl-phthalate, they found good agreement with the Becker and Doring expression for the homogeneous nucleation rate. Only fair agreement was obtained with n-octadecane and sulphur, while agreement in the case of triethylene glycol was poor.

In the study of the condensation of metal vapours, most previous work has been concerned with the nucleation of the vapour on substrates, and has been carried out in

fairly high vacuum. The nucleation of metal vapours in the gaseous phase to form aerosols does not appear to have been studied experimentally. A theoretical study of the formation of metal and metal oxide aerosols by condensation from the fireball of a nuclear explosion was made by Stewart (1956). He considered the case of a large quantity of high melting-point material being vapourised and subsequently cooling to form a fine particulate cloud. Due to the lack of experimental data, he made rough estimates of concentration and temperature. Using the Becker and Doring theory he calculated the supersaturation necessary to initiate condensation of Fe and Si oxides. The values of the supersaturation for nucleation rates of 10^{-2}, 1, and 10^{2} are given in Table (2).

Condensing substance	Temp. ^{o} K	s.v.p. (mm. mercury)	Value of p/p_{∞} for J to be 10^{-2}	1	10^{2}
H_2O	273	4.58	4.03	4.25	4.51
Fe/FeO	2400	6.0	1.0494	1.0514	1.0540
Si/SiO	2500	34	1.0798	1.0831	1.0871

Table (2). Supersaturation necessary to initiate condensation of Fe and Si oxides (Stewart 1956).

The values show the extreme sensitiveness of the nucleation rate to the supersaturation; and also that the supersaturation required at these high temperatures is very small. Values of

100 dynes/cm were assumed for the surface tension of both FeO and SiO, based on values observed for fused salts at high temperatures. He also calculated the variation of the nucleation rate with time, assuming that the temperature fell exponentially, and found that the rate changed by a factor of only 2-3 during the time (200 msec) for 3/4 of the material to condense. This is shown in fig. (4). For his approximate treatment, Stewart therefore took the rate to be constant. He also found that the time taken for a given fraction of the vapour to condense increased slightly as the initial vapour concentration was increased. The main result of the study was that at high temperatures condensation is extremely rapid (300 m sec for 80% condensation), and takes place over a small temperature range.

There has been some controversy as to whether crystals may form direct from the vapour without the intervention of the liquid phase. Pound et al (1955) working with water-saturated air in a Wilson cloud chamber found that spherical particles appeared at terminal temperatures down to -65°C, but at lower temperatures angular ice crystals appeared. The same effect had been previously observed by Sander and Damkohler (1943) who suggested that either crystals were formed direct from the vapour, or -65°C represented the freezing temperature of

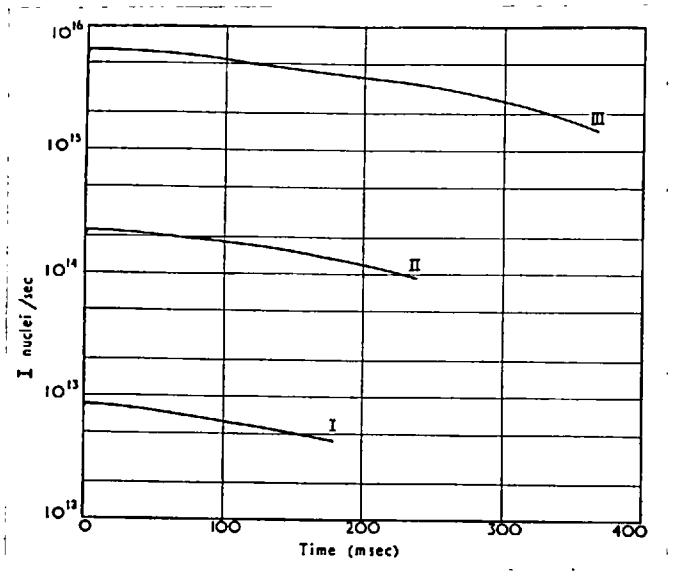

Fig. 4 The variation of the nucleation rate with time after the onset of condensation (Stewart, 1956).

what had been liquid droplets at higher temperatures. Pound et al (1955) suggested that because homogeneous nucleation of liquid water droplets at -40°C had been well established, the particles appearing between this temperature and -65°C were frozen droplets which had not yet developed crystalline faces. Mason et al (1959) found that ice crystals appeared when moist air was subsaturated relative to water but supersaturated relative to ice. No visible water droplets were then produced. They suggested that this could be evidence of crystals forming by a direct vapour-to-solid transition. However, on theoretical grounds, Mason (1960) has concluded that during the cooling of water vapour, the first condensation products would be liquid drops, although at temperatures below -40°C, the drops would freeze in a fraction of a second.

The nucleation and growth of NaCl aerosols was investigated by Buckle and Ubbelohde (1960), who heated a salt bead in a high temperature cloud chamber, and examined the aerosol optically. Maintaining the salt bead at a given temperature, they found that the aerosol was composed of drops or crystals, depending on the chamber temperature. A critical chamber temperature was found below which polyhedral crystals were produced. Droplets were found to be much faster growing than crystals. They

concluded that the condensation process was the nucleation and growth of liquid droplets, since the Becker and Doring theory required a supersaturation of $\sim 10^3$ for the nucleation of crystals. Thus droplets would probably form and rapidly lower the supersaturation before the vapour could cool to the sublimation temperature. Nucleation of crystals would thereby be excluded. However, the rapid growth observed at temperatures near the solidification threshold appeared to be arrested when the chamber temperature was lowered still further, in favour of particle multiplication. The particle size was much reduced. Therefore they suggested that at low chamber temperatures sublimation nuclei may have been formed, further growth not occurring because the supersaturation necessary for surface nucleation was not maintained.

A similar observation of particle multiplication was made by Matusevich (1959), working on crystallisation in stirred solutions. The final size of the crystals depended on the relative rates of nucleation and growth. He found that the mean crystal size decreased with increased stirring speed, indicating that the nucleation rate began to exceed the growth rate.

1.2.5. The growth of aerosol particles.

(i) The "stationary" growth of aerosol particles.

The basis for the theory of the growth of an aerosol droplet was laid by Maxwell, considering the reverse process of evaporation, in 1877. The same equation was obtained independently by Langmuir (1918), who arrived at it by analogy with the theory of heat conduction.

The simplest case is that of the stationary growth of a single spherical droplet, motionless relative to an infinite uniform medium. The word "stationary" is used to indicate that neither change in vapour concentration nor change in particle radius with time is taken into account. Assuming that the vapour concentration at the surface of the drop is equal to the equilibrium concentration c_∞ (the concentration of the saturated vapour at the temperature of the drop), the rate of diffusion of vapour to the droplet across any spherical surface of radius x is given by :

$$I = 4\pi x^2 \frac{dc}{dx} D \quad \text{gms./sec} \qquad \ldots(7)$$

Integration of this equation, with the boundary conditions $c = c$ when $x = \infty$; $c = c_\infty$ when $x = r$, give Maxwell's equation :

$$I = 4\pi r D(c - c_\infty) \qquad \ldots(8)$$

r is the radius of the drop. Thus the rate of growth of

the drop is completely determined by the rate of diffusion of the vapour in the gaseous medium. Early work on the evaporation of droplets (Langmuir, 1918) indicated that equation (8) was true for the evaporation of drops of about 1 mm diameter in air at atmospheric pressure.

However, equation (8) breaks down when the air pressure is sufficiently reduced, since it indicates that the growth rate would tend to infinity. Similarly, it predicts an infinite rate of growth when the radius of the particle approaches zero.

Bradley et al (1946), and also Fuchs (1949), showed that these difficulties could be overcome by supposing that droplet growth (and evaporation) proceeds by a two-stage process. The drop is imagined to be surrounded by a virtually vacuous space, of thickness of the order of the mean free path of the vapour molecules. Across this space, of thickness Δ, vapour passes by Knudsen flow, or molecular distillation. A shell of vapour of concentration c_1, less than c_∞, is built up round the drop, and this value c_1 is set by balancing the rate of growth of the drop, and the rate of supply of vapour by diffusion from the gas. This gives :

$$4\pi r^2 \sqrt{}\alpha(c_\infty - c_1) = 4\pi(a + \Delta)\, c_1 D$$

where $\sqrt{} = (kT/2\pi m)^{\frac{1}{2}}$, and m_1 and m_2 are the molecular masses

of the gas and the diffusing vapour.

Thus : $$c_1 = \frac{cr^2\sqrt{\alpha}}{(r+\Delta)D+r^2\sqrt{\alpha}}$$

and hence $$\frac{dM}{dt} = \frac{4\pi D\ c\ m_2}{D/(r\sqrt{\alpha})+r/(r+\Delta)} \qquad \ldots(9)$$

Bradley (1950) gives : $\Delta = \frac{8D(n_1/m_2)}{3\pi\sqrt{}}$

Equation (9) leads to the correct expression for the rate of evaporation in a vacuum. Bradley (1950) and Fuchs (1959) have also pointed out that when r approaches zero, equation (9) predicts that the rate/unit area $\frac{dM}{dt}(1/4\pi r^2) \rightarrow \sqrt{\alpha} c_o m_2$. This is the vacuum rate, even though the pressure of the gas may be atmospheric or higher. Bradley (1950) has concluded that even for high pressures, of several atmospheres, sufficiently small drops will grow at the vacuum rate, the growth rate being controlled by the condensation coefficient rather than by the diffusion coefficient.

(ii) <u>The "non-stationary" growth of aerosol particles</u>.

In the theoretical treatment of the stationary growth of aerosol particles, the change of the radius of the particle with time, the variation of the vapour

concentration with time, and the presence of a large number of competing particles, are not taken into account. If any of these factors are included, the problem becomes one of "non-stationary growth".

The variation of the vapour concentration with time is then given by the equation :

$$\frac{\partial c}{\partial t} = D \frac{\partial^2 c}{\partial x^2} + \frac{2}{x} \frac{\partial c}{\partial x} \qquad \ldots(10)$$

where c = vapour concentration, x = radial distance from centre of drop, and t = time.

As in the case of stationary growth, the rate of growth of a particle is given by :

$$I = 4\pi x^2 \frac{\partial c}{\partial x} \qquad \ldots(11)$$

It is necessary to solve these two equations for the growth rate, subject to certain boundary conditions.

The effect of the increase in size of the growing droplet on the growth rate was considered by Frisch and Collins (1953). They solved equations (10) and (11) subject to the conditions $c(x,t) = c_{\infty}$ when $t = 0$, and $c(x,t) = c_{\infty}$ when $r = \infty$, $t = 0$. They obtained the solution :

$$1 \cdot \left[r(t) - r_o \right] + \tfrac{1}{2} \left[r^2(t) - r_o^2 \right] = c_{\infty} k D t \qquad \ldots(12)$$

where l' = a length of the order of the mean free path of the vapour molecules, r_o = initial radius, $r(t)$ = radius after time t. This solution simply indicates that when $r \gg$ mean free path, growth proceeds by a diffusion mechanism, and when $r \ll$ mean free path, by a kinetic mechanism (i.e. as in a vacuum). This is a similar result to that obtained from the two-stage mechanism for stationary growth proposed by Bradley (1950) and Fuchs (1959).

The effect of the increase in size of a growing particle was investigated theoretically by Fuchs (1959). He found that the rate of growth in the non-stationary case could be represented by:

$$I = I_o\left(1+\sqrt{\frac{c - c_{oo}}{\gamma}}\right) \qquad \ldots(13)$$

where I_o is the growth rate in the stationary case. Thus the effect of the change on radius on the growth rate is small under ordinary conditions. Fuchs concluded that the effect could be ignored in most circumstances, the growth rate being considered as quasi-stationary.

The theoretical treatments of the growth process given above took as their model a single particle in an infinite uniform medium. In reality a growing or evaporating aerosol will consist of a large number of competing particles. Reiss and La Mer (1950) and Fuchs (1959) stated that this situation could be represented, to a good approximation, by the growth of a single particle in a spherical

volume of radius h, where 2h is the mean distance between neighbouring particles in the system. Fuchs (1959) obtained a solution of equations (10) and (11) for the evaporation of a system of drops, and showed that for the case of $r/h < 0.1$, and $t > h^2/20D$, :

$$I = 4\pi r D c_o \exp\left(-3rDt/(h-r)^3\right) \qquad \ldots(14)$$

Reiss and La Mer (1950) studied the same problem for the growth of a sulphur hydrosol, with the addition that the saturated vapour concentration at the drop surface was taken as an exponential function of time : $c(r,t) = c_o \exp(-At)$, where A = constant. This was to take into account the change in temperature of the drop surface. They obtained the equation for the increase of radius r with time :

$$\frac{d}{dt}(r^2) = (2WD/A\rho)\, KT - (2D/h^3)r^3 + (2WD/A\rho)c_o \qquad \ldots(15)$$

where W = molecular weight.

1.2.6. A survey of previous work on the growth and evaporation of aerosols.

(i) Stationary growth and evaporation.

Previous studies of the vapour/liquid or vapour/solid phase transition in aerosol systems have been concerned almost exclusively with evaporation. Evaporation rates were first determined by Sreznevsky (1882), for liquid drops of diameter ~2mm. on a flat surface. He found that the rate of evaporation was inversely proportional to the drop radius. This result was also obtained by Morse (1910), who studied the evaporation in air of iodine droplets. Whytlaw-Gray et al (1927) studied the evaporation of drops, of radii 1-2 mm., of water, aniline and other organic liquids, and found that the surface area decreased linearly with time.

The first quantitative support for Maxwell's theory was obtained by Topley and Whytlaw-Gray (1927) for the evaporation in air of spheres of iodine, radius ~1mm., suspended from a quartz fibre. The results obtained agreed with Maxwell's equation, equation (8).

Reasonable agreement with Maxwell's theory was obtained by Houghton (1933) who measured the evaporation rates of suspended water drops of diameter 50 - 1000μ in air at atmospheric pressure. Langstroth et al (1950) also found agreement with the theory for evaporation of drops of water and of several organic liquids suspended from glass fibres

in air at atmospheric pressure.

La Mer et al (1950) studied the growth of aerosols of sulphuric acid and dibutyl phthalate produced in a Sinclair-La Mer aerosol generator. In this method of aerosol production, vapour from a boiler and air were cooled slowly and uniformly from the boiler temperature to room temperature. They found that the final particle radius was controlled by the boiler temperature, the ratio of the mass of vapour to the number of nuclei formed, and the vapour pressure of the aerosol substance. They found that the aerosol was almost monodisperse, and proposed that if the growth process followed Maxwell's theory, the final radius would be given by :

$$r^2 = r_o^2 + At$$

where r_o, r are initial and final radii, A is a constant, and t = time. Thus, since the square of the particle radius varies linearly with time, continued uniform growth by diffusion would obliterate initial inhomogeneities in radii, and lead to a monodisperse aerosol. La Mer et al also gave the lower limit of particle size as 10 A, the size of a nucleus.

In order to study the correction to Maxwell's theory when the radius of a drop approaches the mean free path of vapour molecules in the gas, Bradley et al (1946,

1949, 1951) worked with drops of dibutyl phthalate, butyl stearate and several hydrocarbons in air at gas pressures ranging from atmospheric down to about 0.1 mm. The droplets, of radius about 0.5 mm., were suspended from quartz fibres. The results for the evaporation rate agreed with equation (9), thus confirming, for drops of this size, the two-stage model for evaporation and growth of drops suggested by Bradley et al (1946).

Some work on micro-drops, with radii of the order of 1μ, has been carried out using the Millikan condenser. Nestle (1932) calculated the evaporation rate of mercury drops, of initial radius about 0.3μ, from their rate of fall in a Millikan condenser, and found that the mass of a drop decreased linearly with time. He used CO_2, N_2, and H_2 as carrier gases. Schafer (1932) measured evaporation rates of mercury drops of 0.5μ initial diameter in H_2 and CO_2 at atmospheric pressure. He compared his results with theoretical values calculated from an equation of the form of equation (9), and found moderate agreement.

Monchik and Reiss (1954) found the evaporation rates of drops of diamyl sebacate with initial radii $\sim$1μ in air at reduced pressures, between 10 and 100 mm Hg. This is in the important region where the drop radius is of the same order as the mean free path. They found that the evaporation rates were in good agreement with a

theoretical expression of the form of equation (9).

Bradley (1950) has concluded that an equation of the form of equ. (9) applies to droplets evaporating in air at atmospheric pressure, and that for drops smaller than 10^{-4} cm. radius, equ. (9) is probably very nearly correct.

Wright (1961) made a theoretical study of the rate of growth of lead oxide particles in engine gases. Assuming a value of 0.05 cm. per sec. for the diffusion coefficient of lead oxide vapour in air at 10 atm., he calculated the value of Δ in equ. (9) as 200 - 400 A. From known growth times he calculated the final particle radius to be 25 A. With these values for Δ and r, he calculated the denominator of equ. (9) and found it to be 1.0035. Hence he concluded that diffusional retardation of growth was negligible, so that even at 10 atm. gas pressure, the growth of sufficiently small particles proceeded at the rate it would in a vacuum.

(ii) The non-stationary growth of aerosol particles.

There are practically no data for the non-stationary growth or evaporation of aerosols. However, the non-stationary growth of hydrosols was investigated by La Mer and Dinegar (1950). They prepared sulphur hydrosols by adding adding acid to thiosulphate; the reaction yielded

molecularly dispersed sulphur, which then condensed to form sulphur droplets. They considered the process of production of the hydrosol in three stages (fig.5).

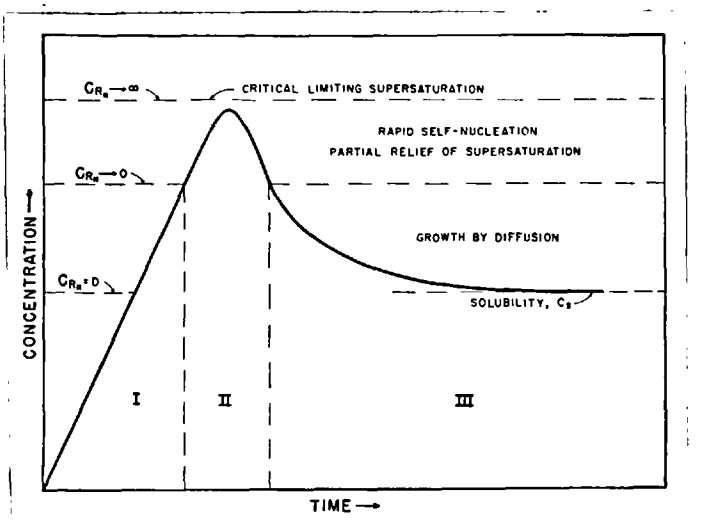

Fig. 5 The variation of sulphur concentration with time during the formation of a sulphur hydrosol (La Mer and Dinegar, 1950).

During Stage I the concentration of sulphur builds up, at a rate depending on the concentration of reactants, until a critical concentration is reached. This critical concentration represents the limiting stage of supersaturation C_{ss} (above this value the nucleation rate $\rightarrow \infty$). The appearance of nuclei in Stage II partly relieves the supersaturation, at least rapidly enough so that the nucleation rate approaches zero. When the concentration falls below C_s, (no more nuclei being produced), the system is still supersaturated, so growth on the existing nuclei can proceed by the diffusion of molecular sulphur (Stage III).

By controlling the initial concentrations of the reactants, La Mer and Dinegar were able to make the nucleation period very short, thus producing a monodispersed colloid. They found that if the initial concentrations were higher, the rate of production of sulphur was so great that the sulphur concentration was continually greater than the value for which $R_n \simeq 0$. A continual cascading of nuclei then ensued, in addition to growth. The size of any particle thus depended on when it was formed; non-uniform growth and a polydisperse sol resulted in this case. They also found that high concentrations favoured the production of crystalline sulphur. They proposed that a small number of crystalline nuclei were produced, along with a large number of supercooled liquid drops. Collisions between the nuclei and the drops would result in the drops being crystallised.

They found that the final size of the particles depended on the number of nuclei produced, the total amount of diffusable sulphur, and the diffusion coefficient of the sulphur. Using the theory of Reiss and La Mer (1950) they obtained an equation for the growth of sulphur particles :

$$\frac{d(r^2)}{dt} = \left[C_{ss} - C_s(t)\right] \frac{2D}{\rho} - \frac{2D}{h^3} r^3 \qquad \ldots(16)$$

This equation could not be solved in closed form, but was solved numerically. La Mer and Dinegar compared the values obtained with the results of experiment, and found very good agreement.

1.2.7 The coagulation of aerosol particles

i) The coagulation of uncharged particles

The phenomenon of continuous and spontaneous coagulation is one of the most striking properties of aerosols. The particles, of whatever substance they may be composed, stick together if they come into contact. This process goes on continuously, so that the aerosol becomes coarser and eventually flocculates out.

The first evidence of coagulation in smokes was obtained by Tolman et al (1919) who measured the diminution with time of the intensity of a Tyndall beam in a confined volume of smoke. The true nature of the coagulation process was elucidated by Whytlaw-Gray and Patterson (1932), who showed that the coagulation of aerosol particles could be described by the theory proposed by Smoluchowksi (1916, 1917) for the coagulation of sols.

Thus if n is the number of particles/c.c. at any time t, and n_o is the number of particles present immediately the smoke is formed, then:

$$1/n - 1/n_o = Kt \qquad \ldots(17)$$

where K is the "coagulation constant".

If this equation is differentiated, then we obtain:

$$-\frac{dn}{dt} = Kn^2 \qquad \ldots(18)$$

Thus the rate at which particles disappear depends only on K and n.

Hence coagulation will be rapid during the early stages, but will fall off quickly with time. Smoluchowski supposed that particles in a coagulating sol collided owing to Brownian movement, and that particles stuck to one another in a certain fraction of these collisions. He obtained the expression for the coagulation constant:

$$K = \frac{2 R T s}{3 \eta N}$$

where R = gas constant, T = absolute temperature, η = viscosity of medium, N = Avogadro's number, and s = sphere of influence of particle. However, for gaseous media, the Cunningham correction to Stokes law must be applied, since the particle radius may be similar to the mean free path ℓ of the particle in the gas. (Green and Lane, 1957). Hence we obtain for the coagulation constant:

$$K = \frac{2 R T s}{3 \eta N} \left(1 + \frac{A l}{r}\right) \qquad \ldots(19)$$

ii) The coagulation of electrically charged particles

A theory for the coagulation of electrically charged aerosols has been developed by Fuchs (1934b). For equal numbers of positively and negatively charged particles, the theory gives rise to the equation:

$$m = \frac{\lambda \exp(\lambda + 1)}{2 \exp(\lambda - 1)}$$

where m is the ratio of particle diminution rates for charged and uncharged particles, $\lambda = q_1 q_2 / 2rkT$, q_1 and q_2 are the charges

on two coagulating particles.

By expanding this as a series it can be shown (Green and Lane, 1957) that $m > 1$; thus a symmetrical bipolar charging should increase the coagulation rate. However, Whytlaw-Gray and Patterson (1932) were unable to show experimentally that the electrification normally acquired by smokes affected the rate of coagulation. They found no clear distinction in coagulation rate of charged and uncharged zinc oxide aerosols. Similarly, Fuchs and Petrjanov (1935) found that symmetrical bipolar charging of oil smokes to an average value of 4-6e per particle had practically no effect on its stability. Gillespie (1953) concluded that somewhat higher charges than this might appreciably alter the coagulation rate. The situation has been summed up by Green and Lane (1957) who state that since an adequate theory has not been developed, the ageing of a charged aerosol cannot be predicted in detail even when the initial conditions are fully known.

iii) Coagulation in an electric field

Electric fields can promote the forced coagulation of aerosols.' (Fuchs 1964). Spherical conducting particles of radius r in an electric field of strength E have induced in them an electric dipole of moment $P = E r^3$. The theory of coagulation, taking into account this polarization, is complex and will not be gone into here. The theory predicts that the coagulation of mists should only be affected by very strong electric fields (Fuchs, 1964).

However, the effect of polarization on solid particles is more interesting. A doublet formed by the coagulation of two primary particles orientates with its long axis parallel to the field, and its dipole moment in this position is much greater than that of the primary particles. The doublet will coagulate with other particles mainly at the ends, and thus grows lengthwise. The aggregates thus acquire chain-like shapes. This has been called "directed coagulation". Experiment (Fuchs,1964) has shown that smokes coagulate in a strong electric field faster than in the absence of a field, but the magnitude of the effect appears to be difficult to predict from the theory.

1.3. A survey of previous related work on the combustion of metals and the temperature and structure of the reaction zone.

The combustion of metallic solids has not received much attention, and hence there is relatively little information on the detailed mechanism of the combustion reaction.

Davis and Hottel (1934) investigated the structure of the flame surrounding burning carbon spheres. They found that the sphere was surrounded by a blue corona, which they attributed to the oxidation of CO, with evidence of a dark zone between the carbon surface and the corona. Spalding (1950, 1951) studied theoretically the combustion of carbon spheres and kerosene drops. Neglecting convection, he proposed as a theoretical model a stagnant gas film surrounding the solid sphere or liquid drop. Through this film, fuel vapour diffused outwards, and air inwards, the reaction zone being defined by the region where the two components were in stoicheiometric proportions.

The combustion of magnesium ribbon in air at atmospheric pressure was studied by Coffin (1945), with the aim of finding out whether a vapour phase or surface reaction mechanism was involved. A vapour-phase combustion process was strongly indicated on the basis of comparison of experimental observations with theoretical burning times calculated from hypotheses involving heat transfer and diffusion. As a theoretical model, the "stagnant film"

approach of Spalding was used. A distinct zonal structure was visible in photographs of the burning magnesium ribbon. A bright zone immediately adjacent to the metal surface was separated from an outer bright zone by an intermediate dark region. The outer bright zone was tentatively attributed to the recalescence of MgO. The inner bright zone is presumably the region of oxidation of magnesium, although this was not explicitly stated. Coffin suggested a model in which Mg vapour was produced at the metal surface at its boiling point; this vapour then moved outwards through a zone of radially increasing temperature until it reached a constant temperature reaction zone at the boiling point of MgO; the condensed MgO vapour then passed through a zone of radially decreasing temperature, producing smoke.

The combustion of Ti and Zr in air at atmospheric pressure was studied by Harrison (1958). He concluded that the combustion takes place at the surface of these metals, since there was no appreciable vaporisation of metal, and thus no appreciable smoke formation, in contrast to the combustion of magnesium.

The combustion of a number of metals in oxygen at pressures ranging from atmospheric to 10 atm. was investigated by Grosse and Conway (1958). They stated that with metals such as Na, Mg, and Ca, which have low boiling

points, considerable volatilisation took place, causing combustion to take place at quite large distances above the metal surface. With Al, Ti, and Zr, which have high boiling points, the combustion zone was close to the metal surface. During the combustion of Al, they observed that very little smoke was produced so long as the oxygen supply rate was low. As the oxygen rate was increased the combustion rate increased, and the pool of liquid Al began to boil vigorously, producing copious amounts of Al_2O_3 smoke. They also calculated the combustion temperature from thermodynamic data. The temperature obtained by combustion was given by :

$$\text{Heat of formation of product at } 298^{\circ}K = \int_{298}^{T} C_p dT.$$

Allowing for dissociation at the boiling point, they found that the combustion temperature for most metal-oxygen systems was the boiling point of the oxide. They studied metal combustion at gas pressures above atmospheric, and found that flame temperatures were a function of total pressure. High pressure increased the boiling point of the oxide, so that higher flame temperatures were produced even where the oxide decomposed on vaporisation. The combustion of Al in oxygen at 10 atm. resulted in a flame temperature of $4400^{\circ}K$, compared with $3800^{\circ}K$ at 1 atm.

Flames of metal powders burning in air have been

studied by a number of workers. The temperatures of these flames have been found usually to coincide with the boiling point of metal oxide. This was observed by Westermann (1930) for Pb, Sn, Zn, Cd, and Cu flames in air. Wolfhard and Parker (1949) found that it was also true for Al and Mg powder flames, but not for boron. For Al and Mg flames, they observed that the combustion product consisted of condensed oxide, present as tiny liquid spheres, which upon cooling became solid oxide particles. They also found that the colour temperature of the Al and Mg was higher than the boiling point of the oxide. They explained this anomalously high temperature as being due to emission from the incandescent oxide droplets present in the flame.

The emission of light from incandescent particles in flames is also familiar from studies of carbon formation in flames of organic compounds. The effect of ambient air pressure on carbon particle formation in premixed ethylene/air flames was studied by Smith (1940), who found that carbon formation increased with pressure. The same pressure dependance was found by Parker and Wolfhard (1950), who investigated carbon formation in diffusion flames of hydrocarbons burning in air.

The formation of boric oxide particles in pentaborane/air flames was studied by Olsen and Setze (1958). They stated that calculation showed that particles of diameter less than 3μ would always remain in temperature and velocity equilibrium with the carrier gas.

1.4. A survey of previous work on the structure of aerosols.

A large proportion of the previous work has been concerned with the coagulation of aerosols. Kohlschutter and **Ehlers** (1912) were the first workers to study aerosols of metals and metal oxides. They formed the aerosols by striking metal arcs in air at atmospheric pressure, and examined the aerosols optically. They found that some substances (zinc and cadmium oxides) tended to form chains of particles, but others did not (copper oxide, silica, bismuth oxide). They attributed this difference in behaviour to the difference in volatility of the material, its tendency to crystallise, and to the form of the crystals themselves. They also produced arc smokes in CO_2 at atmospheric pressure, and observed that "the collected powder was finer than in air, in agreement with the general rule that the degree of dispersion varies directly with the density of the medium".

The first systematic investigations of aerosol systems were carried out by Tolman (1919). He dispersed smokes, formed from various organic compounds, in a chamber and found the change in mass concentration with time, using a Tyndallmeter to observe light scattered by the aerosol cloud. He found that the intensity of the Tyndall beam diminished with time, and thus established that the process of coagulation takes place in smokes. Tolman's work was extended by Wells and Gerke (1919) and also by Whytlaw-Gray (1922),

whose classic experiments with the Zsigismondy slit ultramicroscope enabled individual particles to be counted. Whytlaw-Gray examined aerosols of organic substances of high boiling point, and also aerosols of non-volatile materials. He obtained aerosols of various metal oxides and of metals (Ag, Au, Pt) by striking electric arcs of the metal in air at atmospheric pressure. Using the slit ultramicroscope, he found that the more heterogeneous an aerosol, the more rapidly it coagulated. Thus arc smokes, being formed at high concentration and temperature were found to be very heterogeneous and rapid in coagulating. The coagulation rate was found to be different for different materials. Whytlaw-Gray estimated the particle sizes in the aerosols from the known particle number and mass concentration, and obtained values of the order of 1×10^{-5} cm.

The early workers were interested in finding parallels between the behaviour of aerosols and hydrosols, which had already been the subject of considerable study. Whytlaw-Gray (1922) found the coagulation of aerosols could be very well described by the theory proposed by Smoluchowski (1918) for the coagulation of hydrosols. The theory was applied to aerosols by Whytlaw-Gray, and developed by him to show the dependence of coagulation rate on heterogeneity.

Previous work by Thomson (1906) had established that a certain degree of supersaturation must be attained before

condensation can take place. Whytlaw-Gray (1922) suggested that in arc smokes, ions produced by the electric discharge could act as condensation nuclei, allowing the condensation to take place at a lower supersaturation. He observed that particles in arc smokes tended to form long chains, and interpreted this as being characteristic of the coagulation of charged particles. He observed that the larger particles in metal and metal oxide smokes were crystalline, but thought that smaller particles were probably amorphous. He suggested that the form of the particles was mainly determined by three factors: the temperature of formation, the rate of crystallisation, and the electrification.

However, Walmsley (1927) carried out an X-ray diffraction study of cadmium oxide arc smokes, and found that their ultimate structure was crystalline, the primary particles being crystals of about 5×10^{-6} cm in diameter. Later, Walmsley (1929) examined, by X-ray diffraction, smokes produced from arcs in air of about twenty common metals (Pt, Ag, Au, Mg, Co, Ni, Cd, Ca, Th, Cr, Fe, Cu, Al, As, Sb, Pb) and found them to be crystalline. Silver, gold and platinum gave aerosols of the metal, but the other metals (Cu, Fe, Pb, Al, etc.) formed oxides. In some circumstances, silver gave a proportion of the oxide, Ag_2O. Smokes consisting of oxides which are polymorphous usually gave the modification stable at high temperature, smokes from Cu and Fe arcs gave

mixed oxides. Walmsley concluded that the formation of the smoke particles was completed at a high temperature, and in the immediate vicinity of the electrodes. He measured the densities of the individual smoke particles, and found them to have the normal values of the bulk material.

Kohlschutter (1927) produced metal vapour in an indifferent gas, and allowed it to condense. He found that the size of the metal globules produced increased as the pressure was lowered from atmospheric. He attributed this behaviour to the increase in number of collisions between metal particles at lower pressure, and to the decrease in adsorption of gas at lower pressure.

Cawood and Whytlaw-Gray (1936) investigated ferric oxide aerosols produced by the photo-decomposition of iron pentacarbonyl with air as the carrier gas. They studied the effect of pressure below atmospheric on the structure of the aerosols, and found that the coagulation rate increased as the pressure was lowered. They also found that the primary particles formed at low pressure were much larger than those formed at atmospheric pressure. Fuchs (1936) explained that this result could only be due to a difference in the growth rate, since according to nucleation theory, the number of nuclei formed in unit time is independent of the air pressure. For particles

smaller than the mean free path of the gas molecules, the rate of growth is also independent of the air pressure. A perceptible difference in the growth rate could only begin when the growing particles had reached a size of 10^{-6} - 10^{-5} cm. The growth rate beyond this size would be greater, the greater the diffusion coefficient of the vapour i.e. the lower the air pressure.

The electron diffraction technique was first used for the examination of smokes by Finch, Quarrell and Wilman (1935), who evaporated zinc in air and obtained a ZnO diffraction pattern from the resulting aerosol. Electron diffraction has since been used by a number of workers, notably Yearian (1935), and Erhardt and Lark-Horowitz (1940).

With the invention of the electron microscope, the investigation of aerosols of involatile substances was greatly facilitated. Electron micrographs of metal oxide smoke particles were among the first ever to be obtained with the electron microscope. However, although a considerable number of electron micrographs of metal and metal oxide smokes have been obtained, a surprisingly small amount of systematic work on these aerosols has been carried out with the electron microscope.

Schechter et al (1946) used the electron microscope to investigate smokes produced by various metal arcs and metal-cored carbon arcs in air at atmospheric pressure.

Their most notable observation was the frequent occurrence of spherical particles in the smokes. Thus Au, Al, KCl and NaCl smokes were found to be composed entirely of spheres, while Ag and Cu gave a mixture of spheres and polyhedral crystals. Mg gave cubes, and Zn needle shaped crystals. They suggested that the spherical shape could be either : (a) An unstable intermediate growth formation, (b) An equilibrium state which each small crystal attains if its dimensions are sufficiently small, or (c) A solidified liquid droplet. They did not carry out any particle size analysis, but gave only rough estimates of the mean particle sizes; all were in the range 100 - 2000A.

Harvey, Matthews and Wilman (1960) used electron microscopy and electron diffraction to investigate the structure of aerosols produced by metal arcs in air. They found that the smokes from Au and Ag consisted of spherical particles of the metal alone, while smokes from Pb and Bi consisted of spheres of metal with an outer layer of oxide. Other metals gave smokes consisting of oxide particles which were spherical, or nearly so, for oxides having a high temperature of crystallisation (Al, Ti, Zr and Ta); or polyhedral for those having a low temperature of crystallisation (Cu, Zn, Cd, Sn, Fe, Co, Ni, W). Mo and Sb gave a mixture of spheres and polyhedral particles. They proposed that the recrystallisation temperature of the particular

oxide gave a lower limit to the temperature of formation of the particles. Thus the TiO_2 smoke consisted of the anatase form, which is stable only between 550°C and 800°C. Similarly, the Ta_2O_5 smoke indicated a temperature of at least 700 C. The Sb_2O_3 smoke was found to contain both the orthorhombic form (stable only above 570°C) and the normal cubic form, indicating a temperature of formation above 570°C, the orthorhombic form remaining stable due to rapid quenching.

From electron micrographs, they estimated the mean particle sizes in the smokes to be between 300 and 650 A, which agreed approximately with the value of 500 A obtained from electron diffraction measurements. This led them to conclude that many or most of the particles were single crystals. They also investigated the effect of air pressure between 10 mm. Hg and atmospheric on Au and Ag aerosols, and found that the chain-like aggregation appeared to become more extensive as the pressure was raised.

Kimoto et al (1963) used the electron microscope to study metal aerosols produced by evaporating various metals in an atmosphere of argon, at pressures ranging from 1 mm. Hg to atmospheric. They estimated mean particle sizes from micrographs, and found that the particle size appeared to increase with increase in argon pressure.

1.5. The distribution of particle sizes.

It is well known that the sizes of small particles, such as grains of sand, are not uniform, but differ from one to the other. Closer inspection reveals that there must be some law governing that variability. Firstly, the particle sizes are confined within a certain range. Also, if the particles are grouped together in classes of magnitude, each class covering a certain interval of size, it will be found that some classes contain more particles than others. Usually, there will be one class which contains the largest number of particles, and the numbers of particles in the other classes will be found to decrease progressively towards the two ends of the range. The law which describes these features is called a "frequency distribution law".

In order to obtain the distribution law, the size of each particle must be measured. However, such a measurement need not be very accurate, since it merely serves to establish to which size class a particle belongs. Only for particles at the class limits might there be doubt as to how to classify the particles, and misclassification might occur. However, if the number of particles belonging to a class is large, the effect of such misclassification will be small. The effect will be more pronounced if the class frequency is small, as it is near the ends of the frequency scale.

1.5.1. The form of the distribution law.

(i) The Normal Law.

One of the best known statistical laws is the Gaussian Law of Errors, or the Normal Law. It has been suggested (Green, 1921) that since the differences in particle size in a material are not due to definite assignable causes, but only to a large number of small causes whose presence is governed by unknown factors, a function of the type of the Normal Law might be suitable for describing particle size distributions.

The Normal Law has the form :

$$y = \frac{1}{\sigma\sqrt{2\pi}} \exp\left(-r^2/2\sigma^2\right) \qquad \ldots(20)$$

where y = probability density, σ = standard deviation of r, and r = particle size.

The importance of the Normal Law lies in the fact that it provides an idealised error distribution based on the assumption that the elementary small causes combine at random to produce the observed effect.

Doeglas (1946), stated that he did not suppose that the size frequency distribution of particles was a probability distribution, since the particle size is due to determinate laws, and not to the laws of chance. However, Herdan (1953) pointed out that the concept of chance does not exclude the operation of determinate laws,

but is only a comprehensive concept for the simultaneous operation of a large number of small causes. He therefore concluded that there was no reason why a particle size distribution should not be a probability distribution.

Attempts to apply the Normal Law to particle size distributions were made by Green, (1921) for ZnO particles, Sheppard et al, (1923) for silver halide grains in photographic emulsions, and Martin et al, (1925) for crushed silica. In all cases they found that the size distributions were not fitted by the Normal Law.

(ii) The Log-Normal Law.

According to this distribution law, it is not the differences of equal amount in excess or defect from a mean value which are equally likely, but ratios of equal amount in excess or defect from a mean value. The Log-Normal distribution has the form:

$$y = \frac{1}{\log\sigma\sqrt{2\pi}} \exp - \frac{(\log r - \log r_g)^2}{2 \log^2 \sigma_g} \qquad \ldots(21)$$

where y = probability density, r = particle size, r_g = geometric mean, σ_g = geometric standard deviation

The great range of sizes covered by the Log-Normal distribution makes it suitable for describing particle size distributions. Kolmogoroff (1941) and Epstein (1948) treated the grinding of solids as a stochastic process, and were able to show theoretically that the size dis-

tribution obtained by grinding should be a Log-Normal one. It has since been found empirically that for many materials this is the case. Kottler (1950) showed that the distribution of grain sizes in photographic emulsions followed the Log-Normal distribution.

Particle size analysis of aerosols has mainly been concerned with dusts and mists. Many of these systems have been found to follow the Log-Normal distribution (Drinker, 1925). The distribution of particle sizes in atmospheric dusts was found to be Log-Normal by Billington and Saunders (1947).

Very little is known about the size distribution in smokes, since very little attention has been paid to measurement of size distribution in these systems. Cartwright et al (1956) made an electron microscope study of solid smoke particles present in atmospheric pollution. They found that the particle sizes were in the range 0.01μ -1μ. The size distribution appears to be Log-Normal, although this fact was not brought out in the paper. Meetham (1950) also made an electron microscope study of atmospheric smoke. Again the size distribution appears to be of the Log-Normal type.

1.5.2. The correlation between particle size distribution and particle growth mechanism.

Galton (1897) pointed out that since particle

size could not be less than zero, it was unlikely that a particle size distribution would follow the Normal Law. To remove the absurdity of negative sizes, Galton suggested that an exponential law for the growth of a single particle should be assumed. He suggested a growth law of the form :

$$\frac{dr}{dt} = kr \qquad r = \text{particle radius, } k = \text{constant}$$

Thus $\log r = kt + A$

or $t = a + b \log r$

This "logarithmic transformation" would thus convert sizes r into times t, which would be distributed according to some statistical law. Kottler (1950) has suggested that the distribution of growth times should be assumed to be Normal, since the time zero is arbitrary, and thus does not suffer the restriction ($r>0$) encountered with size. Kottler assigned, asymptotically, $t = -\infty$ to the initiation of growth, and $t = +\infty$ to the end of the growth process. The combination of an exponential law of growth with a Normal distribution of growth times leads immediately to a Log-Normal distribution of particle sizes.

A similar approach was used by Brodynan (1960), considering the growth of latex particles. He pointed out that to use the statistical method for relating particle size distribution to the growth mechanism, it must be assumed that growth takes place in discrete time intervals

by completely random processes. If this is the case, the Central Limit theorem of mathematical physics may be used. The Central Limit theorem states that a random variable, which is the result of a large number of random events, will have a Normal (Gaussian) distribution. Brodynan showed that there must be some parameter (radius, log of the radius, volume, etc.) which has a growth probability independant of the radius.

For the growth of a particle, generally :

$$\frac{dr}{dt} = kr^x \qquad \ldots(22)$$

thus for $x = 0$, $\frac{dr}{dt} = k = \text{constant}$

Hence for $x = 0$, the growth of the radius is independent of the radius. Applying the Central Limit theorem, the particle radii are found to have a Normal distribution.

for $x = 1$, $\frac{dr}{dt} = k\,r$

thus $$\frac{d(\log r)}{dt} = k = \text{constant} \qquad \ldots(23)$$

Hence for $x = 1$, the rate of change of the log of the radius is independent of radius. Hence the particle radii are found to have a Log - Normal distribution.

For $x = -1$, the squares of the radii are Normally distributed, i.e. the particle surface areas are Normally distributed.

For $x = -2$ the cubes of the particle radii (particle volumes) are Normally distributed.

Brodynan found that the particle sizes in emulsions were distributed according to the Log - Normal law, and hence he concluded that the growth law was $dr/dt = k\,r$. Zaiser and La Mer (1948) studied the diffusion-controlled growth of sulphur hydrosols, and found that the growth law was of the form dr^2/dt = constant. Brodynan (1960) pointed out that this result indicated that diffusion-controlled growth should lead to the squares of the particle radii being Normally distributed. Since he had found that in the growth of emulsion particles the radii were Log - Normally distributed, he concluded that diffusion could not be the rate-controlling step in emulsion polymerisation.

2. EXPERIMENTAL DETAILS

2.1. Materials

Metal-oxide aerosols were obtained from metal arcs for magnesium, aluminium, magnox and stainless steel, and from cored carbon arcs for zirconium and uranium dioxide; Metal aerosols were obtained by the evaporation of gold from a gold-cored carbon arc.

The magnesium was supplied by the Magnesium Elektron Co. Ltd., and was 99.95% pure, the main impurities being Zn 0.02%, Al, Mn, and Fe 0.01%. "Superpurity" aluminium was supplied by the British Aluminium Co. Ltd. and was 99.99% pure. Spectroscopically pure gold was obtained from Johnson, Matthey and Co. Ltd.; no impurity was present in quantity greater than 3 p.p.m.

The magnox, stainless steel, zirconium and uranium dioxide were supplied by U.K.A.E.A., Windscale. The composition of the magnox was Mg 99.1 -99.3%, Al 0.7-0.9%, Be 0.005-0.03%, with Cu, Fe and Si all present in quantities less than 80 p.p.m. The composition of the stainless steel was Fe 73%, Cr 18%, and Ni 8%, with Nb not more than 0,7%, C 0.032 - 0.05%, Mn 0.55-0.85% and all other impurities less than 0.05%. The uranium dioxide was of reactor fuel grade. The impurities present in the zirconium were Hf 3.10%, Ca 1.25%, Fe 0.41%, Cr 0.09%, Al 0.04%. The graphite

used for the metal-cored arcs was Reactor Grade A material containing Fe, Ba, Ca, Si and V in the range 10 - 100 p.p.m.; all other impurities were less than 10 p.p.m.

2.2. The preparation of specimens.

2.2.1. The preparation of support films.

In order to examine the aerosols in the electron microscope, it was necessary to deposit them on some kind of thin film which was transparent to the electron beam. For this purpose carbon support films, of thickness 200 - 300 A, were prepared in a Metropolitan-Vickers vacuum deposition apparatus. Carbon from a carbon arc passing 60 amps was deposited in vacuum on clean glass slides placed 8 cm. below the arc. The film thickness was monitored by placing a drop of Teepol on a white tile at the same level as the glass slides; the first detectable contrast between the drop and the tile indicated a film thickness of about 100 A. The carbon films were then floated off on distilled water, picked up on copper electron microscope grids, and pumped dry in a vacuum desiccator. The electron microscope grids were 3 mm. in diameter and 200 mesh per inch. After preparation and thorough drying, the carbon films could be stored in a desiccator for several months without deterioration.

For transmission electron diffraction in the

Finch diffraction camera, thin collodion film supports were used. These films were prepared by allowing a drop of 1.5% solution of collodion in amyl acetate to spread on the surface of distilled water. The films were then picked up on metal gauze and dried in vacuum. Collodion films deteriorated very rapidly, and were therefore used immediately after preparation.

2.2.2. The apparatus for the generation of aerosols.

(i) The high-pressure vessel.

The pressure vessel, illustrated in figs. 6 and 7, was made in the workshop of the Chemical Engineering Department, Imperial College, and consisted of a cylindrical stainless steel vessel closed at the top with a screw-in stainless steel plug. Both parts were machined from the solid. The main body of the vessel and the plug were made from different kinds of steel, to prevent seizing of the screw thread. Thus the main body was machined from EN 57 stainless steel, and the plug from EN 58J stainless steel. The plug was screwed tightly down onto a neoprene O-ring to form a high-pressure seal, the screw thread being lubricated with molybdenum disulphide paste obtained from Rocol Ltd. With the plug in position, the internal dimensions of the vessel were 4" high x 4" diameter. The wall and base of the vessel were both 1" thick.

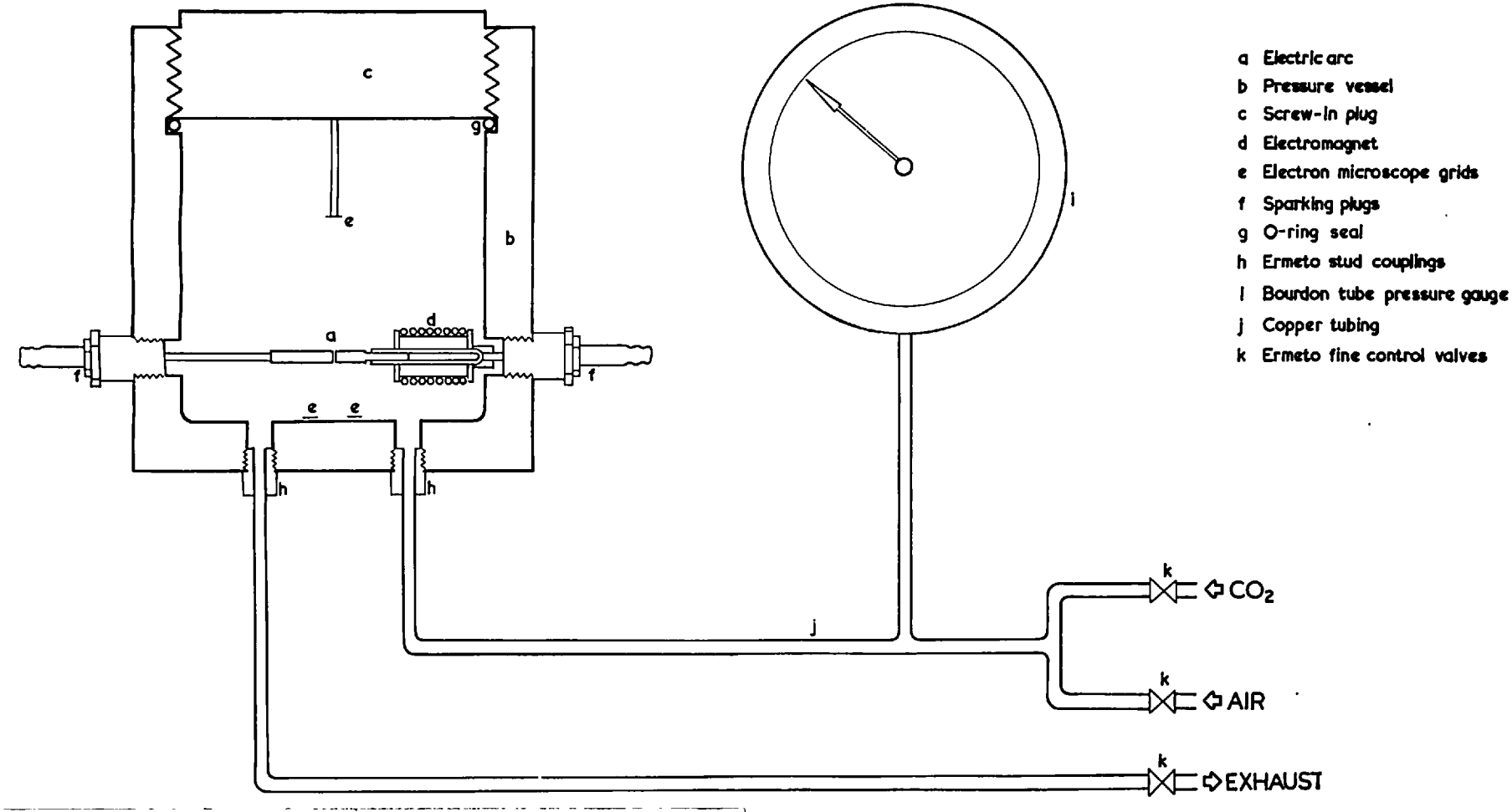

Fig. 6 The high pressure vessel and the associated high pressure system.

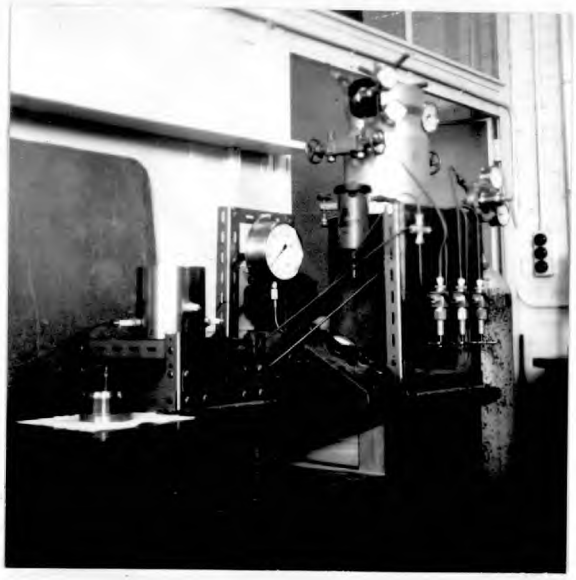

Fig. 7 The high pressure system.

K.L.G. sparking plugs with an extended centre electrode were used to provide high-pressure leads-through for the electric current. Four such sparking plugs were placed in the wall of the vessel, two being 3/4" above the floor of the vessel (one at each end of a diameter) and two at right angles to the first pair, being 2" above the floor of the vessel. Copper rings were used to provide a high-pressure seal between the sparking plugs and the vessel wall. An earthing point was also provided in the floor of the vessel.

The pressure vessel was clamped into a steel frame, which in turn was bolted to the bench. During operation the vessel was surrounded by an explosion shield constructed from 1/4" steel plate.

(ii) The gas supply.

Air was obtained from compressed air cylinders supplied by the British Oxygen Co. Ltd. The composition of the air was the same as that of ordinary atmospheric air: N_2 78.084%, O_2 20.946%, CO_2 0.033%, A 0.934%, Ne 18 p.p.m., He 5 p.p.m. and water vapour 0.01 - 0.05%.

The carbon dioxide was obtained from a Cardice converter supplied by The Distillers Co. Ltd. A muslin bag containing 5 Kg. of silica gel was placed in the bottom of the converter to remove water, and each 25 lb. block of Cardice was scraped clean of condensed water vapour before

being inserted into the converter. After charging with 100 lbs. Cardice, the converter was blown off for 30 minutes to remove any residual air, and then sealed. When equilibrium between the liquid and gaseous CO_2 phases had been reached, the converter was capable of delivering clean dry CO_2 at pressures up to about 800 p.s.i., with a total residual gas content of less than 150 p.p.m., and moisture content less than about 20 p.p.m.

(iii) The high pressure system.

The high pressure system is illustrated schematically in fig.(7). The gas supply (compressed air cylinder and Cardice converter) was connected to the pressure vessel via a system of piping and valves. High pressure gas regulators of the diaphragm type were used on the cylinder nozzles to give rough control of the gas pressure. Ermeto fine-control needle valves were placed in the air and carbon dioxide input lines, and in the exhaust line, to give sensitive control of the gas pressure in the system. All the high pressure piping was of 1/4" diameter copper tube, which could easily be bent to shape, and pipe connections were effected with Ermeto high pressure couplings. The pressure vessel was provided with separate input and exhaust lines, since a single input/exhaust line would have resulted in contamination of the pipe during exhaustion. The total pressure in the system was measured with a Budenburg Bourdon tube gauge reading from 0 - 800 p.s.i.

During work on toxic materials (UO_2), a Volkes absolute filter was placed in the exhaust line, on the low-pressure side of the fine-control valve, to prevent any aerosol particles being released into the atmosphere.

For work using carbon dioxide, a rotary vacuum pump was placed in the exhaust line, to enable air to be removed from the system before admitting CO_2.

(iv) The electric arc.

The electric arc was chosen as a convenient method of generating metal vapour, and also since the method had been used by previous workers (Whytlaw-Gray, 1922; Walmsley, 1927; Finch, Quarrell and Wilman, 1935; Schechter, 1946; Harvey, Matthews and Wilman, 1960). A remote control method had to be devised for striking the arc inside the closed vessel at high pressure. Mechanical methods for doing this were precluded by the difficulty of making movable pressure-tight connections through the wall of the vessel, and therefore an electromagnetic method was chosen. A photograph and diagram of the arc are given in figs.(8a) and (8b).

The electromagnet consisted of a 1 3/4" length of 3/16" bore glass tubing, closed at one end, surrounded by a 1" long cylindrical soft-iron magnet core on which were wound 100 turns of 24 gauge shellac-covered copper wire. The cathode of the arc was machined to fit into a hole in the end of a 1/2" long cylindrical soft iron slider, which could



Fig. 8a The electromagnetically-drawn arc.

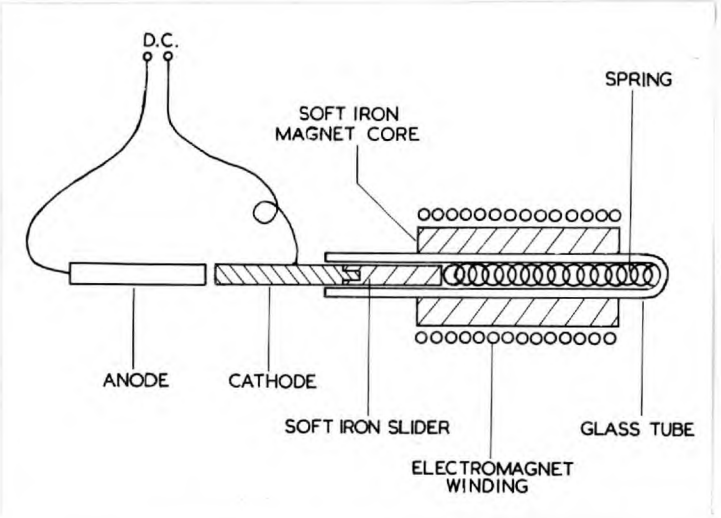

Fig. 8b Schematic diagram of the electromagnetically-drawn arc.

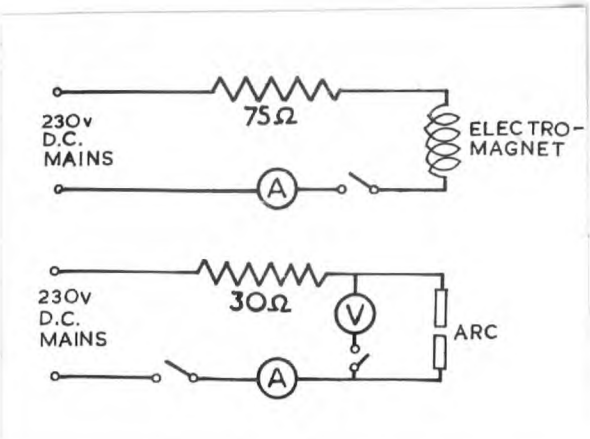

Fig. 9 The electric circuits for the arc and electromagnet.

move freely inside the glass tube. The position of the slider relative to the magnet was determined by a weak spring inside the glass tube.

The electromagnet was supported on the electrode of one of the lower pair of sparking plugs, to which one lead from the magnet coil was connected. The central glass tube provided the insulation between the arc cathode and the magnet lead. The anode of the arc was rigidly attached, with a stainless steel barrel connector, to the opposite sparking plug of the lower pair. To the upper pair of sparking plugs the other magnet coil lead and the arc cathode lead were respectively connected. The arc cathode lead consisted of 3" of 20 gauge tungsten wire, which was connected to the cathode by nipping it between the cathode and the soft iron slider. The leads were connected to the sparking plugs with stainless steel barrel connectors.

The electric circuits for the arc and magnet are shown in fig.(9). The arc and magnet circuits were connected to separate 230 volt D.C. mains supplies, and a 30 amp switch and an ammeter were placed in series in each circuit. A resistance of 30 ohms was placed in series with the arc, and a 75 ohm resistance in series with the electromagnet. The arc was operated at a current of 7.5 amps, and a current of 3 amps was used to operate the electromagnet.

(v) Operation of the electromagnetically-drawn arc.

With the arc in the closed position, the arc circuit was made, causing a current to pass. The magnet circuit was then made, energising the magnet coil, and causing the soft-iron slider and the attached arc cathode to be withdrawn down the centre tube of the magnet. An arc was thus struck between the fixed anode and the movable cathode. The arc gap could be adjusted by altering the anode position, and by adjusting the tension in the magnet spring. In the event of the arc failing to strike, switching off the magnet allowed the cathode to be pushed out by the spring, thus re-establishing contact with the anode.

2.2.3. The generation and collection of aerosols.

For generating aerosols from magnesium, aluminium, magnox and stainless steel, D.C. arcs between electrodes of the metal were used. The electrodes were in the form of rods 1/10" in diameter and about 1" long. This method proved impracticable for zirconium and gold, and was obviously not suitable for UO_2. It was found that arcs between Zr metal electrodes could not be maintained, since an oxide layer formed with great rapidity on the electrodes, insulating them from each other. Similarly, arcs between Au electrodes could not be maintained because the electrodes merely melted when the arc was struck. An alternative method

was obviously required for generating an aerosol from UO_2, this being a highly refractory oxide, and in the form of powder.

For the production of aerosols from Zr, Au, and UO_2, it was therefore decided to use cored carbon arcs, a method which had been previously used by Schechter (1946). The particular material under investigation was placed in a 3/32" diameter hole bored in the end of a carbon rod, 1" long and 3/16" in diameter. This was then used as the anode of a carbon arc. All the other experimental details were the same as for arcs between metal electrodes.

(i) Scope of the experiments.

The aim of the work was to investigate the effect of the composition and pressure of the surrounding gas on the structure of the aerosol produced in the electric arc, and therefore two series of experiments were carried out, one using arcs in air, and one using arcs of the same materials in CO_2. For each material, aerosols were produced at three different pressures; atmospheric pressure, 300 p.s.i., and 500 p.s.i. in both air and CO_2. The experiments with zirconium were exceptional. It was found that no detectable aerosol was produced by a zirconium-cored carbon arc in air, and results were therefore only obtained using CO_2. A full list of the experiments performed is given in Table (3).

Material	Type of arc	Gas pressure at which aerosols generated	
		Air	CO_2
Magnesium	M	A, 300, 500	A, 300, 500
Aluminium	M	A, 300, 500	A, 300, 500
Magnox	M	A, 300, 500	A, 300, 500
Stainless Steel	M	A, 100, 200, 500	A, 300, 500
Uranium Dioxide	C	A, 300, 500	A, 300, 500
Gold	C	A, 300, 500	A, 300, 500
Zirconium	C	No aerosol produced	A, 300, 500

A = Atmospheric pressure, M = metal arc, C = metal-cored carbon arc.
Gas pressures given in p.s.i.

Table (3). Details of the conditions under which aerosols were produced.

(ii) Experimental procedure.

Before each experiment the inside of the pressure vessel, the electromagnet and all the leads and connectors were carefully cleaned and degreased with benzene, and the apparatus was flushed out with large volumes of air or CO_2, depending on which gas was to be used. For experiments using metal arc electrodes (Mg, Al, magnox, stainless steel), the electrodes were prepared by abrading under propyl alcohol (to avoid pick-up of emery particles -αAl_2O_3 and diaspore AlOOH) on several grades of emery paper, with a final polish on 0000 emery, wet with propyl alcohol and then cleaned by immersing

in benzene. In the cases of Au and Zr, where cored carbon arcs were used, a piece of the metal was prepared in the same way, and then fitted into the end of a hollow carbon electrode, which had also been previously cleaned. In the case of UO_2, for which a cored carbon arc was also used, the UO_2 powder was carefully packed into a hollow carbon electrode. After the arc electrodes had been prepared, the electromagnet and the electrodes were placed in position inside the pressure vessel, and the arc gap adjusted to 2 mm. Carbon films on electron microscope grids were then placed inside the vessel, two being placed on the floor of the vessel 2 cm below the arc, and one 6 cm above the arc on a stainless steel specimen holder which was screwed into the lid of the vessel. The vessel was then sealed and gas admitted until the pressure reached the required value. The arc was then struck and continued for 5 - 10 seconds, the smoke produced being deposited on the electron microscope grids by convection and sedimentation. After the arc had been shut off the vessel was left at pressure for 5 mins., and then the pressure was very slowly reduced to atmospheric. The grids were then removed and immediately examined in the electron microscope or the diffraction camera.

For work using CO_2 as the carrier gas, the vessel and the arc were prepared as described above, but after sealing the vessel, the apparatus was pumped out for 10 minutes with a rotary vacuum pump. CO_2 was then admitted until the pressure

reached atmospheric, then the system was pumped out again in order to remove any residual air. CO_2 was then readmitted until the pressure in the system reached the required value.

When preparing aerosols from UO_2 a Volkes absolute filter was placed in the exhaust line, and at the end of an experiment the system was flushed out through the filter for about 10 minutes before opening up the vessel. Standard precautions were taken in the handling of uranium dioxide.

2.3. The examination of specimens.

The two techniques of electron diffraction and electron microscopy were used for the examination of specimens, the first in order to determine the chemical nature and crystalline structure of the aerosols, and the second to determine the form of the aerosol particles and their size distribution.

2.3.1. The electron-diffraction technique.

The diffraction of electrons by single crystals and polycrystals of metals and non-metals, and the interpretation of the resulting electron diffraction patterns has been described in several books and papers - Thomson (1930); Finch, Quarrell and Wilman (1935); Beeching (1936); Finch and Wilman (1937); Thomson and Cochrane (1939); Pinsker (1949, 1953); Wilman (1948a, 1948b, 1950, 1951, 1952). In view of this large quantity of literature on the subject, only a

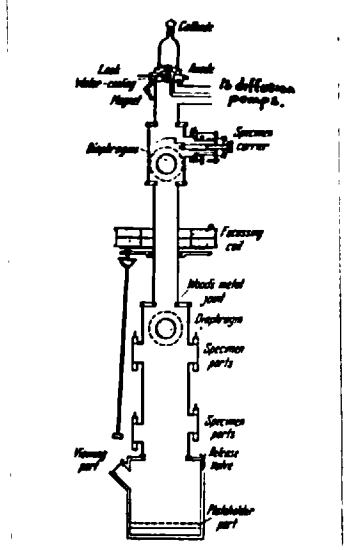

Fig. 10 The Finch electron diffraction camera.

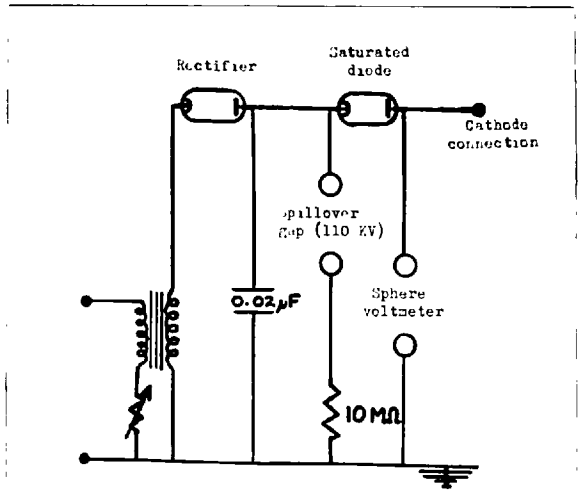

Fig. 11 The high-tension circuit.

brief account of the techniques used and the interpretation of the patterns obtained will be given here.

A Finch electron diffraction camera was used, as described by Finch and Wilman (1937), but with oil diffusion pumps and O-ring seals - see fig.(10). The electron accelerating voltage was in the region 45-65 kV, and the camera length (i.e. the distance from the specimen to the photographic plate) was approximately 50 cm. A diagram of the high tension circuit is given in fig.(11).

Electrons have a low penetrating power, of the order of 1000 A in the beam direction, for atoms of medium atomic weight. In the transmission technique of electron diffraction, which was used exclusively in the present work, it is necessary to ensure that the specimen is thin enough to allow a transmitted beam of sufficient intensity. This condition was fulfilled since all the aerosol specimens examined contained many particles with a diameter less than 500 A.

2.3.2. A brief account of the interpretation of electron diffraction patterns obtained from randomly orientated polycrystalline specimens.

The patterns obtained from randomly orientated crystals may be interpreted in terms of Bragg reflections of the primary beam by net planes in the crystal such that:

$$n\lambda = 2\ d \sin \theta$$

where d is the net plane spacing, and θ the angle between the reflected beam (or the incident beam) and the net plane. The diffracted beams, therefore, lie on a series of cones of semi-apical angle 2θ coaxial with the primary beam. These cones intersect a plane normal to the electron beam (e.g. a fluorescent screen or a photographic plate) in a series of concentric circles (Debye-Scherrer rings). Inserting the camera length and ring radius into the Bragg relationship gives the expression:

$$R_{hkl} = (\lambda L / d_{hkl}) \left(1 + 3/8 \left(\frac{R}{L}\right)^2 + \ldots.\right)$$

The second factor in the expression is negligible to within 0.03% for R less than 1.8 cm. (L is the camera length, d_{hkl} is the net plane spacing and R_{hkl} is the radius of the corresponding ring).

For identification purposes the net plane spacings can be compared with known electron diffraction or X-ray powder pattern data, the latter being tabulated in the well-known A.S.T.M. index. If X-ray data are used for the identification of electron diffraction patterns, it should be noted that the intensities of rings in X-ray and electron diffraction patterns may be different, owing to differential absorption effects if the crystals are not roughly spherical.

A very simple and rapid method of identifying the patterns was used; the radii of the rings were plotted on a logarithmic scale and compared with known data plotted on the same scale. Charts of the Bunn-Bjurstrom type were used in indexing the UO_3 pattern, for which no previous data were available.

The diffraction patterns from the aerosols were calibrated relative to graphite. The use of the carbon-carbon spacing in the basal plane of graphite for calibration purposes was first suggested by Fordham and Finch (1935). Subsequently, Nelson and Riley (1945) found that the a-value and the axial ratio of graphite varied very little with temperature, making it very reliable as a reference material.

For the calibration of the diffraction patterns in the present work, a drop of a solution of colloidal graphite in water was placed on the back of the film supporting the aerosol, allowed to spread over the surface, and pumped dry in a vacuum desiccator. This resulted in a diffraction pattern from the graphite being superimposed on the pattern from the aerosol. The extremely sharp graphite 110 ring (d = 1.230 A) was then used to calibrate the rings in the pattern from the aerosol.

2.3.3. The electron microscopy technique.

The first commercial electron microscope was produced by the Siemens Co. in 1938, from a design of Ruska and Von Borries (1938), and had an ultimate resolving power

of about 50 A. Since that time a considerable amount of work has been done in Germany and the U.S.A., and a steady improvement in resolving power has been achieved. The progress in the design and operation of the electron microscope has been the subject of a large number of articles and reviews - Knoll and Stark (1948), Mahl (1945), Von Borries (1940), Cosslett (1951), Kay (1961). Therefore, a detailed description of the principles and mode of operation of the electron microscope will not be given here, only those points of direct interest to the present work being mentioned.

The instrument used was a Siemens Elmiskop I, a three-stage microscope with double condenser, objective, intermediate and projector lenses, and a magnification range of X1000 - X180,000. The microscope was operated at an accelerating voltage of 80 kV. The vacuum system consisted of an oil diffusion pump backed by a mercury diffusion pump and a rotary pump. The diffusion pumps could also be backed by a vacuum reservoir, allowing the rotary pump to be switched off for long periods and thus removing excess vibration during photography. The instrument has been described in detail by Cosslett (1951).

(i) Resolution.

The resolving power of the electron microscope may be defined in terms of its ability to distinguish separate images of two closely spaced image points. The shape of these image points will not be evident unless they are several times larger

than the resolving power with which they are observed. The relation of particle shape to resolving power has been discussed by Von Borries and Kausche (1940), who estimated that a cube must have an average diameter of four times the smallest separation resolvable for it to be distinguished from a sphere. Isolated particles, if very different in density from their surroundings, can be detected when their size is considerably less than the resolving power, but their size cannot be measured with any accuracy, nor can their shape be determined.

In an electron microscope the equivalent wavelength of the electron beam is about 1/20 A, and a resolution of the same order might be expected. However, other limitations such as lens abberations restrict the maximum aperture which can be employed in electron lenses. As a result an ultimate resolution of a few Angstroms is theoretically possible. The Siemens Elmiskop I used in the present work had an ultimate resolution of 10 A when in perfect alignment. A resolution of about 15 A was in fact normally attained.

(ii) Focusing.

Semi-opaque objects observed in the electron microscope show a series of Fresnel fringes round their edges when the image is slightly defocused. These fringes are due to interference between the direct electron beam and that scattered by the edge of the object. The appearance of the fringes is different in the under-focused and the over-focused

image, the contrast of the fringes being reversed. The condition for the best focused image is the evidence of negligible Fresnel fringes.

Fresnel fringes can only be observed at a magnification greater than about X20,000. In the present work a X10 viewing telescope was used to observe the Fresnel fringes and establish the best focus. Accurate focusing was important, since the presence of a fringe round a particle could have led to spurious values for particle size.

(iii) Magnification.

The Siemens Elmiskop I was equipped with internal calibration for producing fixed magnifications. In order to produce a particular magnification, the lens strengths were adjusted so that the image of a projector aperture of known size was fitted exactly to a 9 cm diameter circle inscribed on the viewing screen. By using different projector apertures a range of magnifications could be obtained. The magnifications used were: X5,000, X10,000, X20,000, X40,000, and X80,000, these values being accurate to $\pm 3\%$.

The criterion for the choice of magnification in any particular case was that the smallest particle in the field of view should have a diameter not less than about 1 mm when observed through the X10 viewing telescope. This limit was set by the smallest size countable with the Zeiss particle size analyser. (See section 2.4.1.).

(iv) Image formation.

The paths of electrons through the microscope under normal conditions for the formation of a "bright-field" image are shown in fig.(12). Electrons are produced at the hot tungsten filament and the condenser lenses produce a focused beam of electrons which illuminates the specimen. The width of the beam is controlled by a condenser aperture inserted in the second condenser lens. From the specimen the electron beam passes into the imaging system, and a first stage image is produced by the objective lens. An objective aperture is placed in the focal plane of this lens to improve the contrast by stopping out elastically scattered electrons. A second stage image is produced by the intermediate lens, and the final image on the fluorescent screen is produced by the projector lens.

(v) Selected-area diffraction.

Ray paths through the lens system with the microscope in the diffraction condition are shown in fig.(13). Diffraction patterns can be obtained from small selected areas of the specimen by removing the objective aperture and placing a diffraction aperture in the image plane of the objective lens. This lens then forms a diffraction pattern at its back focal plane, the pattern resulting from the small area of the specimen selected by the aperture. The intermediate and projector lenses are then used to image the pattern on the screen. By reducing the size of the diffraction aperture the area of the specimen

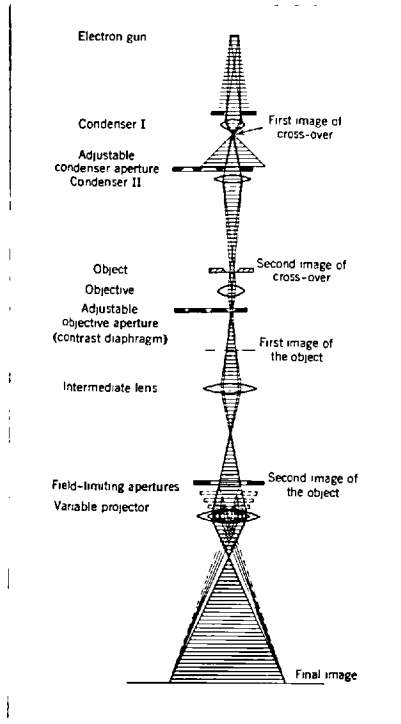

Fig. 12 · The paths of electrons through the electron microscope in the imaging condition.

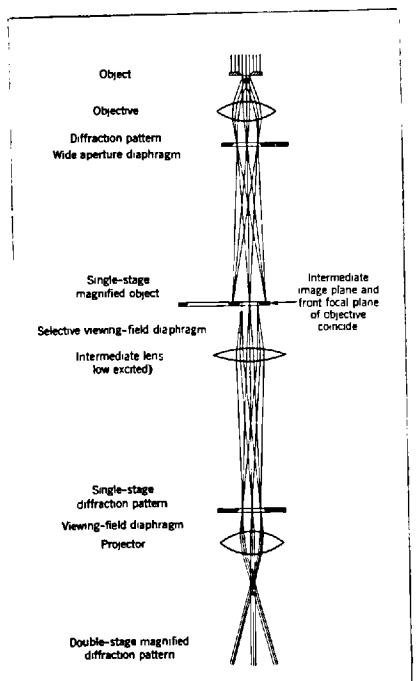

Fig. 13 The paths of electrons through the electron microscope in the diffraction condition.

from which the diffraction pattern is produced can be made a few microns in diameter.

Thus in the present investigations, if aerosol particles of different shape and apparent density appeared in the specimen, the nature of any differences in structure and composition could be determined using this technique.

(vi) Contamination.

In all electron microscopes it is found that the surfaces exposed to the impact of the electron beam acquire a hard insulating carbonaceous deposit. The cause of contamination has been suggested as being due to the deposition of ion clusters formed from residual organic vapours by collision with the beam (Watson 1947, Hillier 1948). The effect is greatest where the current density is greatest i.e. on the apertures and the specimen.

It was found that contamination of the objective aperture reduced the resolving power considerably, and therefore clean apertures were used at all times.

(vii) Photography.

For recording the image produced in the electron microscope Kodak B.4 or Ilford N.50, photographic plates were used. Both types of plate were of high contrast. A minimum of twelve micrographs were taken for each specimen chosen for examination. In selecting a particular area of the specimen to be photographed, every effort was made to ensure that the selection was random, to avoid biasing the

size distribution.

2.4. Particle size analysis.

2.4.1. Technique of size analysis.

The particle size analyses were carried out by U.K.A.E.A. Windscale, using a Zeiss TGZ 3 particle size analyser. Enlarged prints from the electron micrographs were made for use in the analyser; the lower limit on the particle diameter which could be measured with the analyser was 1.2 mm, and therefore the size of the enlargement was made such that the smallest particle seen on the print had a diameter not less than this value. Usually this meant that the total magnification of the image was between X100,000 - X200,000.

In the method of size analysis used, the total particle size spectrum was divided into 24 size classes, each class covering a range of particle diameters. In order that all the particles were placed in their size classes with the same relative precision, the step-width of each class (i.e. the range of diameters covered by each class) was increased exponentially with class size. (Using the same step-width throughout the size spectrum could result in a difference in precision of about 30% between the extremes of the scale). Since the exponential increase in step-width was used, it was necessary to correct the particle counts, using a standard correction table, before plotting the size

distribution.

A minimum of 2000 particles were counted for each aerosol examined, this number being considered the minimum necessary for an accurate determination of the size distribution in such polydisperse specimens.

2.4.2. Graphical representation of the size distribution.

Two methods of plotting the size distribution were used, the frequency distribution histogram and the cumulative distribution curve. In the frequency histogram the numbers of particles in any size class were plotted against the size class, the sizes being on an exponential scale. In the cumulative distribution curve, the percentage of the total number of particles greater than a particular size were plotted against size on probablilty graph paper.

2.5. The investigation of the structure of the arc-flame.

An investigation of the structure of the arc-flame was carried out for stainless steel, magnesium, and gold-cored carbon arcs burning in air at atmospheric pressure. The size of the electrodes, the arc gap, and the current were the same as those used in the actual generation of aerosols. In each case the arc-flame was photographed from a distance of about 15 cm using a plate camera and Ilford Special Rapid plates. Photographs of the flame were taken along the axis of the arc, and perpendicular to the arc. In addition

the arc was observed visually by projecting an image of the arc-flame on to a ground-glass screen, and from the screen drawings showing the flame structure were made.

2.6. The determination of the temperature distribution in the vicinity of the arc.

The temperature gradients round a carbon arc and a stainless steel arc were measured using a 30 gauge chromel-alumel thermocouple. The thermocouple had a temperature range of 0 - 1000°C and was calibrated using the boiling point of water, the M.Pt. of zinc (419.4°C) and the M.Pt. of tin (232°C). The temperature measurements were carried out in situ inside the pressure vessel, under actual operating conditions. It was found that the thermocouple reading taken close to the arc increased very rapidly during the first one or two seconds after striking the arc, and then continued to increase at a much slower rate for a period of up to 20 secs. Under these conditions it was difficult to obtain any really accurate measurement of the temperature. Therefore, to obtain an approximate estimate of the temperature gradient near to the arc, thermocouple readings were taken at intervals of 5 sec. and 10 sec. after striking the arc. Readings were taken for distances of 0.25 cm up to 2 cm away from the arc.

For the stainless steel arc in air at atmospheric pressure the temperature gradient was measured in the vertical direction above and below the arc, and in the same plane as

the arc. The same procedure was carried out for the carbon arc, in air at atmospheric pressure, and also in air at 500 p.s.i.

2.7. The determination of the rate of evaporation of metal from the arc.

Experiments to find the evaporation rate were carried out for stainless steel and gold-cored carbon arcs. Due to sputtering of the arc electrodes and, in the case of stainless steel, the formation of an oxide layer on the electrode surface, the results obtained were regarded as at best only very rough approximations.

The method was simply to weigh the electrodes, using a semi-microbalance, before and after arcing them for a known time. This was done for a stainless steel arc in air at atmospheric pressure, and for a gold-cored carbon arc in air at atmospheric pressure and also at 500 p.s.i. In all cases the experiments were repeated a number of times and the mean value for the evaporation rate calculated.

3. RESULTS

The results are described in two main sections. In the first section the size distribution, mean size, shape, chemical composition and structure of the particles in each aerosol are considered. The second section is devoted to the structure of the arc flames, the temperature distribution in the vicinity of the arcs, and the rate of evaporation of metal from the arc.

3.1. The size, shape and structure of the aerosol particles.

The results for the aerosols obtained from each arc under various conditions are given here. For each arc material, aerosols were generated in air at atmospheric pressure, 300 p.s.i., and 500 p.s.i., and in CO_2 at atmospheric pressure, 300 p.s.i., and 500 p.s.i. For some materials, aerosols were generated at intermediate gas pressures. For each aerosol electron diffraction patterns and electron micrographs were obtained from typical areas of the specimen. The results are given for each arc material in turn, firstly in air, and then in CO_2. A typical electron micrograph and the associated frequency histogram of particle size are given for aerosols produced at atmospheric pressure and at 500 p.s.i. in both air and CO_2. From time to time, repeat experiments were carried out to check the reproducibility of the results. In these cases, more than one value for the mean particle diameter is quoted. For each arc material an

enlargement of the order of X100,000 from an electron micrograph is given to show the finer detail of particle shape. Typical electron diffraction patterns indicating the crystalline nature, composition and structure of the aerosols are shown. One example of the cumulative frequency distribution is given for each material, to show the form of the distribution function.

3.1.1. Aerosols formed by the combustion of magnesium.

(i) General observations.

It proved impossible to maintain an arc between the magnesium electrodes, since the electrodes began to burn shortly after the arc was struck, indicating that the ignition temperature of Mg (625°C according to Fassel, Gulbransen et. al. 1951) had been exceeded. However, this made the results of interest in that a comparison could be drawn between the features of aerosols formed from arcs and those formed in a free combustion process. The combustion of the magnesium proceeded vigorously in both air and CO_2 at all gas pressures. The smoke deposits produced were white in colour, as was the ash remaining after combustion.

(ii) Aerosols from the combustion of magnesium in air.

(a) The composition and crystal structure of the particles.

The electron diffraction patterns obtained with the Finch diffraction camera showed that the particles in the aerosols generated at air pressures from atmospheric to 500

p.s.i. were crystalline and had a structure corresponding to MgO (cubic, a = 4.213A). Fig.18 shows the characteristic MgO pattern obtained from the aerosol produced in air at 500 p.s.i. The ring radii and net plane spacings (d) are compared with the A.S.T.M. data for MgO in Table 4.

Table 4. Electron diffraction data from aerosol formed by combustion of Mg in air at 500 p.s.i., corresponding to MgO, periclase, a = 4.213 A.

Observed rings c.f. fig.18			MgO periclase ASTM card 4-0829		
Intensity*	Radius (cm)	d (A)	d (A)	I/I_1	hkl
M	0.996	2.434	2.431	10	111
VS	1.153	2.110	2.106	100	200
S	1.629	1.492	1.489	52	220
			1.270	4	311
M	2.001	1.214	1.216	12	222
F	2.310	1.052	1.053	5	400
			0.967	2	331
M	2.581	0.942	0.942	17	420
M	2.833	0.858	0.860	15	422
			0.811	3	511
F	3.224	0.754			
F	3.426	0.710			
F	3.617	0.672			
VF	3.817	0.637			

*S = strong, M = medium, F = faint, V = very

(b) The particle shape.

Typical electron micrographs, with the corresponding frequency histograms, of aerosols produced by the combustion of magnesium in air at atmospheric pressure and 500 p.s.i. are given in figs.14 and 15.

The aerosols were found to be composed of tiny perfect cubes of MgO, together with some more spherically-shaped particles. Selected-area diffraction was carried out in the electron microscope in order to determine whether the more spherical particles were of different crystalline structure from the cubes. Diffraction patterns were obtained from particle clusters composed exclusively of spheres, and exclusively of cubes, and were found to correspond identically to MgO. Examination of the aerosols at high magnification, of the order of X100,000 revealed that very few, if any, of the more spherical particles were in fact true spheres. In almost every case these particles were found to have cube facets in various stages of development.

The cubic shape of the particles indicated that each particle was a single crystal. This conclusion was verified by the appearance of "wedge fringes" in the images of particles having the appropriate orientation with respect to the electron beam. Such wedge fringes can only be produced by single crystals. Fig.16 shows an enlargement at X150,000 of aerosol particles produced from the combustion of Mg in air at 300 p.s.i., wedge fringes being clearly evident in several of the

particles.

An interesting feature of arc smokes is the aggregation of particles into long chain-like formations. This has been observed by previous workers (Whytlaw-Gray, 1922; Schechter et al, 1946; Harvey, Matthews and Wilman 1960). This chain-like aggregation was present in all the aerosols examined in the present work, but the MgO aerosols proved to be of particular interest since the well-defined cube shape enabled the relative orientation of neighbouring particles to be observed. It was found that in any individual chain or section of a chain, the particles tended to be of about the same size, contrary to the observations of Walmsley (1927), who stated that in arc smokes, neighbouring particles were of very dissimilar size. Neighbouring particles were also found to be in similar orientation. Most frequently, particles were found to be touching at a cube corner, down the length of a chain, or touching at a cube edge. Where both cubes and more spherical particles were present, it was found that some chains of mixed cubes and spheres did occur, but in most cases a chain was composed exclusively of cubes or exclusively of spheres, and that the particles within such individual chains were again of very similar size.

These observations would seem to indicate that the particles in any particular chain were formed at the same time, and grew under the same conditions, and also coagulated into chains very near to the vapour source before enough time had

elapsed for them to be dispersed.

Another notable feature of the aerosols is that no further growth took place after the coagulation into chains. This is evident from the micrographs, since all the particles are well-defined individual units, with no evidence of additional growth on collections of particles.

The particle shape and mode of aggregation described above were found for all the aerosols formed by the combustion of Mg in air. No marked effect of gas pressure on the particle shape or mode of aggregation was observed.

(c) The particle size distribution.

Frequency histograms for aerosols formed by the combustion of magnesium in air at atmospheric pressure and 500 p.s.i. are shown in figs.14 and 15. Fig.14 shows a marked peak at the low end of the size spectrum. This kind of peak was a feature of many of the histograms, and is simply due to the fact that the particle size-class corresponding to this peak was the lower limit of the Zeiss particle-size analyser, i.e. the size corresponding to a 1.5 mm diameter particle on the enlarged print. Detectable particles with a diameter smaller than this would automatically be counted in this size-class, since there was no smaller size-class on the instrument. Hence the peak at the low end of the size spectrum represents the sum of what would have been the tail of the distribution.

All the aerosols formed by the combustion of Mg in

air were found to have a Log-Normal distribution (see section 1.5.1.). This was indicated by the fact that for each aerosol the cumulative frequency curve plotted on probability graph paper was a straight line. An example of such a plot is given in fig.16.

(d) The effect of the air pressure on the mean particle size.

The mean particle sizes and the standard deviations of the MgO aerosols formed in air were obtained from the cumulative frequency curves. The values for air at atmospheric pressure, 300 p.s.i. and 500 p.s.i. are given in table 5.

Table 5. Mean particle sizes in aerosols formed by the combustion of Mg in air.

Air pressure	Mean particle diameter (μ)	Standard deviation
Atmospheric	0.034	2.18
300 p.s.i.	0.135	1.59
	0.093	1.71
500 p.s.i.	0.235	1.78

These results show that the mean particle size increased as the air pressure at which the aerosol was formed was increased, the relationship between size and air pressure being approximately linear. The results are shown graphically

in fig.21.

(iii) Aerosols from the combustion of magnesium in CO_2.

Typical electron micrographs and the corresponding frequency histograms of the aerosols produced by the combustion of Mg in CO_2 at atmospheric pressure and 500 p.s.i. are given in figs.19 and 20. Most of the features of these aerosols were the same as those of the aerosols formed in air. Thus examination by electron diffraction indicated that the particles were composed of MgO (cubic, a = 4.213 A). The particle shape was again a cube or a sphere showing evidence of cube facets. The chain-like mode of aggregation was again observed, each individual chain tending to consist of particles of similar size, shape and orientation. The cumulative frequency curves for all the aerosols were found to plot as straight lines on probability graph paper, indicating that the size distributions were all Log-Normal.

One feature of the aerosols formed in CO_2 which differed from those formed in air was the effect of gas pressure on the particle shape. There appeared to be a tendency for the particle shape to become more spherical as the CO_2 pressure was increased. The aerosols formed at 500 p.s.i., fig.20, showed a higher percentage of the more spherical particles than the aerosols formed at atmospheric pressure, although perfect cubes were still present.

(a) The effect of CO_2 pressure on the mean particle size.

The mean particle sizes and standard deviation of the aerosols formed by the combustion of magnesium in CO_2 at atmospheric pressure, 300 p.s.i. and 500 p.s.i. are given in table 6.

Table 6. Mean particle sizes in aerosols formed by the combustion of Mg in CO_2.

CO_2 pressure	Mean particle diameter (μ)	Standard deviation
Atmospheric	0.036	1.486
300 p.s.i.	0.033	2.33
500 p.s.i.	0.054	1.869

The results show that the mean particle size increased in an approximately linear fashion as the gas pressure was increased, in a similar manner to the aerosols generated in air. However, a notable result was that the mean particle size of the MgO aerosol generated in CO_2 at any particular gas pressure was smaller than that of the aerosol generated in air at the same pressure. The rate of increase of particle size with pressure was also smaller in CO_2 than in air. The results for both air and CO_2 are shown graphically in fig.21 for comparison.

(iv) Summary of the results for aerosols formed by the combustion of magnesium in air and CO_2.

(a) Since the electrodes began to burn shortly after

the arc was struck, the aerosols may be regarded as having been produced almost entirely by the free combustion of Mg metal.

(b) The aerosol particles were found to consist of cubes or spheres of MgO (f.c. cubic, a = 4.213 A), each cube-shaped particle being a single crystal.

(c) The size distributions of all the aerosols were Log-Normal.

(d) The particle size increased with increasing gas pressure in an approximately linear manner.

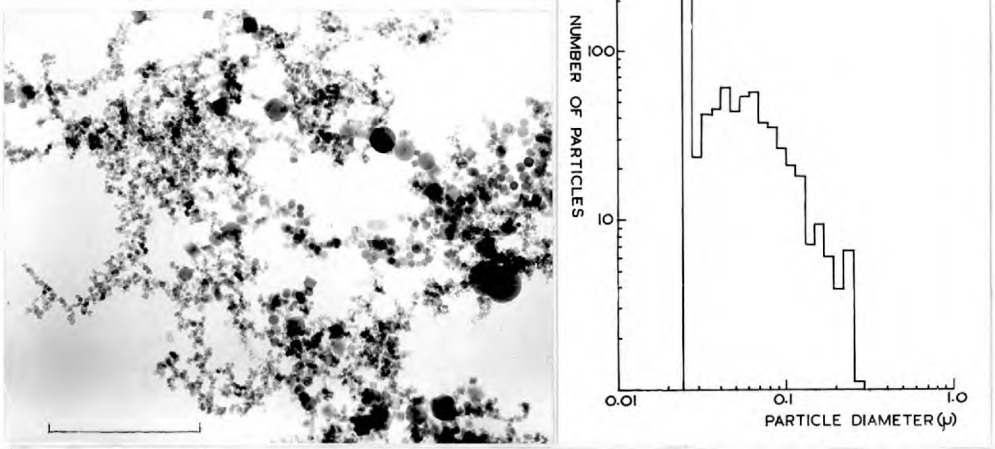

Fig. 14 Electron micrograph (X20,000, Scale = 1μ) and frequency histogram of the aerosol produced by the combustion of magnesium in air at atmospheric pressure.

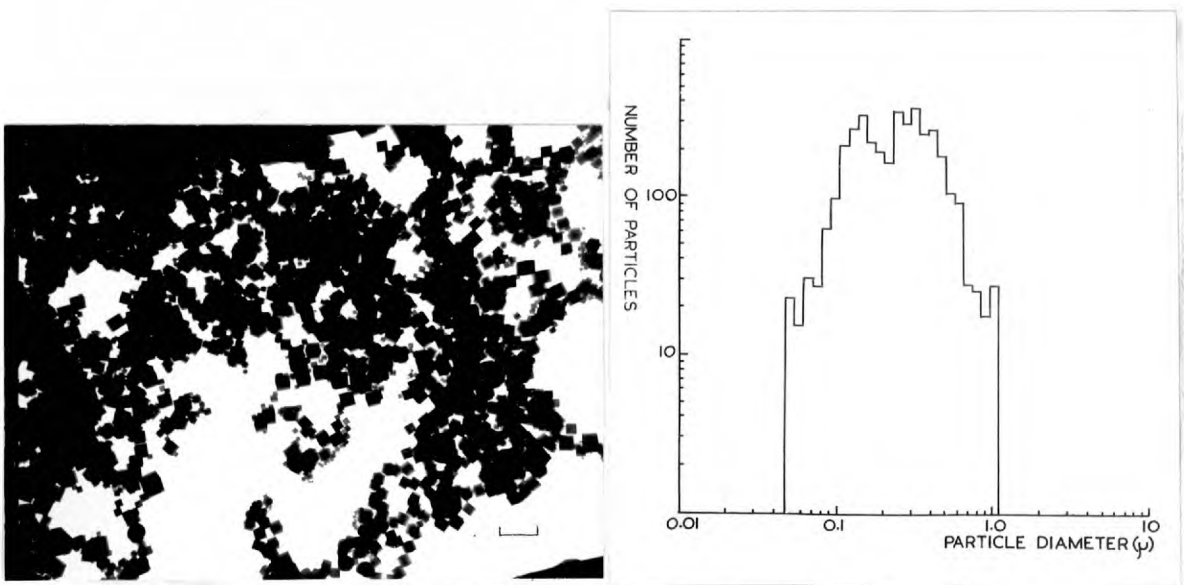

Fig. 15 Electron micrograph (X5,000, Scale = 1μ) and frequency histogram of the aerosol produced by the combustion of magnesium in air at 500 p.s.i.

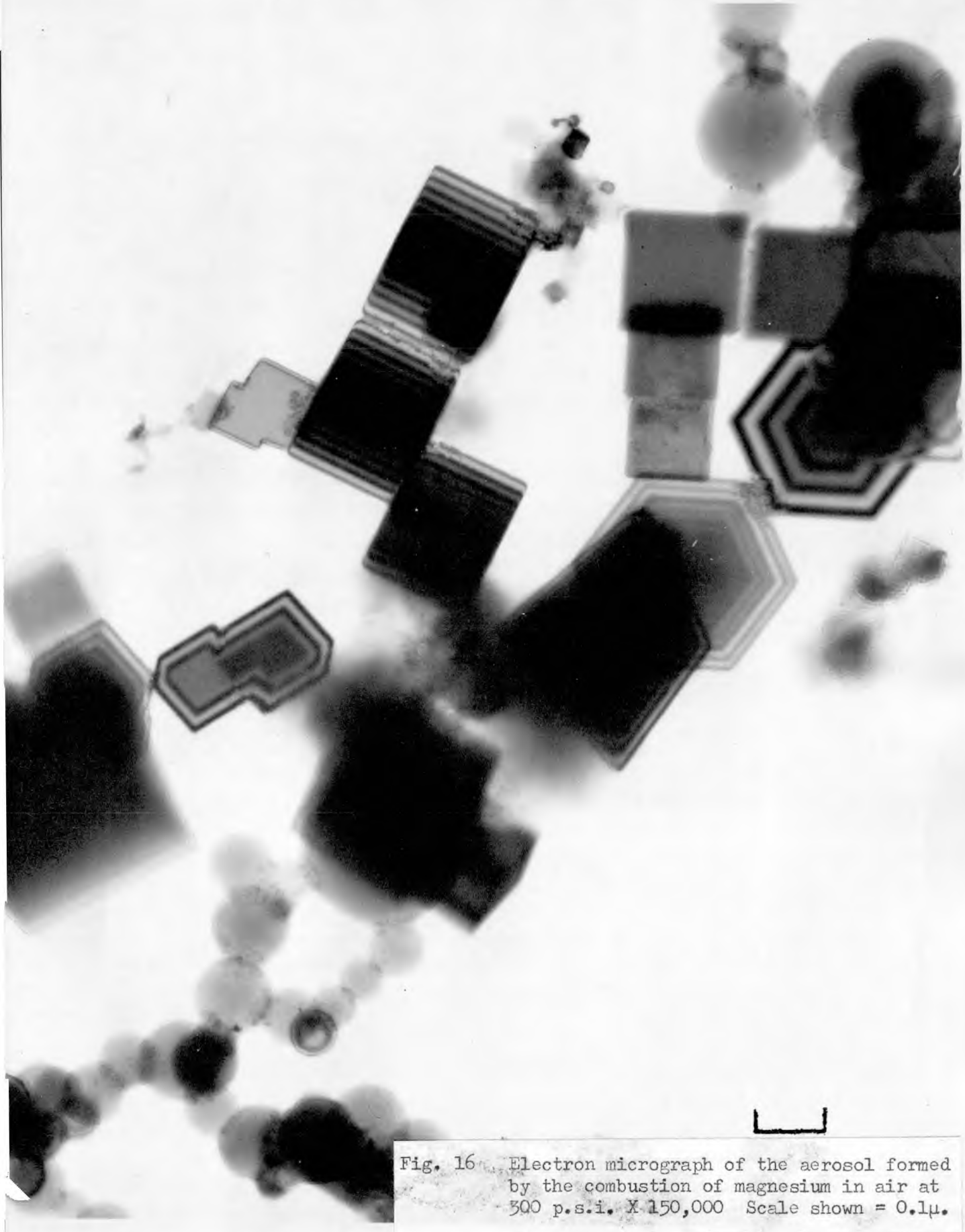

Fig. 16 Electron micrograph of the aerosol formed by the combustion of magnesium in air at 300 p.s.i. X 150,000 Scale shown = 0.1μ.

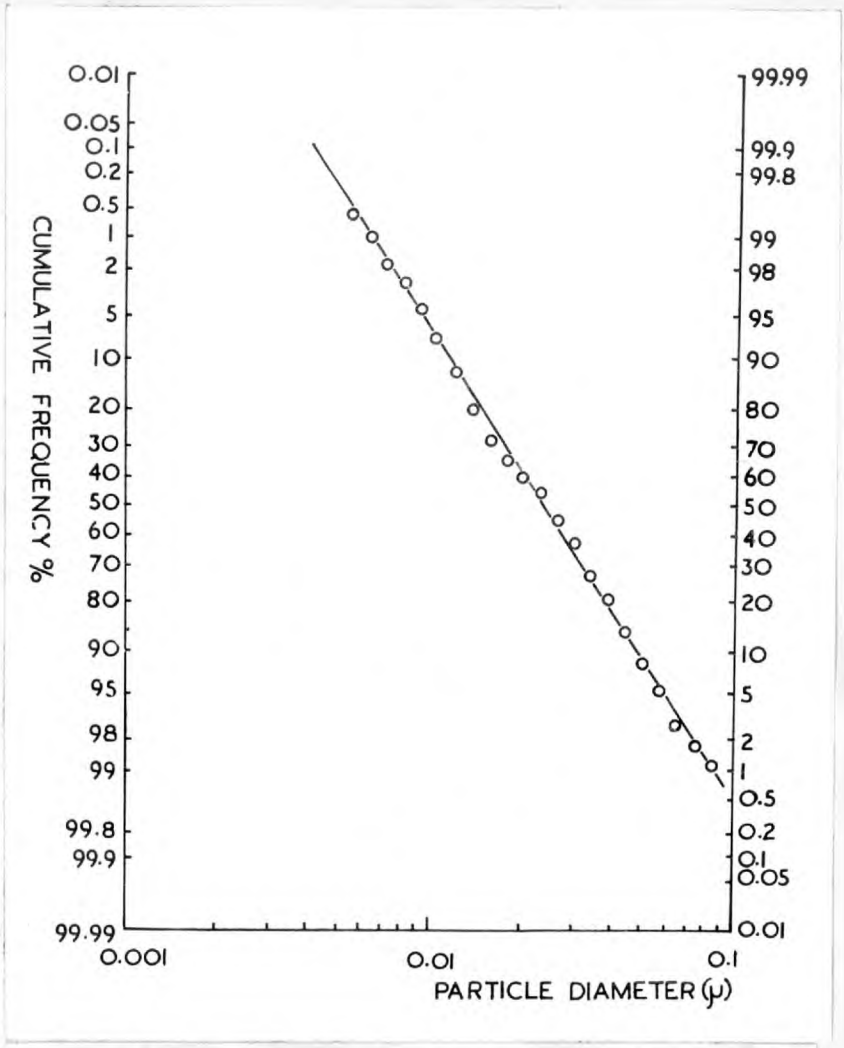

Fig. 17 Cumulative frequency curve for the MgO aerosol formed in air at 500 p.s.i.

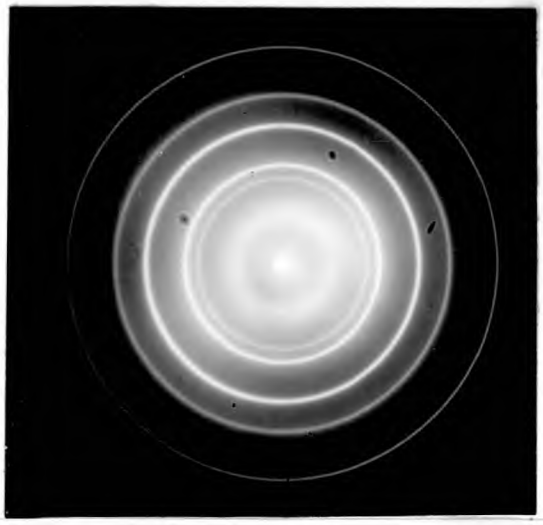

Fig. 18 Electron diffraction pattern from the aerosol formed by the combustion of magnesium in air at 500 p.s.i.

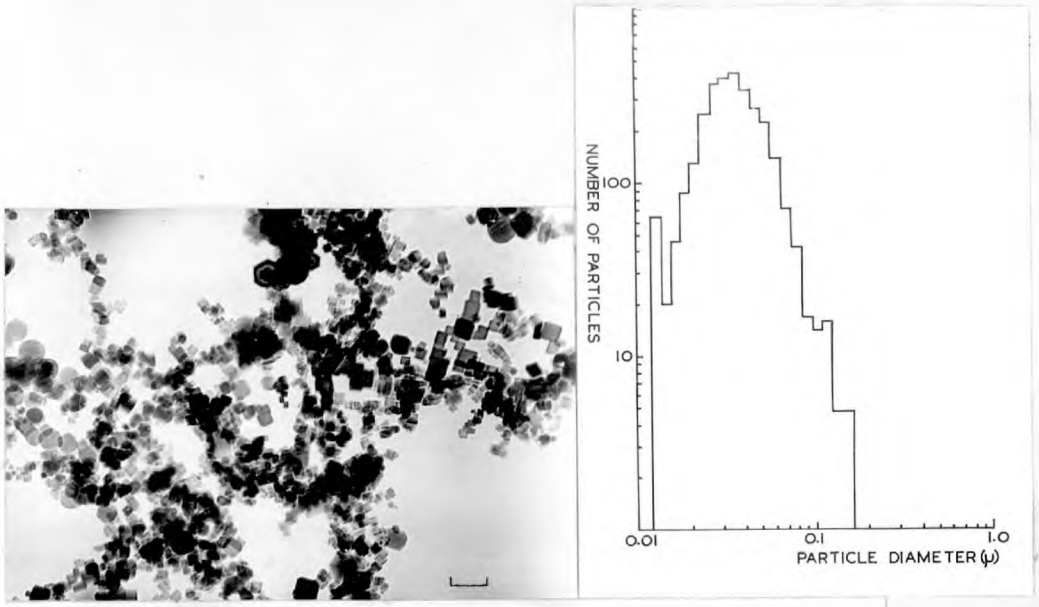

Fig. 19 Electron micrograph (X40,000 Scale = 0.1μ) and frequency histogram of the aerosol produced by the combustion of Mg in CO_2 at atmospheric pressure.

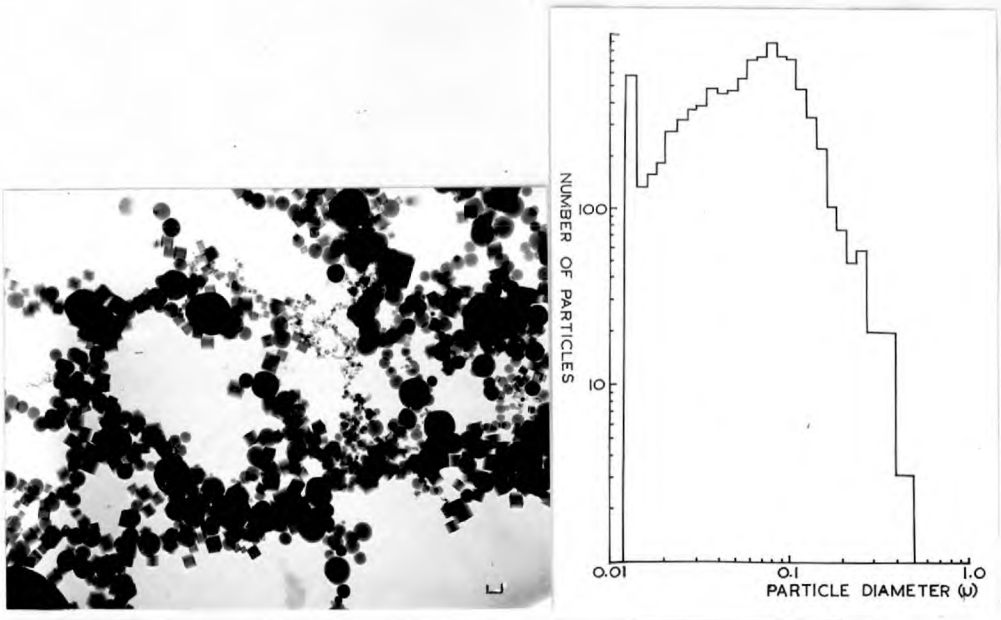

Fig. 20 Electron micrograph (X20,000 Scale = 0.1μ) and frequency histogram of the aerosol produced by the combustion of Mg in CO_2 at 500 p.s.i.

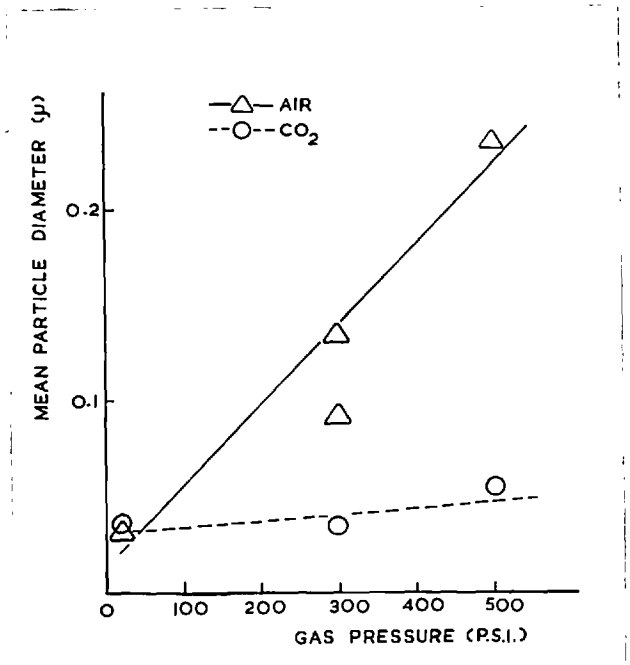

Fig. 21 Plot of mean particle size against gas pressure for MgO aerosols formed in air and CO_2.

3.1.2. Aerosols formed by the aluminium arc.

(i) General observations.

On occasion it was difficult to maintain an arc between aluminium electrodes, particularly at high gas pressures. This was due to the extremely rapid oxidation which took place on the electrode surfaces; a thick layer of oxide tended to be built up between the electrodes, insulating them from each other. Alternatively, the electrodes melted, causing the arc to be broken. Where such difficulties were encountered, repeated attempts were made until a successful arc was obtained.

After arcing a substantial layer of white oxide was found to be present on the aluminium electrodes, but in CO_2 only very small quantities of smoke were generated.

The particles in the aerosols formed in air and CO_2 at atmospheric pressure were extremely small, and contaminated rapidly in the electron microscope. It was found necessary to focus the image and expose the photographic plate in less than about 10 seconds to obtain successful micrographs.

(ii) Aerosols formed from the aluminium arc in air.

(a) The composition and crystal structure of the aerosols.

Electron diffraction patterns were obtained from the aerosols produced by the Al arc in air and in CO_2 at atmospheric pressure, 300 p.s.i., and 500 p.s.i. In all cases the pattern was due mainly to crystalline γ - Al_2O_3 (cubic, a = 15.790 A). However, several of the patterns

showed rings due to high-index planes which could not be readily identified as belonging to any of the forms of Al_2O_3. The results confirm those of Harvey, Matthews and Wilman (1960), who found that the aerosols from an Al arc in air at atmospheric pressure consisted of γ - Al_2O_3. Walmsley (1929) had previously suggested, from X-ray diffraction results, that the Al arc aerosols probably consisted mainly of β - Al_2O_3, with possibly a small quantity of γ - Al_2O_3.

It is of interest to note that γ - Al_2O_3 is the low-temperature form of alumina. The γ form (spinel) is stable up to about 1200°C. Above these temperatures, transformation to the high-temperature form α - Al_2O_3 (corundum) takes place, the change being irreversible. (Runck, 1956).

(b) The particle shape.

Typical electron micrographs, with the corresponding frequency histograms, for the aerosols formed from the Al arc in air at atmospheric pressure and 500 p.s.i. are given in figs.22 and 23. For all the aerosols, throughout the range of gas pressures, the individual particles were found to be almost perfect spheres. When examined at high magnification of the order of X100,000, some surface roughness was evident on the particles, but there was no suggestion of any regular polyhedral facet development.

The aggregation of particles into chains was again observed, as was the tendency for particles in any particular chain to be of similar size.

No wedge fringes were observed to be produced by any of the Al_2O_3 aerosol particles, no matter what their size. Harvey, Matthews and Wilman (1960) found that the particle size estimated from electron micrographs and the size estimated from line broadening in electron diffraction patterns were of the same order for an Al_2O_3 aerosol produced by an Al arc in air at atmospheric pressure. From these data they concluded that the spherical Al_2O_3 particles were probably single crystals. The occurrence of this spherical shape is of interest, and will be discussed further in section 4.

(c) The particle size distributions.

Frequency histograms for aerosols formed from the aluminium arc in air at atmospheric pressure and 500 p.s.i. are shown in figs.22 and 23. The particle sizes in all the aerosols formed from the Al arc, throughout the range of gas pressures studied, were found to follow the Log Normal distribution. Fig.24 shows the typical straight line plot obtained on probability graph paper for the aerosols obtained from the Al arc in air at atmospheric pressure. The tailing-off of the curve at high values of the particle diameter is due to misclassification in the size analysis, which may be expected at the ends of the size spectrum.

(d) The effect of air pressure on particle size.

The mean particle sizes and standard deviations of the aerosols formed from the Al arc in air are given in Table 7.

Table 7. Mean particle sizes in aerosols formed from the Al arc in air.

Air pressure	Mean particle diameter (μ)	Standard deviation
Atmospheric	0.029	1.71
300 p.s.i.	0.092	1.52
500 p.s.i.	0.160	1.59

The mean particle size was found to increase with increase in air pressure, in a similar manner to the MgO aerosols. The relationship between particle size and gas pressure again appeared to be approximately linear, see fig.29.

Change in the gas pressure was found to have no effect on the individual particle shape or on the manner in which the particles were aggregated together.

(iii) Aerosols formed from the aluminium arc in CO_2.

(a) The particle shape, structure and size distributions.

Typical electron micrographs and the corresponding frequency histograms for the aerosols produced by the Al arc in CO_2 are shown in figs.25 and 26. Again, most of the features of these aerosols were found to be similar to those of the Al-arc aerosols formed in air. Investigation by electron diffraction indicated that the aerosols formed in CO_2 at atmospheric pressure, 300 p.s.i. and 500 p.s.i. were composed mainly of γ - Al_2O_3, (cubic, a = 15.790 A). The

Table 8. Electron diffraction data from the aerosol formed by the aluminium arc in CO_2 at atmospheric pressure, corresponding to γ - Al_2O_3, cubic, a = 15.79 A.

Observed rings (cf. fig. 27)			γ-Al_2O_3 cubic ASTM card 3-0914		
Intensity*	Radius (cm)	d(A)≠	d(A)	I/I_1	hkl
			5.59	40	220
			4.59	20	222
			3.24	30	422
M	0.7924	2.81	2.80	50	440
			2.65	8	600
			2.50	8	620
VS	0.9325	2.39	2.38	100	622
F	0.9735	2.29	2.28	30	444
			2.20	5	711
			2.12	5	642
VS	1.1402	1.955	1.98	70	800
			1.92	1	
			1.87	8	660
			1.73	20	842
			1.69	3	664
			1.65	1	
			1.61	40	844
			1.58	1	
			1.55	10	862
M	1.4988	1.485	1.52	60	666
			1.47	20	864
			1.44	20	
VS	1.6420	1.370	1.40	100	880
F	1.9376	1.150			
MF	2.0178	1.105			
VF	2.2514	1.036			
MF	2.3625	0.943			
VVF	2.5642	0.868			
M	2.6438	0.843			

* S = strong, M = medium, F = faint, V = very.

≠ Relative to graphite d_{110} = 1.23 A.

electron diffraction pattern obtained from the aerosol produced in CO_2 at atmospheric pressure is shown in fig.27. The ring radii and net-plane spacings are compared with ASTM data for γ - Al_2O_3 in Table 8.

The individual particles were found to be almost perfect spheres, with no evidence of any facet formation. Fig.28 shows a X280,000 enlargement of the aerosol produced from the Al arc in CO_2 at atmospheric pressure. Even at this high magnification there is no suggestion of any regular polyhedral facet development, although slight irregular surface asperities are evident.

The aggregation of particles into chains was observed at all the CO_2 pressures investigated, as was the tendency for particles in a particular chain to be of a similar size. The particle sizes of all the aerosols were found to follow the Log-Normal distribution.

(b) The effect of CO_2 pressure on particle size.

The mean particle sizes and standard deviations for the aerosols formed from the Al arc in CO_2 at atmospheric pressure, 300 p.s.i. and 500 p.s.i. are given in Table 9.

Table 9. Mean particle sizes of aerosols from Al arc in CO_2.

CO_2 pressure	Mean particle diameter (μ)	Standard deviation
	0.027	1.48
Atmospheric	0.021	1.52
	0.024	1.31
300 p.s.i.	0.044	1.64
500 p.s.i.	0.114	1.61

The mean particle size increased approximately linearly with increase in the CO_2 pressure, as in air. At any particular pressure the mean particle size of the aerosol formed in CO_2 was smaller than that formed in air, this difference becoming greater at higher gas pressures. Thus the curve of particle size against gas pressure showed a smaller slope for CO_2 than for air. The curves for air and CO_2 are shown in fig.29.

(iv) Summary of the results for aerosols formed from the aluminium arc in air and CO_2.

(a) The aerosol particles were found to consist of γ - Al_2O_3, (cubic, a = 15.790 A).

(b) No effect of gas pressure on particle shape was observed, the particles being almost perfect spheres.

(c) The size distributions of all the aerosols were Log-Normal.

(d) The mean particle size increased with increasing gas pressure, in an approximately linear manner. This effect was greater in air than in CO_2.

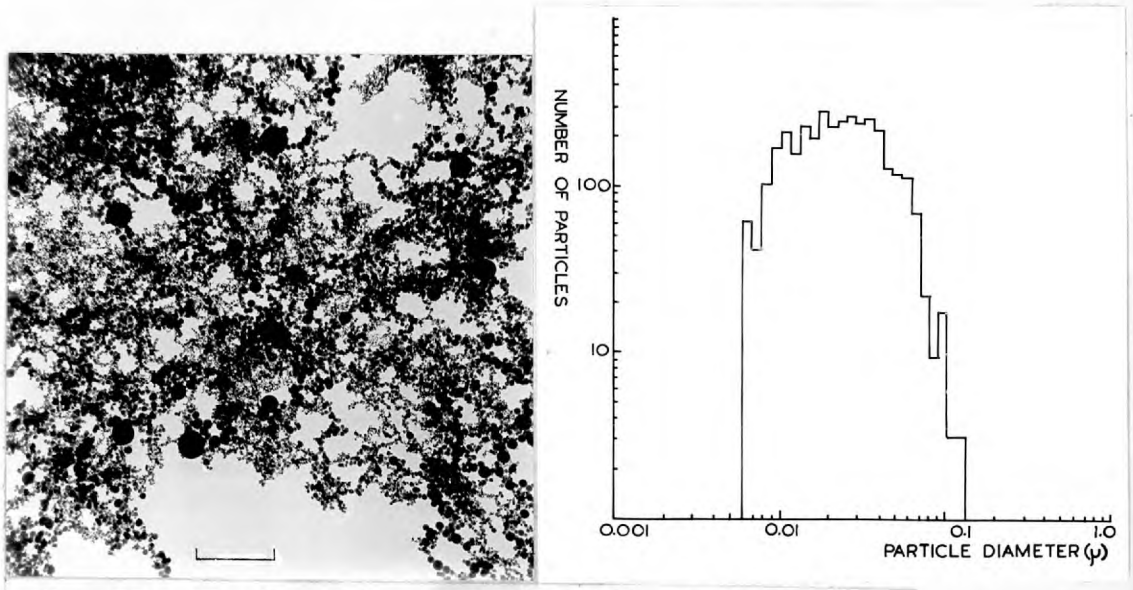

Fig. 22 Electron micrograph (X10,000 Scale = 1μ) and frequency histogram of the aerosol formed by the Al arc in air at atmospheric pressure.

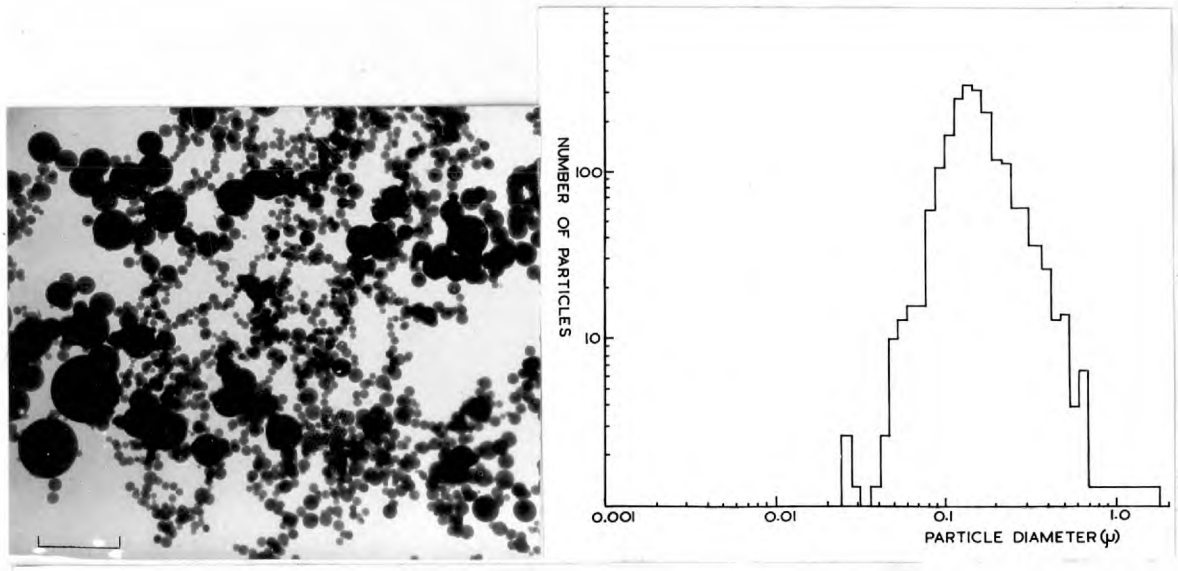

Fig. 23 Electron micrograph (X10,000 Scale = 1μ) and frequency histogram of the aerosol formed by the Al arc in air at 500 p.s.i.

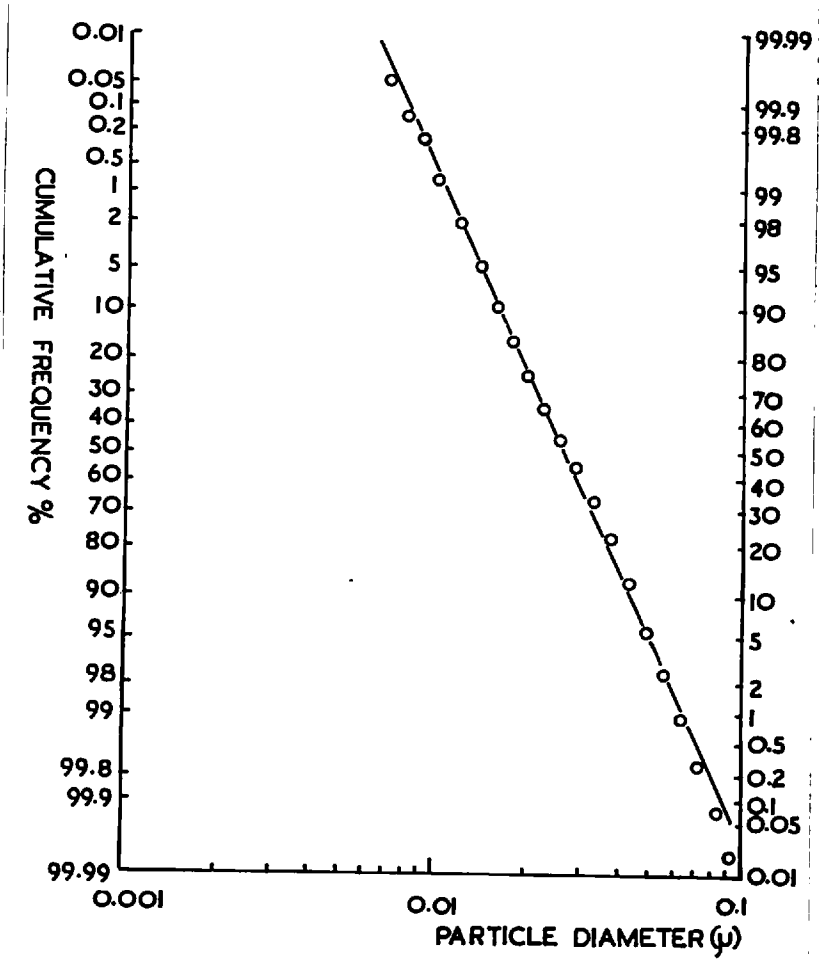

Fig. 24 Cumulative frequency curve for the Al_2O_3 aerosol formed in air at atmospheric pressure.

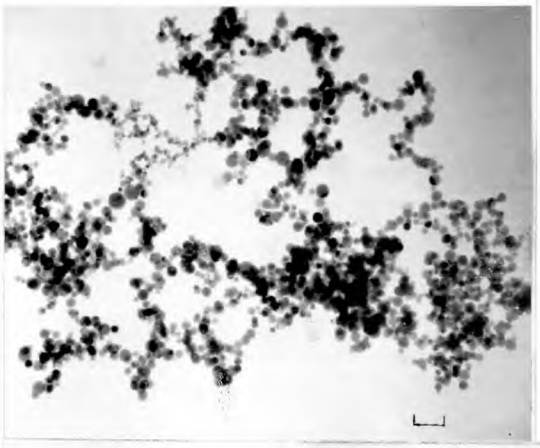

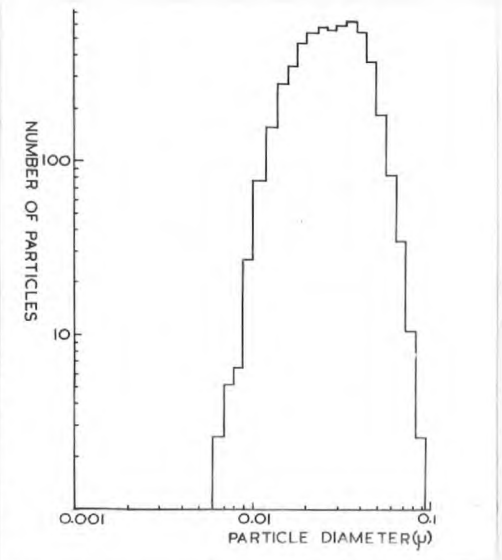

Fig. 25 Electron micrograph (X40,000 Scale = 0.1μ) and frequency histogram of the aerosol formed by the Al arc in CO_2 at atmospheric pressure.

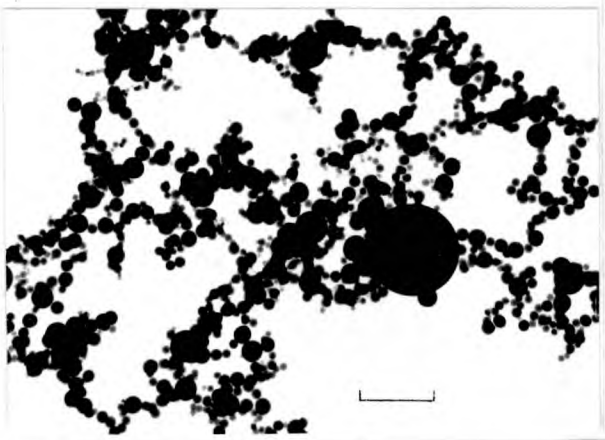

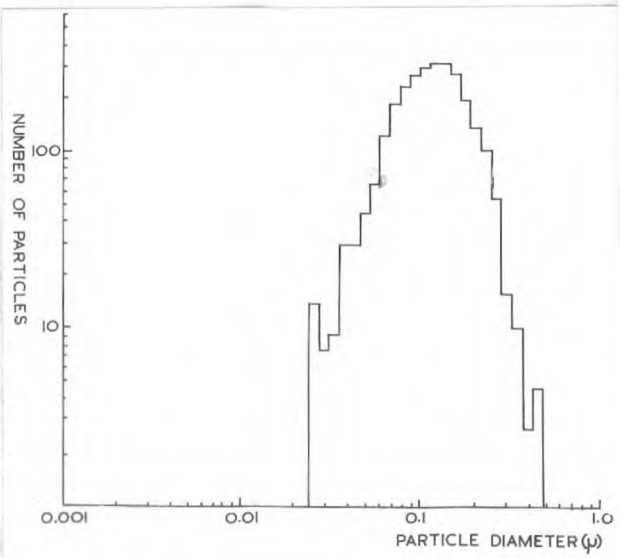

Fig. 26 Electron micrograph (X10,000 Scale = 1μ) and frequency histogram of the aerosol formed by the Al arc in CO_2 at 500 p.s.i.

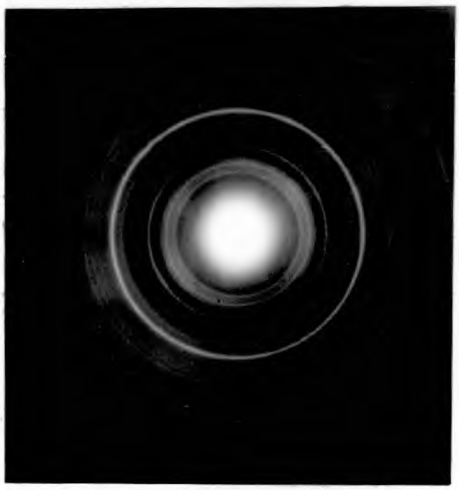

Fig. 27 Electron diffraction pattern from the aerosol formed by the Al arc in CO_2 at atmospheric pressure.

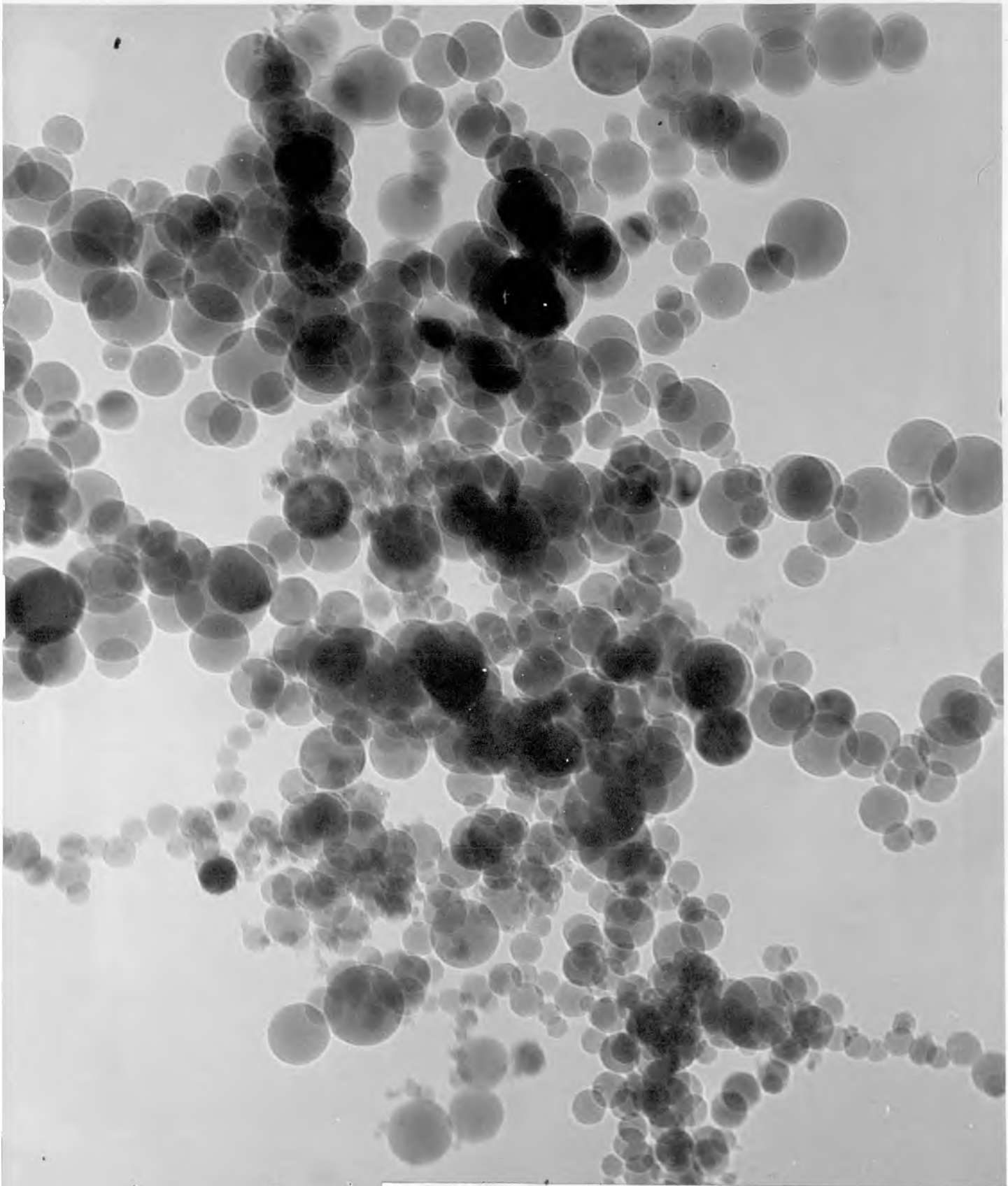

Fig. 28. Electron micrograph of the aerosol formed by the Al arc in air at atmospheric pressure (X280,000 Scale = 0.1μ).

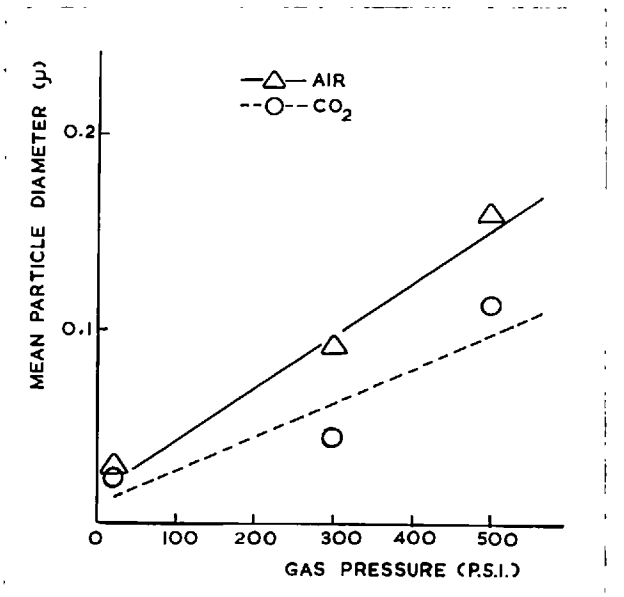

Fig. 29 Plot of mean particle size against gas pressure for Al_2O_3 aerosols formed in air and CO_2.

3.1.3. Aerosols formed from the magnox arc.

(i) General observations.

When an arc between magnox electrodes was struck in air, the electrodes began to burn after a short time of arcing, as had occurred previously with the magnesium electrodes. Dense clouds of white oxide smoke were produced. However, in CO_2 the electrodes did not ignite, and a normal arc could be maintained, in contrast to the case of magnesium electrodes in CO_2. Only very small quantities of smoke were produced by the magnox arc in CO_2 at atmospheric pressure, but larger quantities were obtained at higher pressures.

(ii) Aerosols formed by the combustion of magnox in air.

(a) The composition and crystal structure of the particles.

The aerosols produced by the combustion of magnox at air pressures from atmospheric to 500 p.s.i. were found to be composed of crystalline MgO (cubic, a = 4.213 A). This was not unexpected, in view of the composition of magnox (Mg 99.1 - 99.3%, Al 0.7 - 0.9%). It was thought that there was a possibility that some traces of Al_2O_3 or the spinel $MgO.Al_2O_3$ might be present. However, in any of the large number of diffraction patterns obtained there were no rings which were not accounted for as due to MgO. The diffraction pattern from the aerosol produced by the combustion of magnox in air at 500 p.s.i. is shown in fig.33. The ring radii and net-plane spacings are compared with the ASTM data for MgO

(periclase) in Table 10.

Table 10. Electron diffraction data from aerosol formed by the combustion of magnox in air at 500 p.s.i., corresponding to MgO, periclase, a = 4.213 A.

Observed rings (cf.fig.35)			MgO periclase ASTM card 4-0829		
Intensity*	Radius (cm)	d (A)+	d (A)	I/I	hkl
M	1.133	2.370	2.431	10	111
VS	1.302	2.062	2.106	100	200
S	1.818	1.475	1.489	52	220
			1.270	4	311
MS	2.220	1.215	1.216	12	222
F	2.563	1.047	1.053	5	400
			0.967	2	331
M	2.856	0.942	0.942	17	420
M	3.123	0.858	0.860	15	422
VVF	3.314	0.807	0.811	3	511
F	3.606	0.743			
M	3.821	0.702			
F	4.026	0.667			

*S = strong, M = medium, F = faint, V = very

+Relative to graphite d_{110} = 1.230 A.

(b) The particle shape.

Typical electron micrographs and the corresponding frequency histograms, for the aerosols produced by the combustion of magnox in air at atmospheric pressure and 500 p.s.i. are shown in figs.30 and 31. It was found that the majority of the particles in the aerosols formed at atmospheric pressure were perfect cubes of MgO. A small percentage of the particles were more spherical in shape. Examination of these more spherical particles under high magnification in the electron microscope showed that most of them showed slight development of cube facets; the spherical appearance could be due to the presence of high index facets which would round off the cube corners. The cube shape, together with the appearance of wedge fringes in the images of many of the particles indicated that they were single crystals. The aggregation of particles into chains was again observed. The particles in a particular chain tended to be of similar size and, as with the aerosols from the combustion of magnesium, neighbouring particles tended to be in the same orientation. This kind of parallel orientation is strikingly evident in fig.32, an enlarged micrograph of the aerosols from the combustion of magnox in air at 300 p.s.i.

As the gas pressure at which the aerosols were formed was increased, it was found that the percentage of the more spherical particles increased, until at 500 p.s.i. there were very few perfect cubes, fig.31. Examination at

high magnification in the electron microscope again revealed that most of the apparently spherical particles showed very slight development of cube facets. Many of these faceted spheres in the aerosols produced at 300 and 500 p.s.i. showed wedge fringes, indicating that they were single crystals, as were the perfect cubes.

Since this tendency towards a more spherical particle shape with increasing gas pressure was not nearly so evident in the aerosols formed by the combustion of magnesium, its occurrence in the magnox aerosols may be due to the Al content (0.7 - 0.9%) of the alloy.

(c) The particle size distributions.

The frequency histograms for the aerosols formed by the combustion of magnox in air at atmospheric pressure and 500 p.s.i. are shown in figs.30 and 31. The increase in mean particle size with increasing gas pressure is clearly evident in the histograms. The peak at the smallest particle diameter in fig.31 is due to this being the lower limit of the particle size analyser in this particular case.

A probability plot of the cumulative frequency against particle diameter for the aerosol formed in air at 300 p.s.i. is shown in fig.34; the straight line indicates a Log-Normal distribution. Misclassification during the size analysis again accounts for the divergence from a straight line at high particle diameters. The particle sizes in all the aerosols formed by the combustion of magnox in air were

found to follow the Log-Normal distribution.

(d) The effect of air pressure on the particle size.

The mean particle sizes and standard deviations of the aerosols formed by the combustion of magnox in air are given in Table 11.

Table 11. Mean particle sizes in aerosols formed by the combustion of magnox in air.

Air pressure	Mean particle diameter (μ)	Standard deviation
Atmospheric	0.046	1.62
300 p.s.i.	0.086	1.37
	0.101	1.66
500 p.s.i.	0.150	1.47
	0.190	1.41

These results show that the mean particle size increased approximately linearly with increase in air pressure, as was found previously with other materials. The results are shown graphically in fig.37.

(iii) Aerosols from the magnox arc in CO_2.

(a) The particle shape, structure and size distribution.

As with the previous aerosols investigated, the aerosols formed from the magnox arc in CO_2 were found to be similar in most features to those formed in air, even

though the mode of generation was different from those formed in air. (The electrodes did not ignite in CO_2, as has been stated earlier). The particles were found to be composed of MgO (cubic, a = 4.213 A). The same effect of gas pressure on particle shape was observed: mostly perfect cubes at atmospheric pressure and almost entirely slightly faceted spheres at 500 p.s.i. Cumulative frequency curves plotted on probability graph paper showed that all the aerosols followed the Log-Normal distribution of particle size.

Electron micrographs of the aerosols formed from the magnox are in CO_2 at atmospheric pressure and 500 p.s.i. are shown in figs.35 and 36.

(b) The effect of CO_2 pressure on the particle size.

The mean particle sizes and standard deviations of the aerosols formed from the magnox arc in CO_2 at atmospheric pressure, 300 p.s.i. and 500 p.s.i. are given in Table 12.

Table 12. Mean particle sizes in aerosols formed from the magnox arc in CO_2.

CO_2 pressure	Mean particle diameter (μ)	Standard deviation
Atmospheric	0.018	1.61
300 p.s.i.	0.082	1.45
500 p.s.i.	0.093	1.60

Again, the mean particle size was found to increase linearly with increase in gas pressure, as was found in air. This can also be seen from the histograms of particle size for the aerosols formed in CO_2 at atmospheric pressure and 500 p.s.i., illustrated in figs.35 and 36.

As for the previous materials investigated, the particle size of the aerosol formed in CO_2 at any particular pressure was smaller than that of the aerosols formed in air at the same pressure, and the slope of the particle size/pressure graph was smaller for CO_2 than for air. The two curves for CO_2 and air are shown in fig.37.

(iv) Summary of the results for aerosols formed by the combustion of magnox in air, and from the magnox arc in CO_2.

(a) The aerosols were found to consist of MgO (cubic, a = 4.213 A).

(b) The particle shape of the aerosols formed in both air and CO_2 was found to become more spherical as the gas pressure at which they were formed was increased.

(c) The size distributions of all the aerosols were Log-Normal.

(d) The mean particle size increased with increasing gas pressure, in an approximately linear manner. The effect was greater in air than in CO_2.

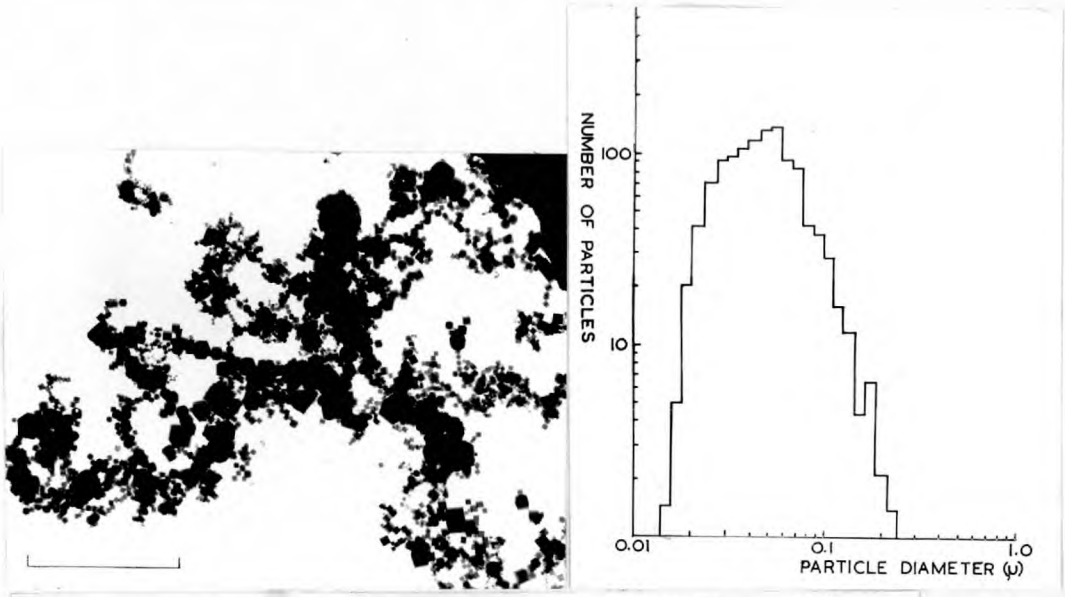

Fig. 30 Electron micrograph (X20,000 Scale = 1μ) and frequency histogram of the aerosol formed by the combustion of magnox in air at atmospheric pressure.

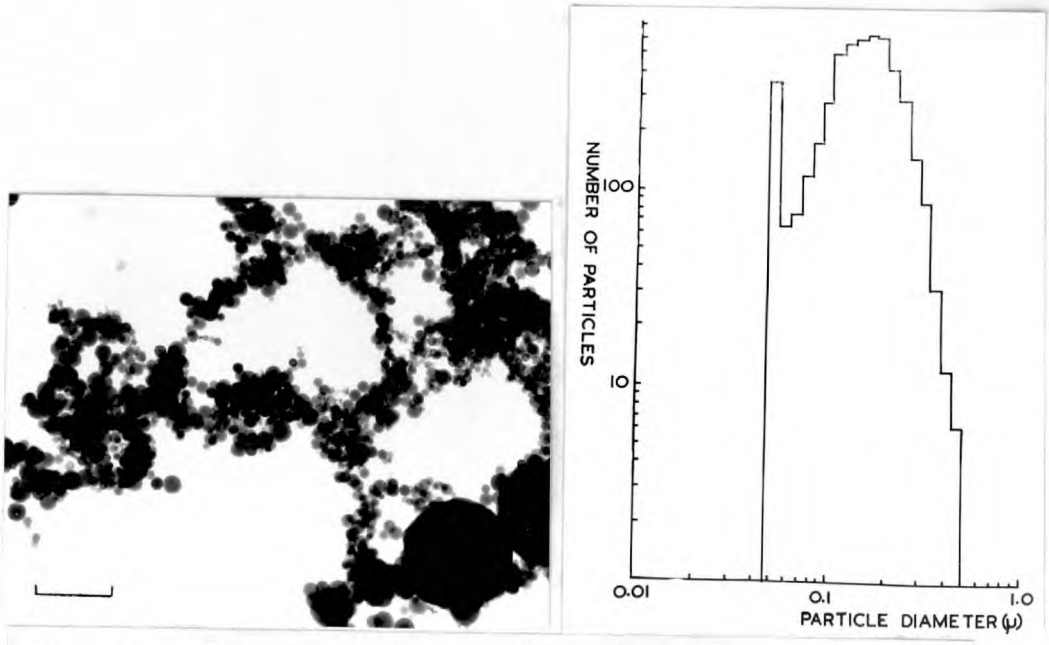

Fig. 31 Electron micrograph (X10,000 Scale = 1μ) and frequency histogram of the aerosol formed by the combustion of magnox in air at 500 p.s.i.

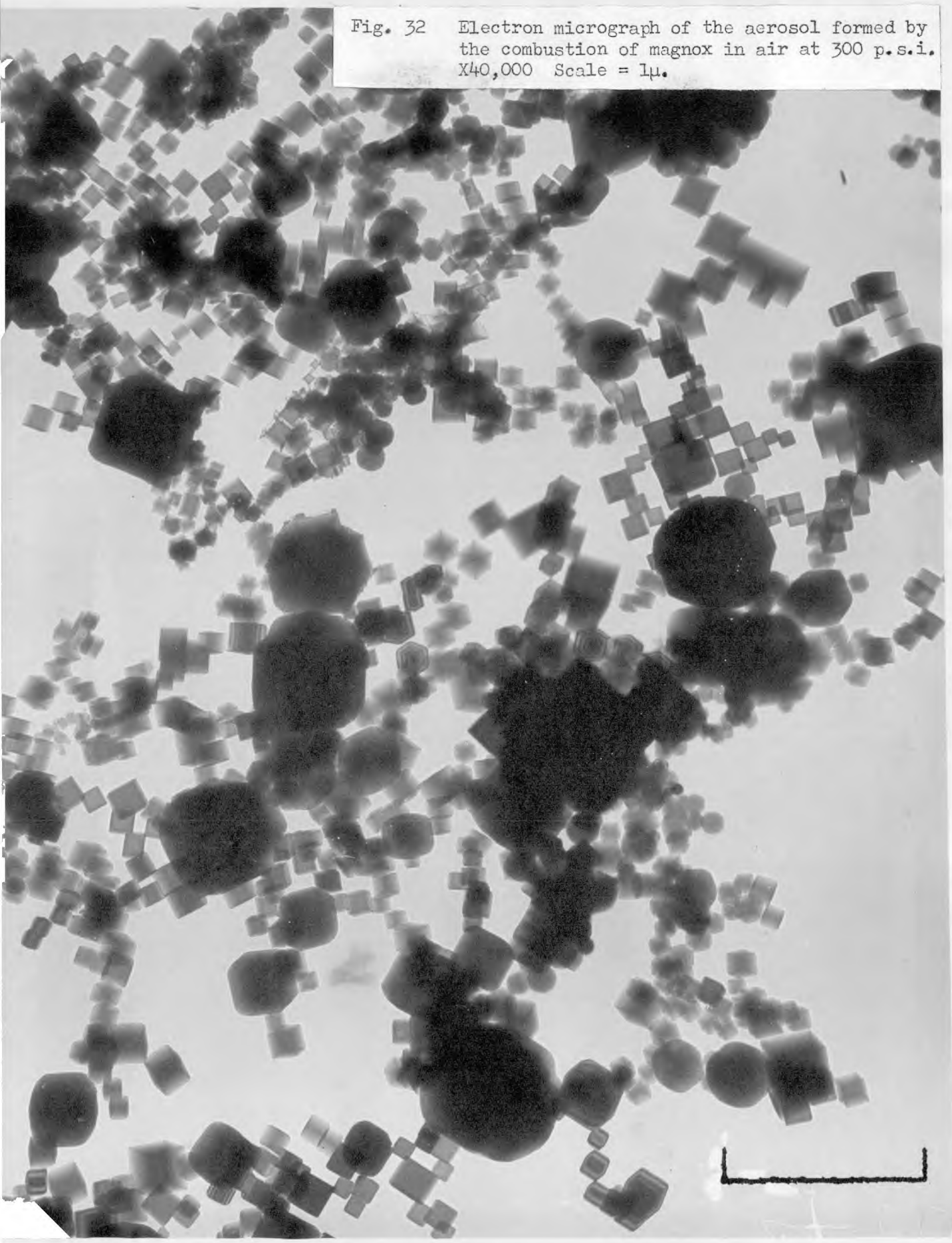

Fig. 32 Electron micrograph of the aerosol formed by the combustion of magnox in air at 300 p.s.i. X40,000 Scale = 1μ.

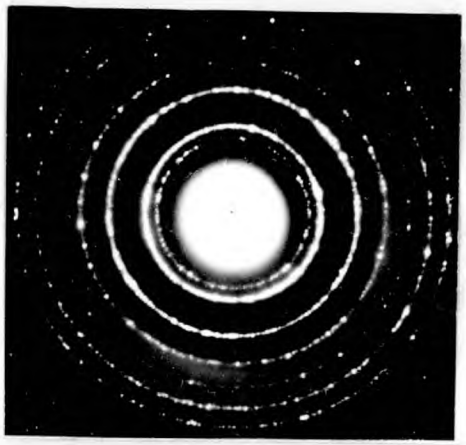

Fig. 33 Electron diffraction pattern from the aerosol formed by the combustion of magnox in air at 500 p.s.i.

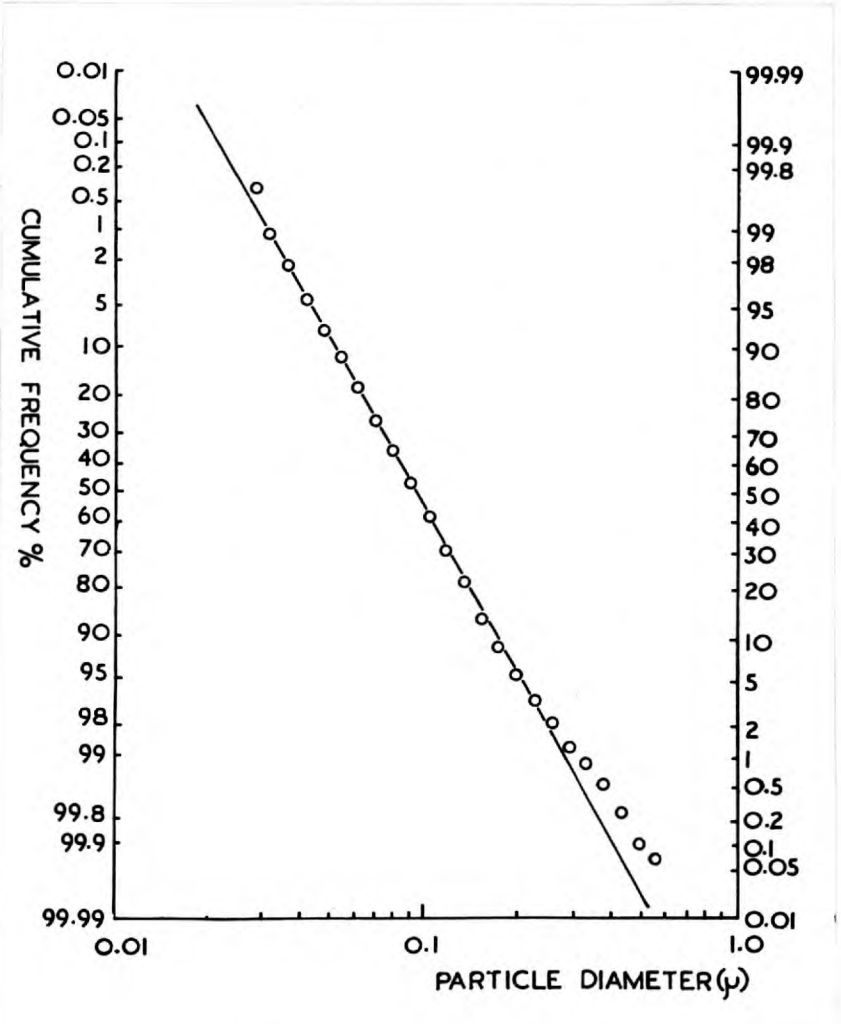

Fig. 34 Cumulative frequency curve for the aerosol formed by the combustion of magnox in air at 300 p.s.i.

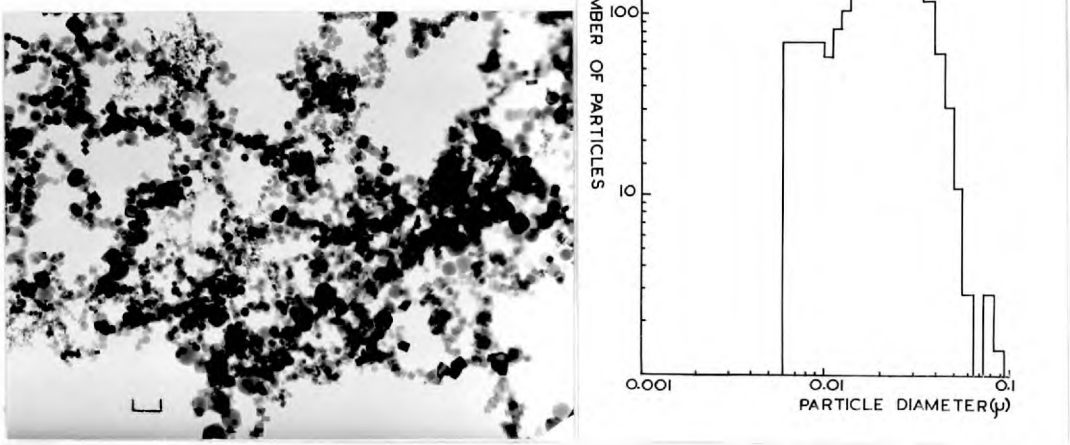

Fig. 35 Electron micrograph (X40,000 Scale 0.1μ) and frequency histogram of the aerosol formed by the magnox arc in CO_2 at atmospheric pressure.

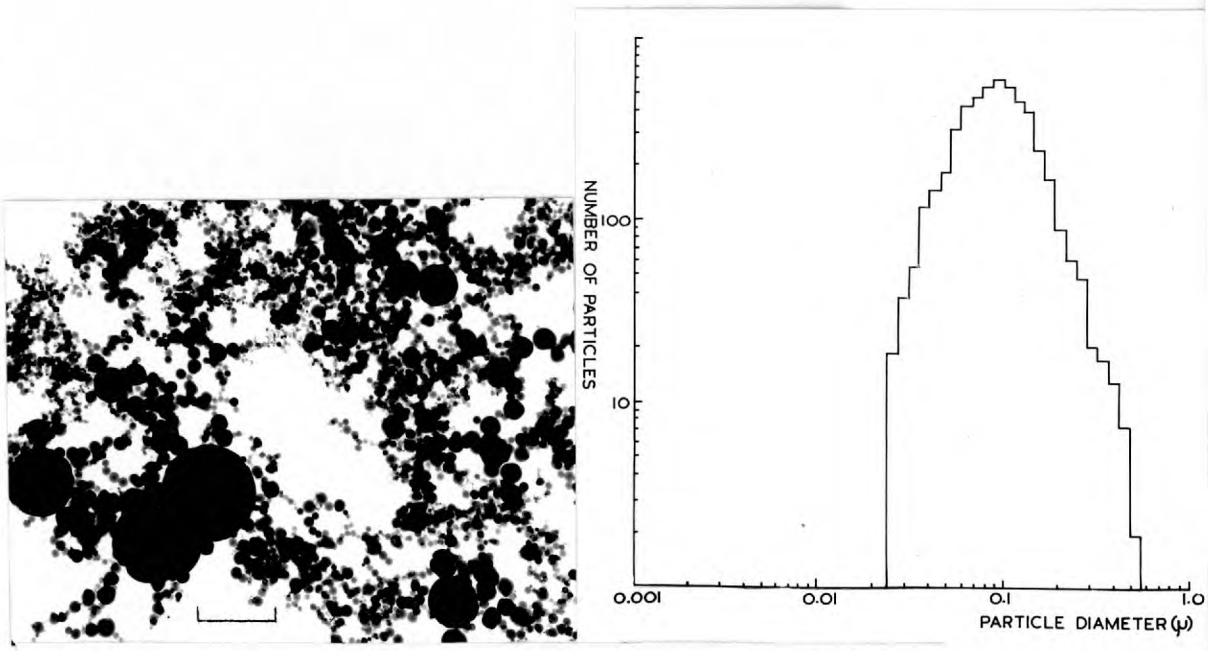

Fig. 36 Electron micrograph (X10,000 Scale = 1μ) and frequency histogram of the aerosol formed by the magnox arc in CO_2 at 500 p.s.i.

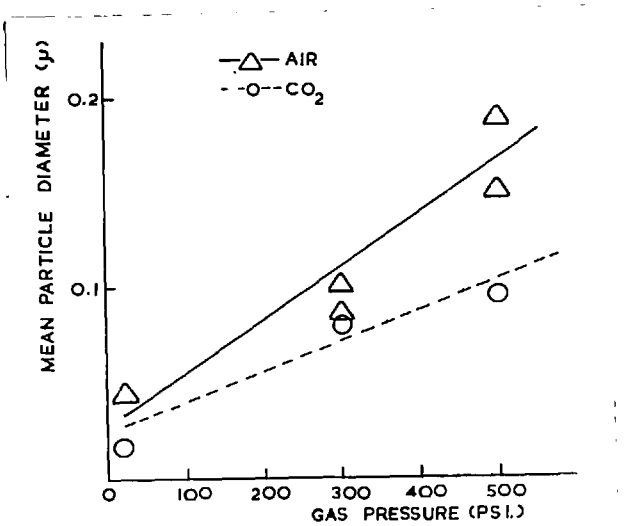

Fig. 37 Plot of mean particle size against gas pressure for the aerosols formed from the magnox arc in air and CO_2.

3.1.4. Aerosols from the stainless steel arc.

(i) General Observations.

The arc between stainless steel electrodes burnt strongly in both air and CO_2 at all the gas pressures investigated. Some sputtering of metal from the arc occurred. The smoke deposits formed were red-brown in colour.

The particles in the aerosols formed at atmospheric pressure were again very small, and some difficulty was experienced due to contamination in the electron microscope. (The relative effect of contamination on the measured particle size becomes more serious as the radius of curvature of the particle decreases).

It was found that in CO_2 at atmospheric pressure only very small quantities of smoke were produced, and after arcing there was much less oxide on the electrode surfaces than at higher pressures in CO_2 and in air.

(ii) Aerosols from the stainless steel arc in air.

(a) The composition and crystal structure of the aerosols.

The stainless steel used for the arc electrodes had the composition Fe 74%, Cr 18%, Ni 8%. It is well known that the oxidation of steel gives rise to double oxides having in many cases the spinel structure (f.c. cubic). In the present case electron diffraction patterns corresponding to a spinel were obtained from the stainless steel arc aerosols generated in air at pressures from atmospheric to

Table 13. Electron diffraction data from the aerosol formed by the stainless steel arc in air at atmospheric pressure, corresponding to $NiO.Fe_2O_3$ cubic, a = 8.339.

Observed rings (cf. fig.42)			$NiO.Fe_2O_3$ cubic ASTM card 10-325		
Intensity*	Radius(cm)≠	d(A)	d(A)	I/I_1	hkl
M	0.5039	4.772	4.82	20	111
S	0.8147	2.952	2.948	30	220
VS	0.9570	2.512	2.513	100	311
			2.408	7	222
S	1.1509	2.089	2.085	25	400
			1.9125	3	331
MF	1.4164	1.700	1.7025	7	222
M	1.5040	1.599	1.6051	30	511
S	1.6377	1.468	1.4760	40	440
			1.4100	1	531
VF	1.8266	1.316	1.3187	5	620
VF	1.9004	1.266	1.2706	9	533
			1.2573	3	622
			1.2306	5	444
M	2.0906	1.153	1.1676	1	711
F	2.1693	1.115	1.1145	5	642
			1.0857	15	731
			1.0424	5	800

* S = strong, M = medium, F = faint, V = very.

≠ Relative to graphite d_{110} = 1.23 A.

500 p.s.i. The diffraction pattern obtained from the aerosol formed in air at atmospheric pressure is shown in fig.42, and the ring radii and net plane spacings are given in Table 13.

Calibration of the electron diffraction patterns with graphite (d_{110} = 1.230 A) gave a=8.335 $\pm$ 0.007 A for the aerosol material. There were four possible compounds which could have been produced by the oxidation of the steel. These were Fe_3O_4 (a = 8.374 A), $NiO.Cr_2O_3$ (a = 8.299 A), $NiO.Fe_2O_3$ (a = 8.340), and $FeO.Cr_2O_3$ (a = 8.344 A). All these compounds have the spinel structure, have very similar a-values, and give rise to almost identical diffraction patterns. On the basis of the measured a-value, $NiO.Fe_2O_3$ and $FeO.Cr_2O_3$ appeared to be the more probable of the alternatives. The ring intensities were then compared; the faint ring at d = 1.91 A agreed with the X-ray data for $NiO.Fe_2O_3$, but not with $FeO.Cr_2O_3$, which has a strong ring in this position. Thus $NiO.Fe_2O_3$ (nickel ferrite) was taken as being the most likely composition of the aerosols. However, the possibility of one or all of the other oxides being present cannot be entirely ruled out.

(b) <u>The particle shape</u>.

Electron micrographs of the aerosols produced in air at atmospheric pressure and 500 p.s.i. are shown in figs. 38 and 39. The aerosols consisted of a mixture of regular polyhedral particles and faceted spheres. Some cubes were

observed to be present, and when examined under high magnification in the electron microscope, most of the more spherical particles had indications of cubic symmetry, the general shape being similar to that of the Fe_3O_4 crystal (hexoctahedron). Some rather irregularly shaped particles were also observed, and in general the particles in the stainless steel - arc aerosols had a higher degree of surface irregularity than those in the aerosols of other materials. An enlarged micrograph of the aerosol formed in air at 300 p.s.i. is shown in fig.40.

No marked effect of the air pressure on the particle shape was observed.

(c) The particle size distributions.

The frequency histograms for the aerosols formed from the stainless steel arc in air at atmospheric pressure and 500 p.s.i. are shown in figs.38 and 39. The increase in the mean particle size with increase in the gas pressure at which the aerosol was formed is again evident. The cumulative frequency curve for the aerosol formed in air at atmospheric pressure is shown in fig.41. Again the straight line indicates that the size distribution is of the Log-Normal type. Log-Normal distributions were found for all the stainless steel-arc aerosols formed in air at pressures from atmospheric to 500 p.s.i.

(d) The effect of air pressure on the particle size.

The mean particle sizes and standard deviations of

the aerosols formed from the atainless steel arc in air at atmospheric pressure, 100 p.s.i., 200 p.s.i. and 500 p.s.i. are given in Table 14.

The mean particle size was found to increase approximately linearly with increase in the gas pressure. The results are shown graphically in fig.45.

Table 14. Mean particle sizes in aerosols formed from the stainless steel arc in air.

Air pressure	Mean particle diameter (μ)	Standard deviation
Atmospheric	0.016	1.41
100 p.s.i.	0.028	1.61
	0.017	1.48
200 p.s.i.	0.054	1.84
	0.041	1.51
500 p.s.i.	0.056	1.88
	0.062	1.90
	0.061	1.72
	0.047	1.87

(ii) Aerosols from the stainless steel arc in CO_2.

(a) The particle shape, structure and size distributions.

The aerosols formed in CO_2 were found to be similar to those formed in air in all respects except particle size. The electron diffraction patterns indicated the same spinel structure, corresponding most probably to

$NiO.Fe_2O_3$ for the particles in the aerosols formed in CO_2 at pressures from atmospheric to 500 p.s.i. The particle shape was similar to that of the particles formed in air, and again there was no noticeable effect of gas pressure on the particle shape. The same chain-like mode of aggregation was observed.

The size distributions of all the aerosols formed in CO_2 were found to be of the Log-Normal type.

Typical electron micrographs, with the corresponding frequency histograms, of the aerosols produced by the stainless steel arc in CO_2 at atmospheric pressure and 500 p.s.i. are shown in figs.43 and 44.

(b) <u>The effect of the CO_2 pressure on the particle size</u>.

The mean particle sizes and the standard deviations of the aerosols formed from the stainless steel arc in CO_2 are given in Table 15.

<u>Table 15.</u> Mean particle sizes in aerosols formed from the stainless steel arc in CO_2.

CO_2 pressure	Mean particle diameter (μ)	Standard deviation
Atmospheric	0.022	1.67
300 p.s.i.	0.031	2.07
500 p.s.i.	0.038	2.08

Again the particle size was found to increase approximately linearly with increase in the CO_2 pressure at which the aerosol was formed and, as with the other materials investigated, the slope of the particle size/pressure graph was smaller for the aerosols formed in CO_2 than for those formed in air. (See fig.45).

(iv) Summary of the results for the aerosols formed from the stainless steel arc in air and CO_2.

(a) The aerosol particles were found to consist of a double oxide, probably nickel ferrite, $NiO.Fe_2O_3$ ($a = 8.340$ A).

(b) No marked effect of the gas pressure on the particle shape was observed, the particles being polyhedral.

(c) The size distributions of all the aerosols were of the Log-Normal type.

(d) The mean particle size increased with increase in gas pressure, the effect being greater in air than in CO_2.

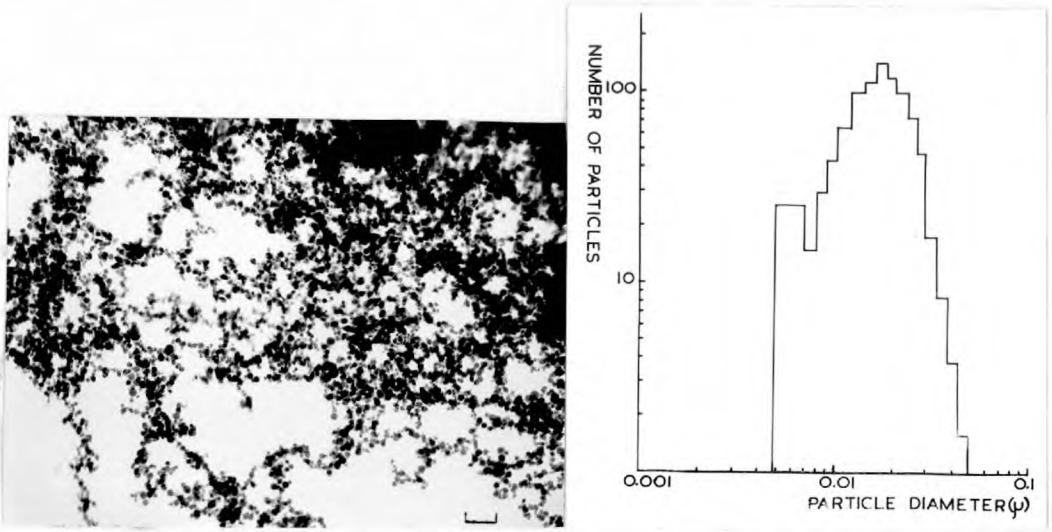

Fig. 38 Electron micrograph (X40,000 Scale = 0.1μ) and frequency histogram for the aerosol formed by the stainless steel arc in air at atmospheric pressure.

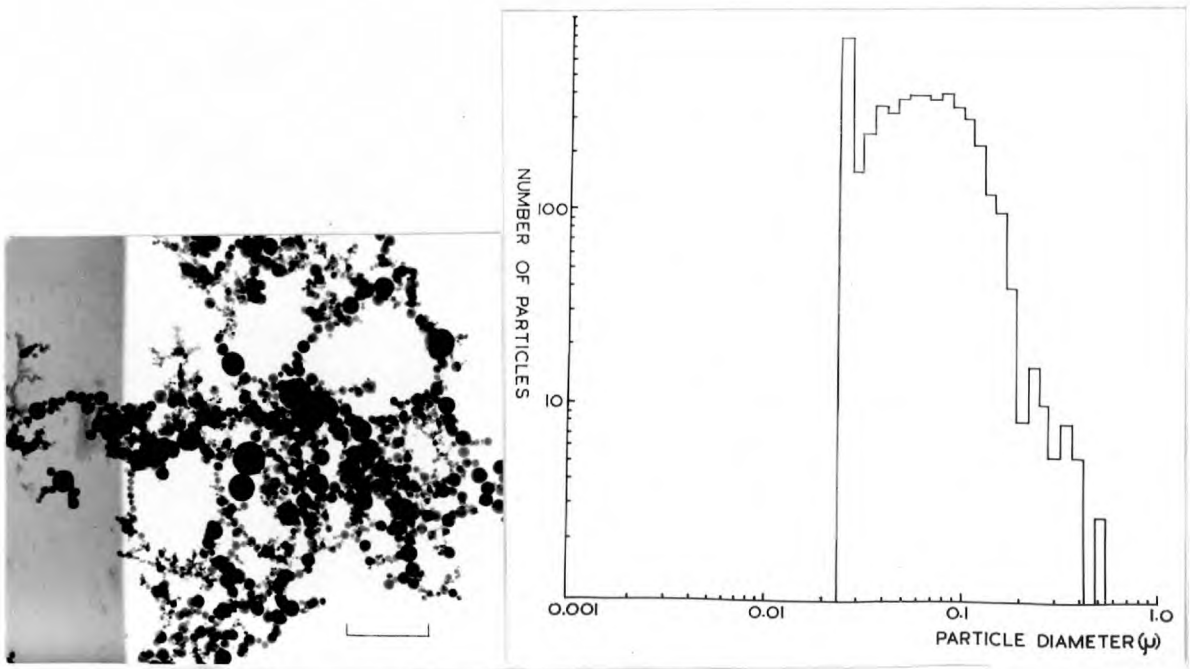

Fig. 39 Electron micrograph (X10,000 Scale = 1μ) and frequency histogram of the aerosol formed by the stainless steel arc in air at 500 p.s.i.

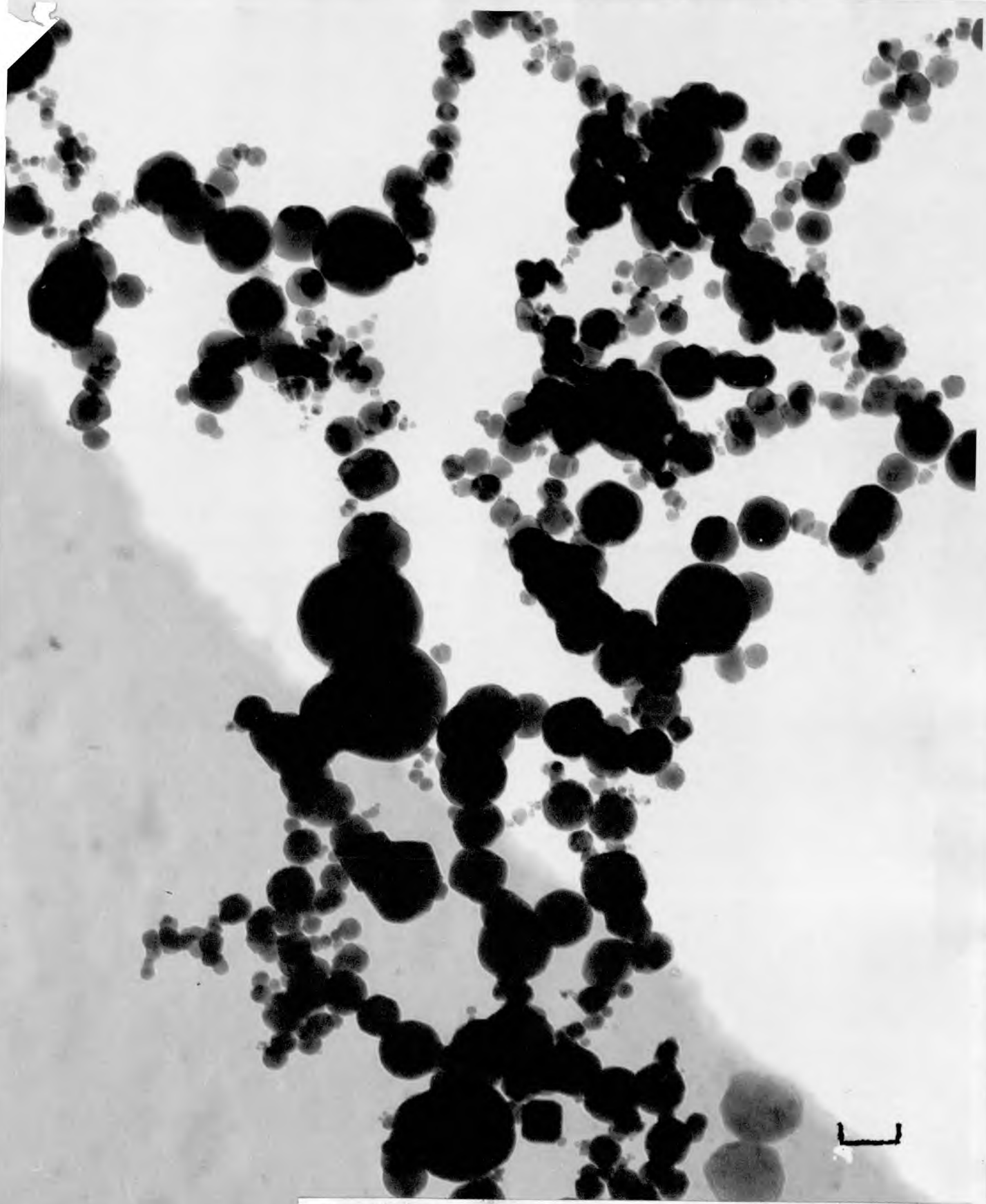

Fig. 40 Electron micrograph of the aerosol formed by the stainless steel arc in air at 300 p.s.i. (X120,000 Scale = 0.1μ).

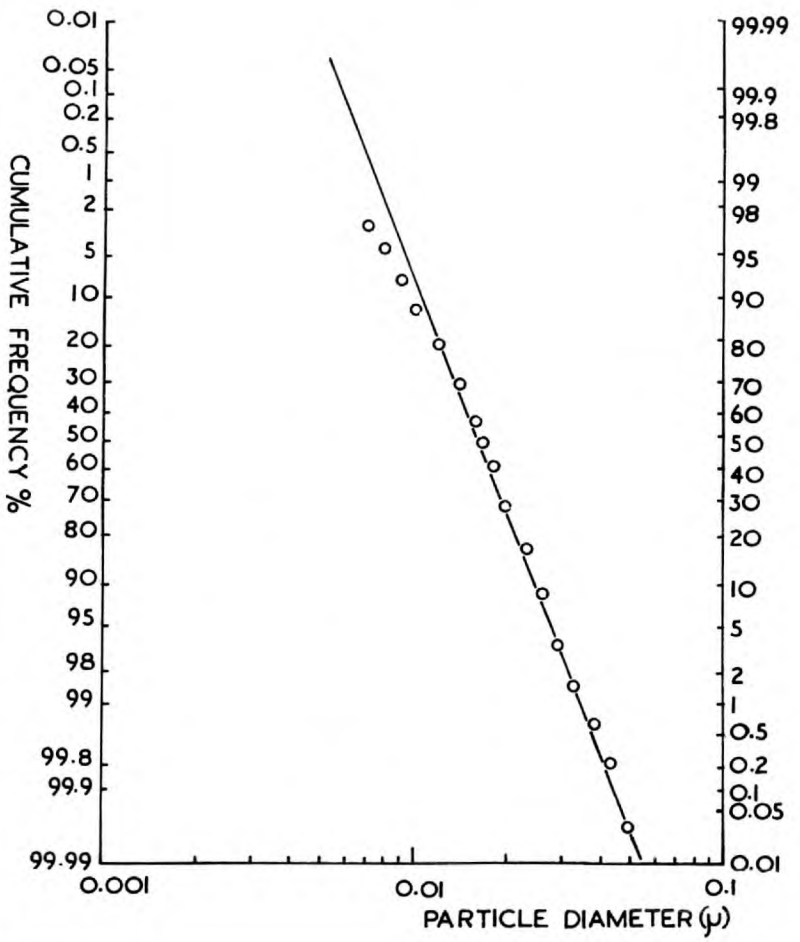

Fig. 41 Cumulative frequency curve for the aerosol formed by the stainless steel arc in air at atmospheric pressure.

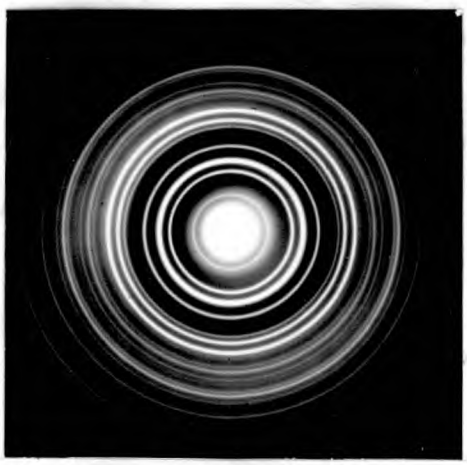

Fig. 42 Electron diffraction pattern from the aerosol formed by the stainless steel arc in air at atmospheric pressure.

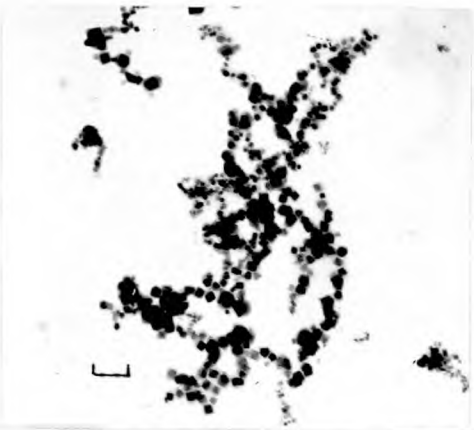

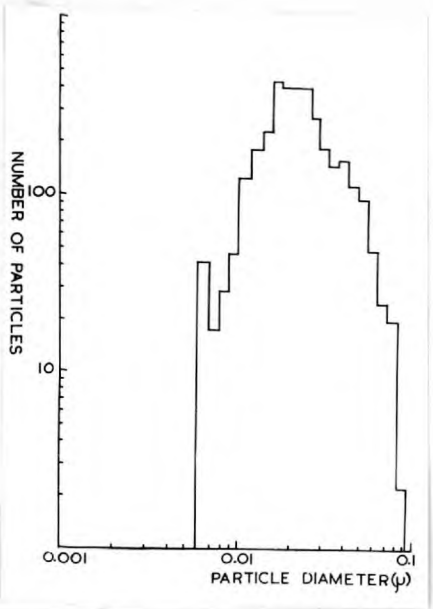

Fig. 43 Electron micrograph (X40,000 Scale = 0.1μ) and frequency histogram of the aerosol formed by the stainless steel arc in CO_2 at atmospheric pressure.

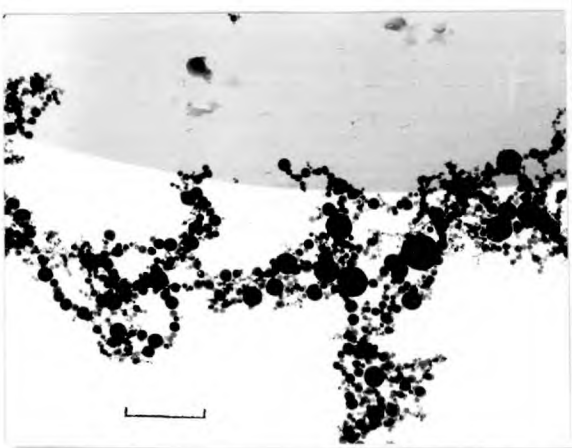

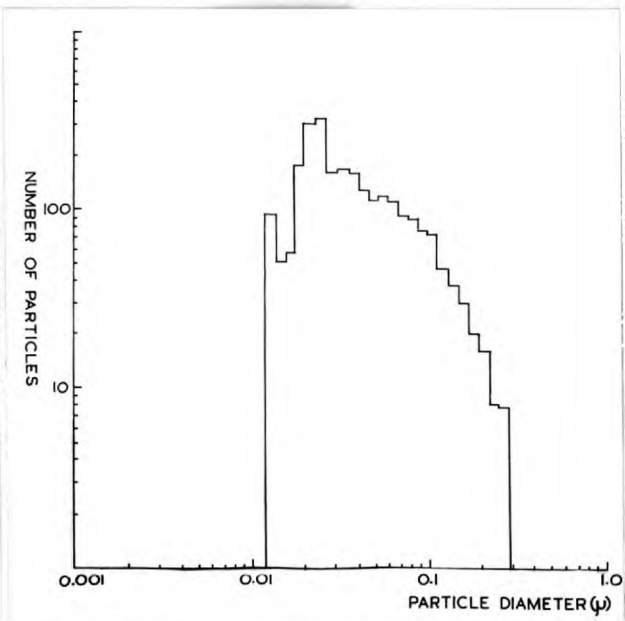

Fig. 44 Electron micrograph (X10,000 Scale = 1μ) and frequency histogram of the aerosol formed by the stainless steel arc in CO_2 at 500 p.s.i.

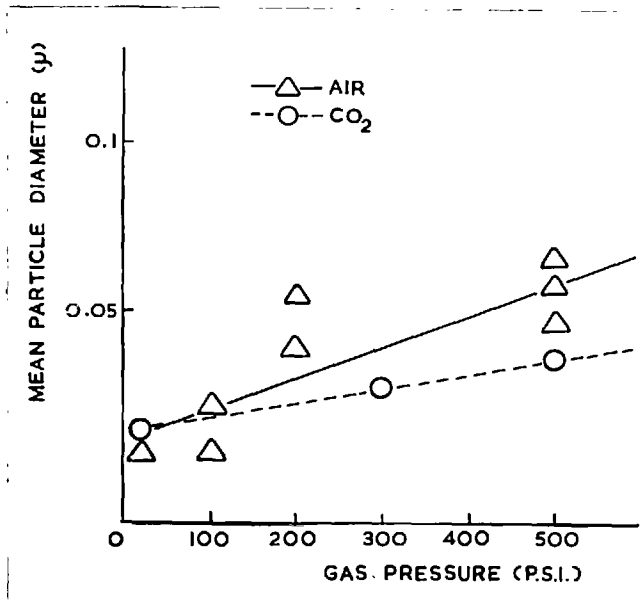

Fig. 45 Plot of the mean particle size against pressure for the aerosols formed by the stainless steel arc in air and CO_2.

3.1.5. Aerosols from UO_2 on a carbon arc.

(i) General observations.

A cored carbon arc was used for the generation of aerosols from UO_2, the UO_2 powder being placed in a hole in the anode. The arc burnt strongly in both air and CO_2 at all the gas pressures investigated, and copious volumes of smoke were produced. The UO_2 powder was initially red-brown in colour, while after arcing the colour of the substance remaining in the anode ranged from bright green to very dark green or black. The smoke deposits were yellowish-grey in colour. After arcing, the carbon anode was found to be dark brown at the tip, changing to yellowish-grey further from the tip (the cooler region of the electrode).

(ii) Aerosols from UO_2 on a carbon arc in air.

(a) The composition and crystal structure of the aerosols.

In all cases but one the electron diffraction patterns obtained from the UO_2/carbon arc aerosols formed in air at pressures from atmospheric to 500 p.s.i. indicated that they were composed mainly of UO_2 together with small traces of U_3O_8. The electron diffraction pattern from the aerosol formed in air at 300 p.s.i. is shown in fig.46, and the ring radii and net plane spacings are compared with the ASTM data for UO_2 and U_3O_8 in Table 16. In the several diffraction patterns examined, all the rings which were not part of the UO_2 pattern could be accounted for by the U_3O_8 pattern.

Table 16. Electron diffraction data from the aerosol formed from the UO_2/carbon arc in air at 300 p.s.i., corresponding to UO_2, cubic, a = 5.4682.

Observed rings (cf. fig. 46)			UO_2 cubic ASTM card 5-0550		
Intensity*	Radius (cm)	d(A)≠	d(A)	I/I_1	hkl
VS	0.721	3.156	3.157	100	111
MS	0.834	2.730	2.735	48	200
S	1.184	1.918	1.934	49	220
MS	1.381	1.645	1.649	47	311
M	1.443	1.577	1.579	13	222
F	1.672	1.361	1.368	9	400
MF	1.815	1.253	1.255	18	331
F	1.867	1.219	1.223	15	420
MF	2.050	1.109	1.116	13	422
F	2.165	1.051	1.052	15	511
			0.967	6	440
			0.924	15	531
			0.911	8	600
			0.865	9	620
			0.834	7	533
			0.824	7	622

* S = strong, M = medium, F = faint, V = very.

≠ Relative to graphite d_{110} = 1.230 A.

Table 17. Electron diffraction data from the aerosol formed by the UO_2 arc in air, corresponding to UO_3, hexagonal, a = 3.971.

Observed rings (cf. fig. 47)			
Intensity*	Radius (cm)	d(A)≠	hkl
VVF	0.443	5.76	
MS	0.615	4.14	001
VS	0.748	3.406	100
VS	0.967	2.635	101
F	1.155	2.206	
VF	1.226	2.080	002
S	1.293	1.970	110
VS	1.434	1.785	111, 102
VVF	1.498	1.701	200
F	1.612	1.581	201
VF	1.678	1.516	
M	1.782	1.431	112
F	1.985	1.284	210, 103
F	2.235	1.194	

* S = strong, M = medium, F = faint, V = very.

≠ Relative to graphite d_{110} = 1.230 A.

However, in one isolated case, an aerosol generated in air at atmospheric pressure, electron diffraction results indicated a structure corresponding to UO_3 with a trace of U_3O_8. There was no evidence of UO_2 in this pattern. The diffraction pattern, with the graphite calibration, is shown in fig.47, and the ring radii and net plane spacings are given in Table 17. There were no ASTM data available for UO_3, and the pattern was therefore indexed from the Bunn-Bjorstrom type of chart. Several rings not corresponding to UO_3 were tentively identified with U_3O_8.

The presence of UO_3 was an interesting result, and appeared to be somewhat anomalous in that the aerosols formed at higher air pressures were all found to be composed of UO_2 with traces of U_3O_8; if an oxide of higher oxygen content were to be formed, it might be expected to be formed more readily at a higher oxygen partial pressure.

A low temperature of formation of the aerosol particles is also indicated when UO_3 is present, since UO_3 decomposes above 450°C, to give UO_2. Hence the UO_3 aerosols must have been formed at a temperature lower than this.

These facts made the result of special interest, and therefore several more aerosols were generated in air at atmospheric pressure from the UO_2/carbon arc. However, careful examination of these aerosols by electron diffraction (including selected area diffraction) failed to reveal the

presence of any UO_3. These aerosols were found to be composed entirely of UO_2.

(b) The particle shape.

Typical electron micrographs, with the corresponding frequency histograms, of the aerosols formed by the UO_2/carbon arc in air at atmospheric pressure and 500 p.s.i. are shown in figs.48 and 49. All the particles in the aerosols formed at atmospheric pressure showed a well-defined polyhedral shape, being cubes or either rhombic or square-shaped tablets. These particle shapes conform with the shapes observed for large crystals of UO_2 by previous workers, which have been listed by Katz and Rabinowitz (1951): metallic lustrous scales (Peligot, 1842); fine strongly reflecting octahedra (Hillebrand, 1893); brilliant cubes (Hofmann, 1915); microscopic regular octahedra (Arfvedson, 1924).

A change in the particle shape with increase in the gas pressure was particularly evident in the UO_2/carbon arc aerosols. In the aerosol formed at 500 p.s.i. most of the particles showed only slight evidence of facet development, and were very nearly spherical. There were very few well-defined polyhedra.

The aggregation of particles into chains was again observed, and individual chains tended to contain particles of a similar size.

(c) The particle size distributions.

The frequency histograms for the UO_2/carbon arc

aerosols formed in air at atmospheric pressure and 500 p.s.i. are shown in figs.48 and 49. The increase of the mean particle diameter with increase in the air pressure is evident. The cumulative frequency curve of the aerosols formed in air gave straight line plots indicating that the particle size distributions were of the Log-Normal type, as for the other materials studied. Log-Normal distributions of particle size were found for all the UO_2/carbon arc aerosols investigated.

(d) The effect of the air pressure on particle size.

The mean particle sizes and standard deviations of the aerosols formed from UO_2 on a carbon arc are given in Table 18, and are shown graphically in fig.55.

Table 18. Mean particle sizes in aerosols formed from the UO_2/carbon arc in air.

Air pressure	Mean particle diameter (μ)	Standard deviation
Atmospheric	0.042	1.45
	0.029	1.54
	0.033	1.42
300 p.s.i.	0.080	1.60
500 p.s.i.	0.135	1.63

The mean particle size was found to increase approximately linearly with increase in the air pressure, as was found for the other materials.

(ii) Aerosols formed from UO_2 on a carbon arc in CO_2.

(a) The particle shape, structure and size distributions.

Electron micrographs of the smokes formed in CO_2 at atmospheric pressure and 500 p.s.i. are shown in figs. 50 and 51. The aerosols formed in CO_2 were found to be similar to those formed in air in all respects apart from particle size. For all gas pressures, the aerosols were composed of UO_2 (cubic, a = 5.468 A), together with a trace of U_3O_8. The particle shapes were similar to those formed in air, and the same tendency towards a more spherical shape with increasing gas pressure was observed. Since the change in particle shape was so evident with the UO_2/carbon arc aerosols, two enlarged micrographs are shown, (figs. 52 and 53). The tabular particle shape in the aerosol formed at atmospheric pressure can be seen in fig.52, while the much more spherical particle shape in the aerosol formed at 300 p.s.i. is shown in fig.53. A layer due to contamination in the electron microscope is evident on the particles in fig. 52.

The size distributions of all the aerosols formed in CO_2 were of the Log-Normal type. The cumulative frequency curve of the aerosol formed in CO_2 at atmospheric pressure is shown in fig.54. The tailing off of the curve at low particle diameters is again due to misclassification during the size analysis.

(b) The effect of the CO_2 pressure on particle size.

The frequency histograms for the aerosols formed in CO_2 at atmospheric pressure and 500 p.s.i. are shown in figs.50 and 51. The peaks at the lowest particle diameter correspond to the cut-off value of the particle size analyser.

The mean particle sizes and standard deviations of the aerosols formed in CO_2 are given in Table 19.

Table 19. Mean particle sizes of the aerosols formed from the UO_2/carbon arc in CO_2.

CO_2 pressure	Mean particle diameter (μ)	Standard deviation
Atmospheric	0.027 0.022	1.33 1.83
300 p.s.i.	0.056	1.66
500 p.s.i.	0.066	1.73

The mean particle diameter increased with increase in the gas pressure at which the aerosol was formed. Again the particle size of the aerosol formed in CO_2 was found to be smaller than that of the aerosol formed in air at the same pressure, and the slope of the particle size/pressure graph was smaller for CO_2 than for air. The results for CO_2 and for air are shown graphically in fig.55.

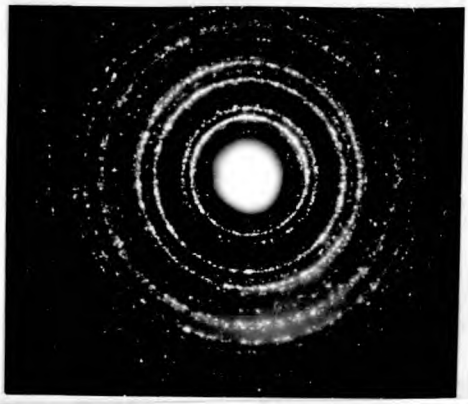

Fig. 46 Electron diffraction pattern from the aerosol formed by the UO_2/carbon arc in air at 300 p.s.i. Pattern corresponding to UO_2.

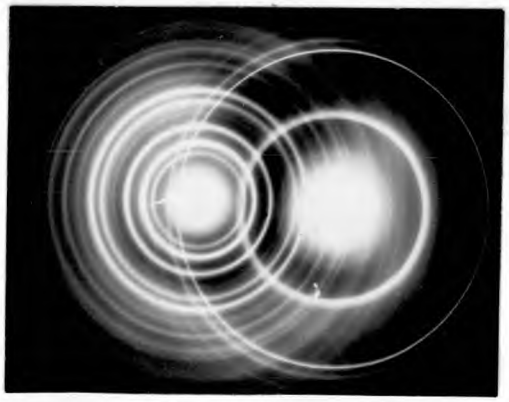

Fig. 47 Electron diffraction pattern from the aerosol formed by the UO_2/carbon arc in air at atmospheric pressure. Pattern corresponding to UO_3.

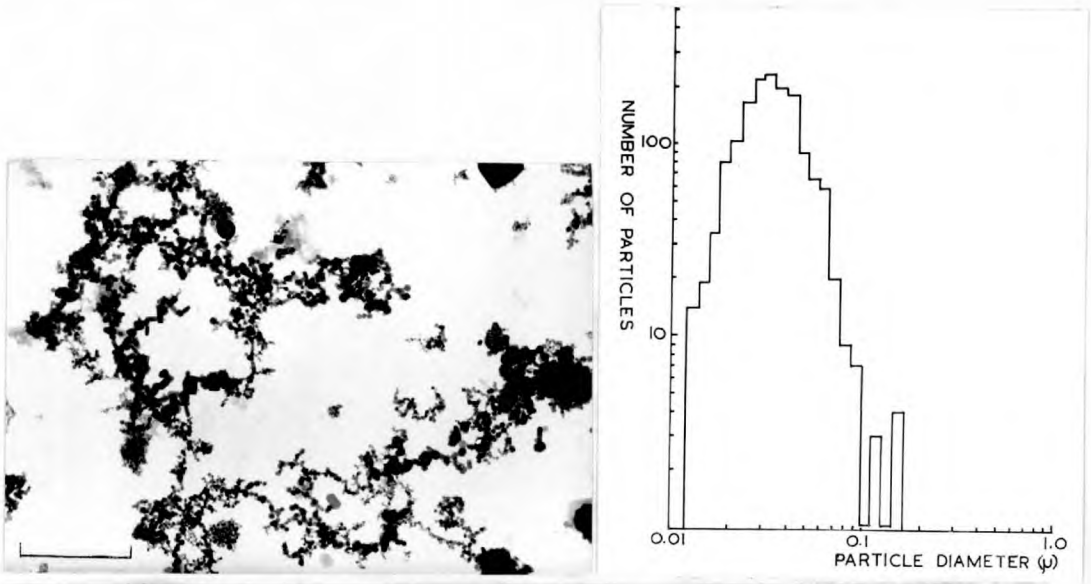

Fig. 48 Electron micrograph (X15,000 Scale = 1μ) and frequency histogram of the aerosol formed by the UO_2/carbon arc in air at atmospheric pressure.

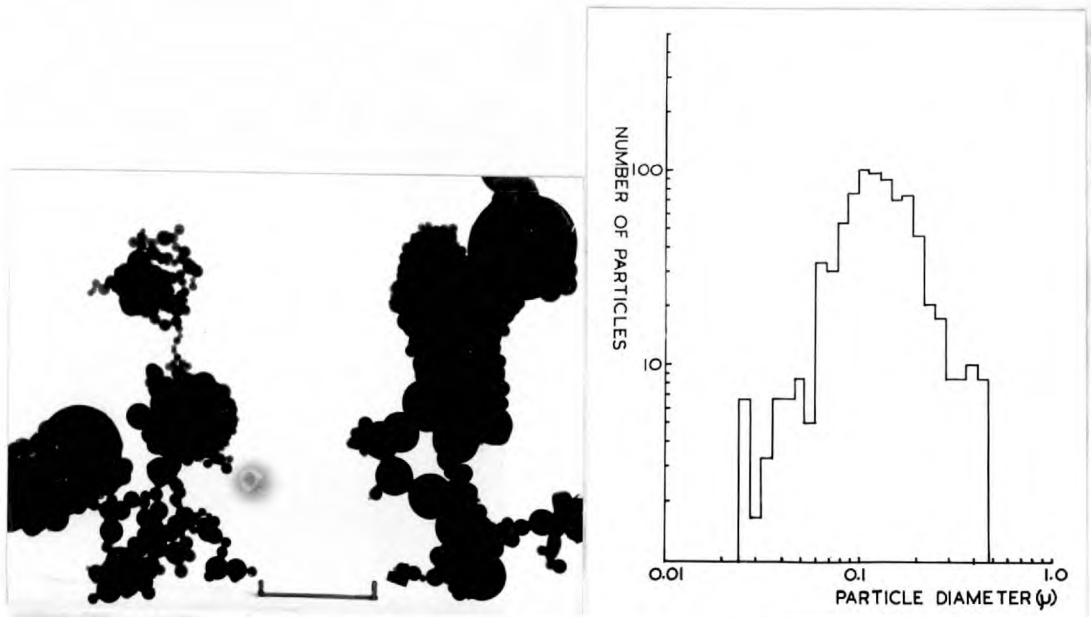

Fig. 49 Electron micrograph (X15,000 Scale = 1μ) and frequency histogram from the aerosol formed by the UO_2/carbon arc in air at 500 p.s.i.

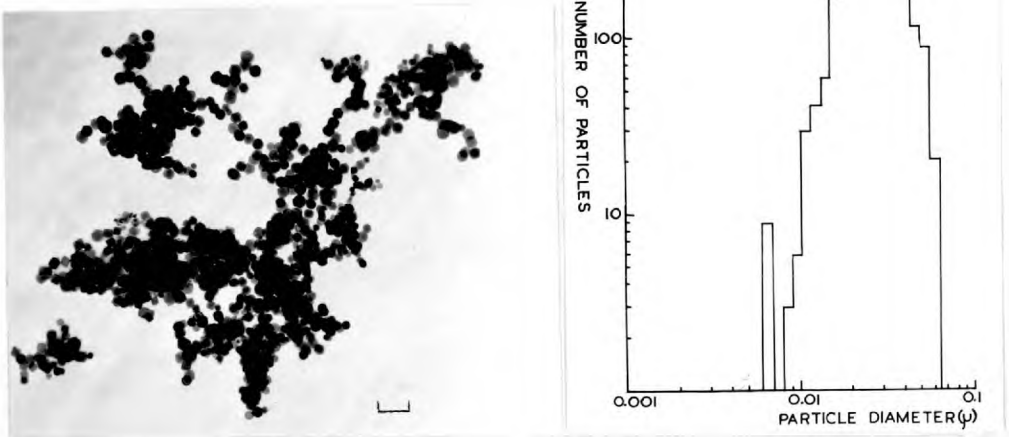

Fig. 50 Electron micrograph (X40,000 Scale = 0.1μ) and frequency histogram of aerosol formed by the UO_2/carbon arc in CO_2 at atmospheric pressure.

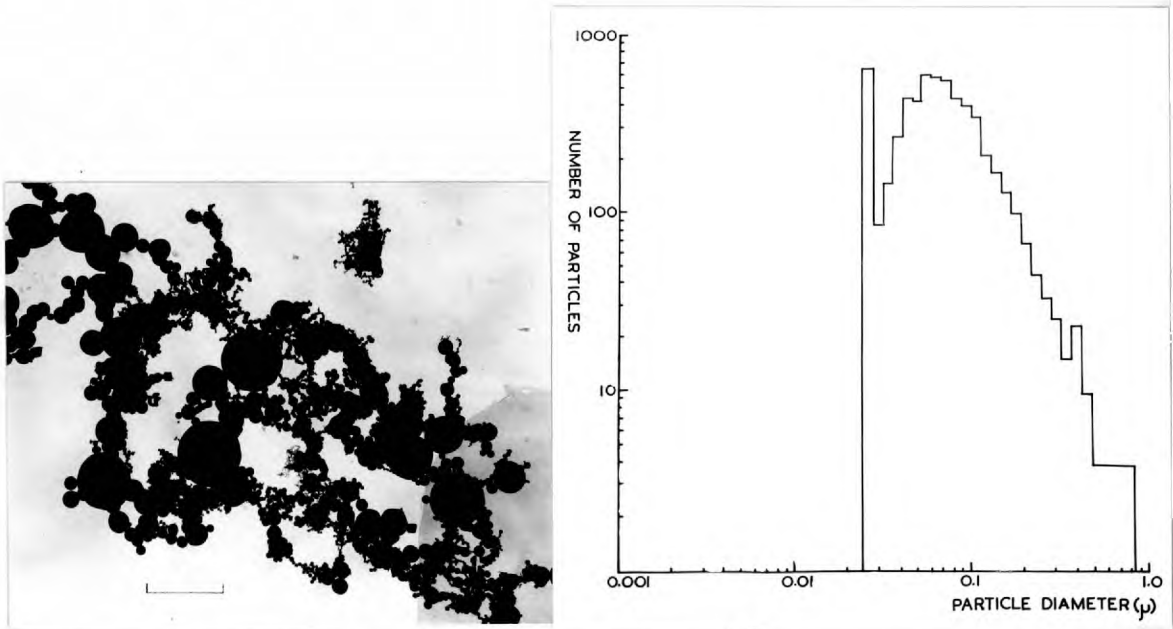

Fig. 51 Electron micrograph (X10,000 Scale = 1μ) and frequency histogram of the aerosol formed by the UO_2/carbon arc in CO_2 at 500 p.s.i.

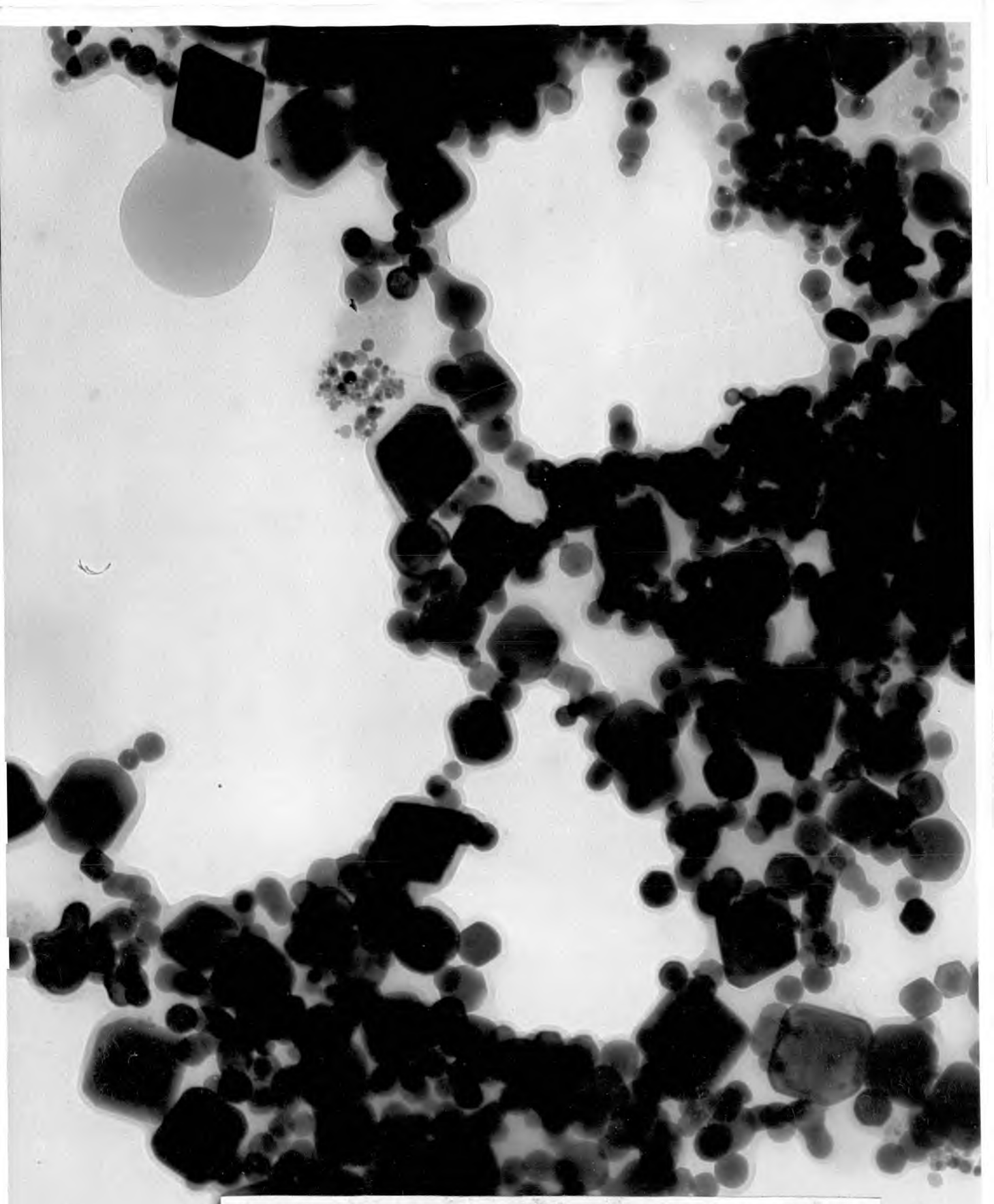

Fig. 52 Electron micrograph of the aerosol formed by the UO_2/carbon arc in air at atmospheric pressure. X200,000 Scale = 0.1μ.

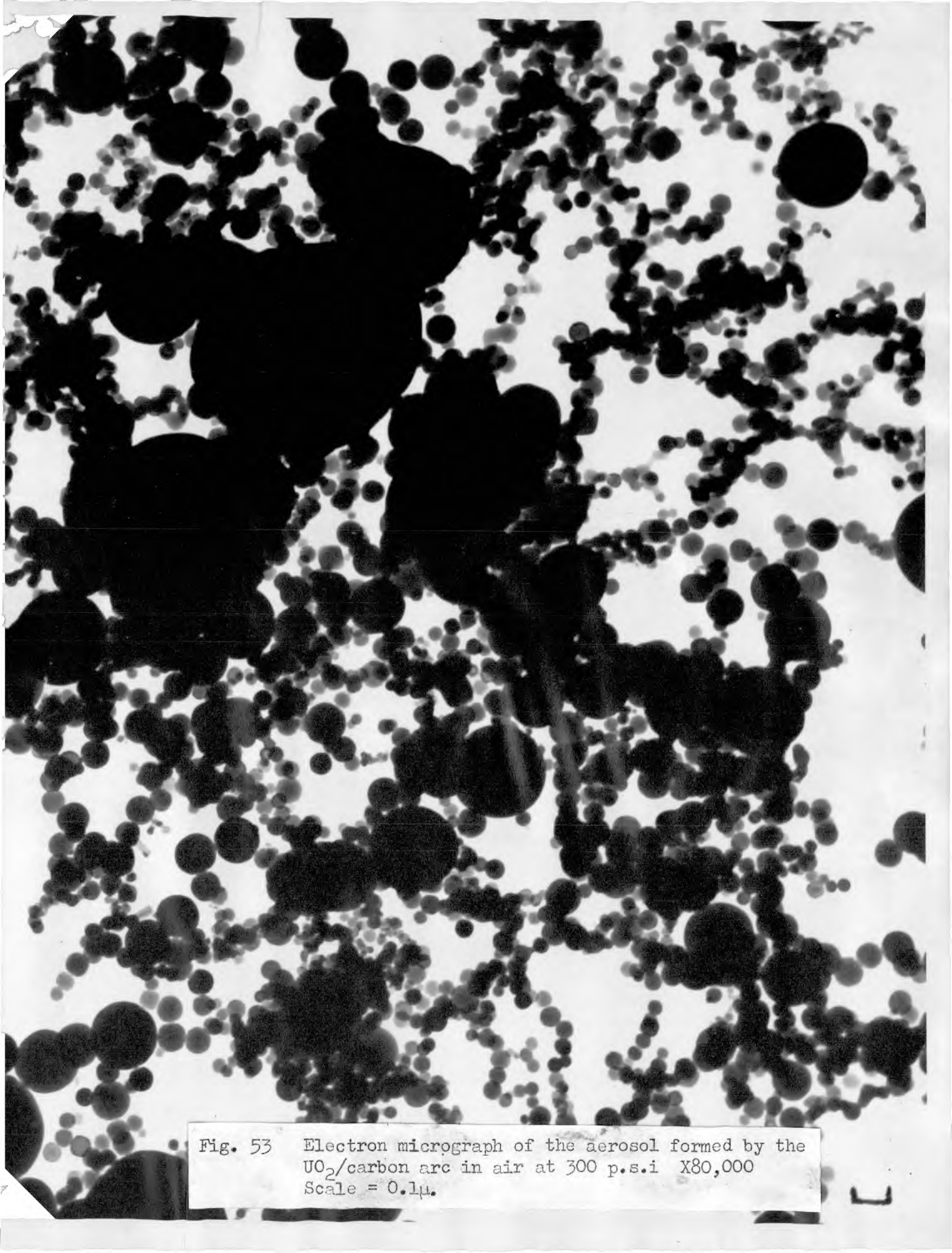

Fig. 53 Electron micrograph of the aerosol formed by the UO_2/carbon arc in air at 300 p.s.i X80,000
Scale = 0.1μ.

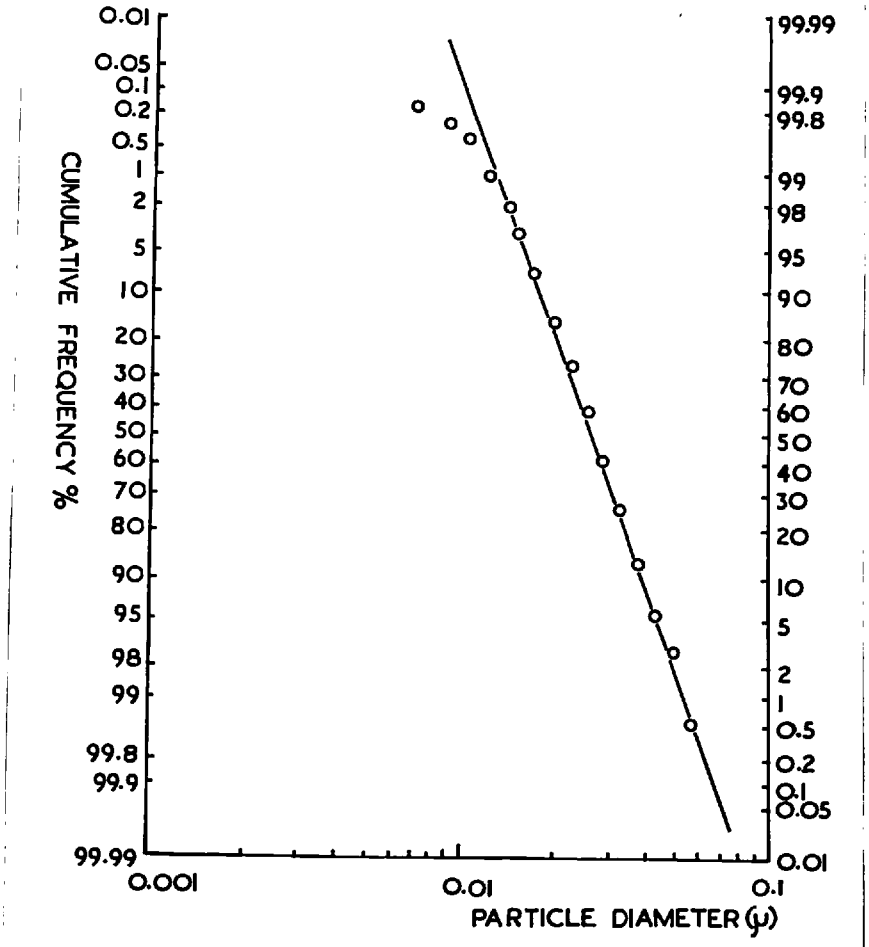

Fig. 54 Cumulative frequency curve for the UO_2 aerosol formed in CO_2 at atmospheric pressure.

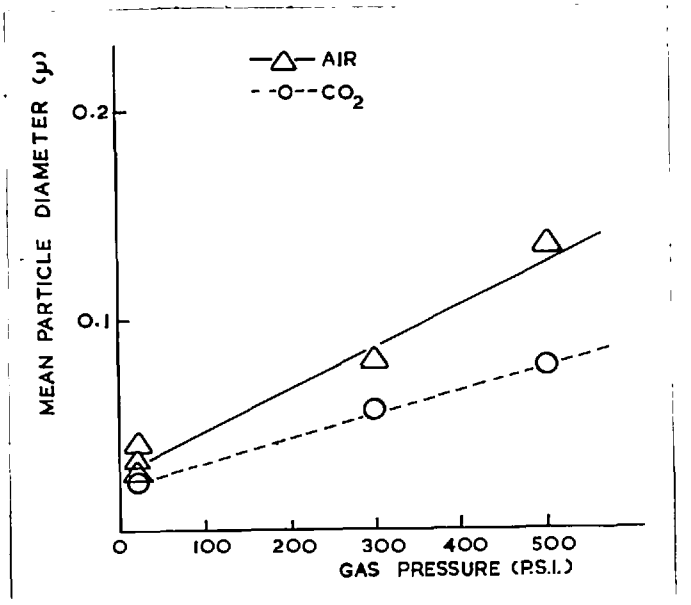

Fig. 55 Plot of mean particle size against gas pressure for aerosols formed by the UO_2/carbon arc in air and CO_2.

3.1.6. Aerosols from the zirconium arc.

(i) General observations.

The first attempts to produce an aerosol from zirconium were made using an arc between electrodes of zirconium metal. It was found that an aerosol of ZrO_2 could readily be produced in air and in CO_2 at atmospheric pressure. However, at pressures above atmospheric, all attempts to produce an aerosol from the metal arc failed due to the extremely rapid oxidation of the metal, which resulted in an insulating layer of oxide on the electrodes.

It was therefore decided to try a Zr-cored carbon arc. In air at pressures above atmospheric (300 and 500 p.s.i.) this method also failed to produce an aerosol, but in CO_2 aerosols were succesfully generated at pressures up to 500 p.s.i.

(ii) Aerosols from the Zr arc in air.

The aerosol generated from the Zr arc in air at atmospheric pressure was found to be composed of ZrO_2 (f.c. cubic, a = 5.103 A). The particle shape was either a cube or a more spherical shape showing cube facets. The size distribution of the aerosol was found to be Log-Normal, and the mean particle size was 0.018μ standard deviation 1.62.

(iii) Aerosols from Zr on a carbon arc in CO_2.

(a) The composition and crystal structure of the aerosols.

Examination by electron diffraction showed that

Table 20. Electron diffraction data from the aerosol formed from the Zr/carbon arc in CO_2 at 300 p.s.i., corresponding to ZrO_2, cubic, a = 5.103.

Observed rings (cf. fig. 59)			ZrO_2 cubic ASTM card 3 - 0642	
Intensity*	Radius(mm)	d(A)≠	d(A)	I/I_1
VS	8.670	2.97	2.96	100
S	9.998	2.56	2.56	24
MF	12.125	2.11		
VS	14.083	1.82	1.81	80
S	16.435	1.56	1.54	60
F	17.197	1.49	1.48	10
F	18.403	1.39		
MF	19.871	1.29	1.28	12
VVF	20.719	1.24		
M	21.58	1.18	1.17	20
			1.14	12
M	24.234	1.05	1.04	16
F	25.749	0.990	0.984	14
			0.904	5
M	29.267	0.876	0.864	8
			0.853	5
			0.809	4

* S = strong, M = medium, F = faint, V = very.

≠ Relative to graphite d = 1.230 A.

the aerosols produced by the Zr/carbon arc in CO_2 at pressures from atmospheric to 500 p.s.i. were composed of crystalline ZrO_2 (f.c. cubic, a = 5.103 A). The diffraction pattern obtained from the aerosol generated in CO_2 at 300 p.s.i. is shown in fig.59, and the ring radii and net plane spacings are compared with the ASTM data for ZrO_2 in Table 20.

The stability of the various forms of ZrO_2 has been described by Runck (1956). The monoclinic form is stable from room temperature to 1000°C, the tetragonal form from 1000°C - 1900°C, and the trigonal form is produced from any other form by prolonged heating at 2000°C. In pure ZrO_2 the cubic form is not stable near its melting point, or at room temperature. The cubic form is normally made by heating the monoclinic form with MgO or CaO; the cubic lattice may also be stabilised by the oxides of Sc, Ce and Y.

The occurrence of the cubic form in the ZrO_2 aerosols investigated in the present work is therefore most probably due to the Ca impurity (1.25%) present in the zirconium metal.

(b) <u>The particle shape</u>.

Electron micrographs, with the corresponding frequency histograms, of the aerosols produced by the Zr/carbon arc in CO_2 at atmospheric pressure and 500 p.s.i. are shown in figs. 56 and 57. Most of the particles in the aerosols formed in CO_2 at atmospheric pressure showed some

facet development, the particle shape being basically a cube, although with well-rounded corners. Some apparently perfectly spherical particles were also present. As with the other materials studied, the aggregation of particles into chains was observed, and particles in sections of individual chains again appeared to be of similar size. In the electron microscope, wedge fringes were observed in the images of some of the particles, indicating their single crystal nature.

The polyhedral particle shape became less evident as the CO_2 pressure was increased. Fig.58 shows an enlargement of a micrograph obtained from the aerosol formed in CO_2 at 300 p.s.i. Faceting is still evident on many of the particles, but is much less marked than on those formed at atmospheric pressure. At 500 p.s.i., fig.57, most of the particles are apparently almost spherical, although a few are still clearly faceted.

(c) The particle size distributions.

The frequency histograms for the aerosols formed from the Zr/carbon arc in CO_2 at atmospheric pressure and 500 p.s.i. are shown in figs.56 and 57. The increase in mean particle size with increasing gas pressure is evident from the histograms. The cumulative frequency curve, plotted on probability graph paper, for the aerosol formed in air at 500 p.s.i. is shown in fig.58a. Similar straight-line plots, indicating a Log-Normal distribution of particle size, were

obtained for the aerosols formed at atmospheric pressure and 500 p.s.i.

(d) The effect of CO_2 pressure on particle size.

The mean particle sizes and standard deviations of the aerosols formed from the Zr/carbon arc in CO_2 at atmospheric pressure, 300 p.s.i., and 500 p.s.i. are given in Table 21.

Table 21. Mean particle sizes in aerosols formed from Zr/carbon arc in CO_2.

CO_2 pressure	Mean particle diameter (μ)	Standard deviation
Atmospheric	0.016	1.51
300 p.s.i.	0.024	1.52
500 p.s.i.	0.048	1.59

As with the other arc materials, the mean particle size was found to increase approximately linearly with increase in the CO_2 pressure at which the aerosol was formed, see fig.60.

(iv) Summary of results for aerosols formed from the Zr arc.

(a) The aerosols were found to be composed of ZrO_2 (f.c. cubic, a = 5.103 A).

(b) The particle shape was polyhedral, cube facets being evident. The particle shape tended more towards a sphere as the gas pressure was increased.

(c) The size distributions of the aerosols were Log-Normal.

(d) The mean particle size increased with increase in gas pressure, in an approximately linear manner.

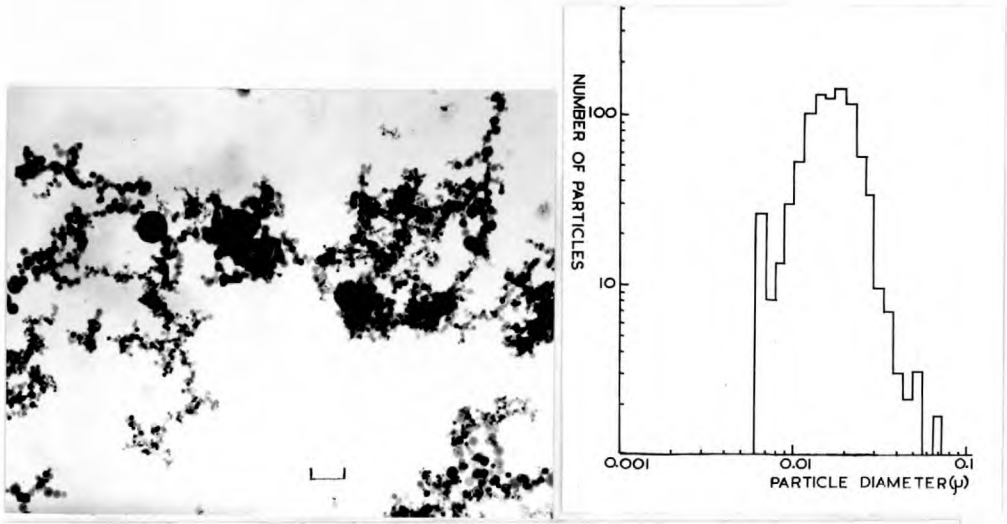

Fig. 56 Electron micrograph (X40,000 Scale = 0.1μ) and frequency histogram of the aerosol formed by the Zr/carbon arc in CO_2 at atmospheric pressure.

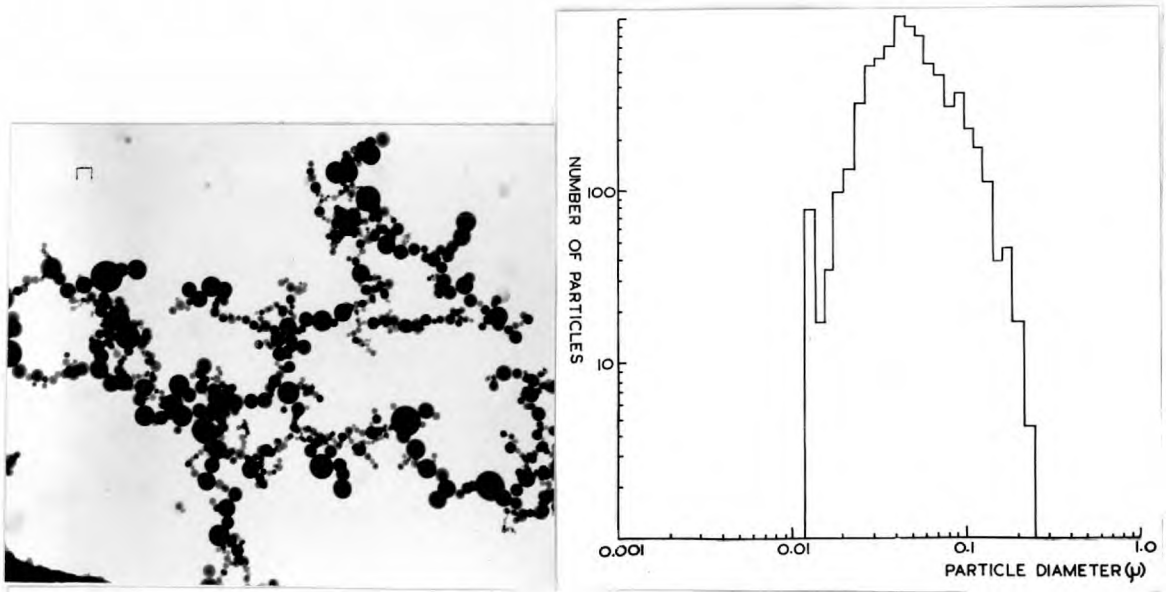

Fig. 57 Electron micrograph (X20,000 Scale = 0.1μ) and frequency histogram of the aerosol formed by the Zr/carbon arc in CO_2 at 500 p.s.i.

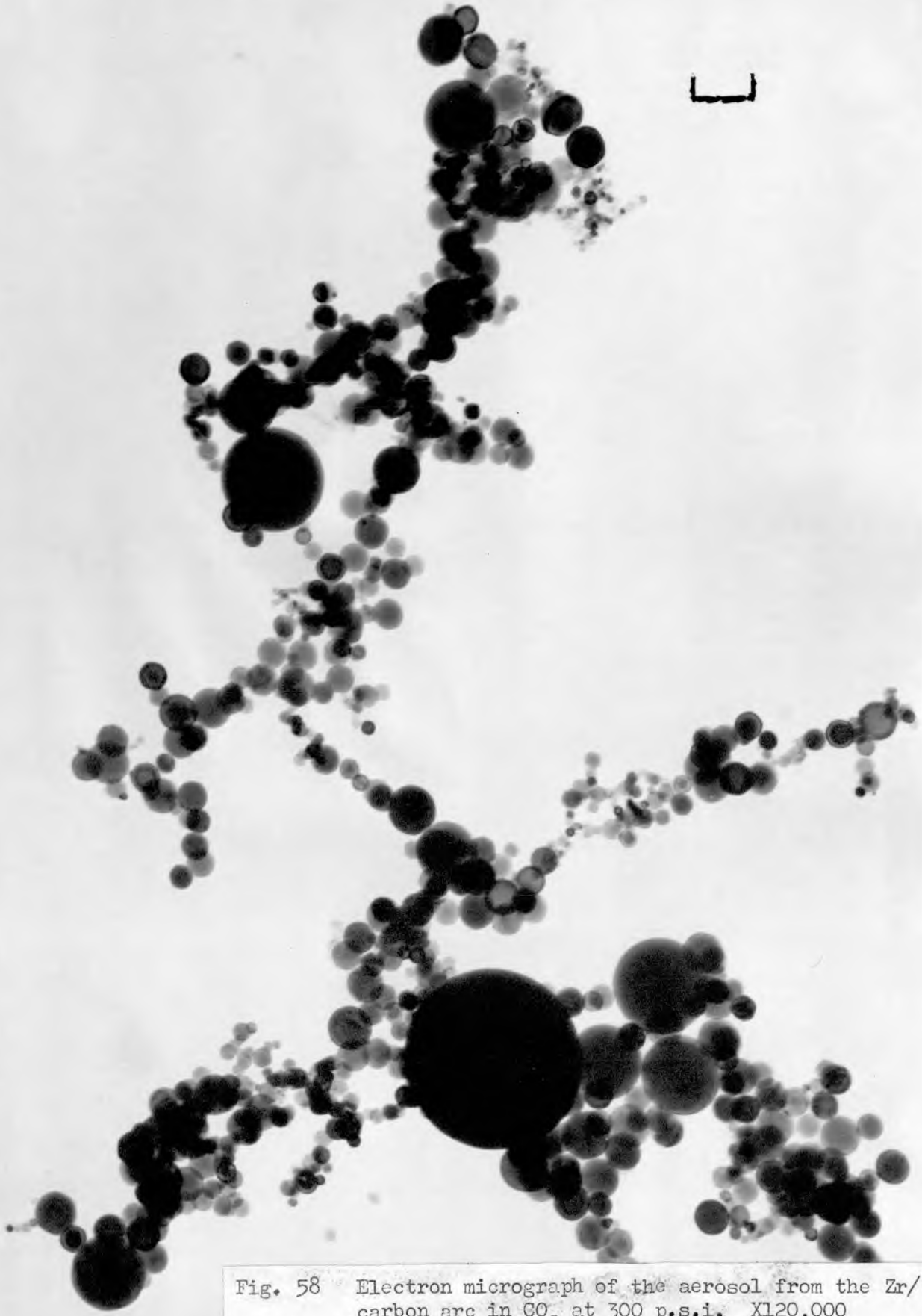

Fig. 58 Electron micrograph of the aerosol from the Zr/carbon arc in CO_2 at 300 p.s.i. X120,000 Scale = 0.1μ.

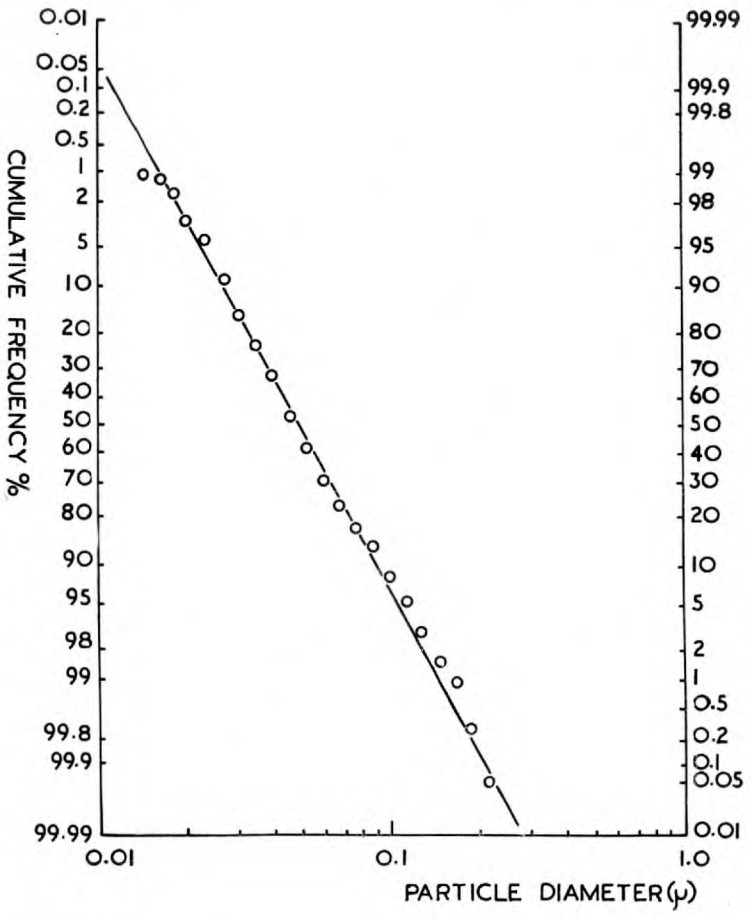

Fig.58a Cumulative frequency curve for the ZrO_2 aerosol formed in air at 500 p.s.i.

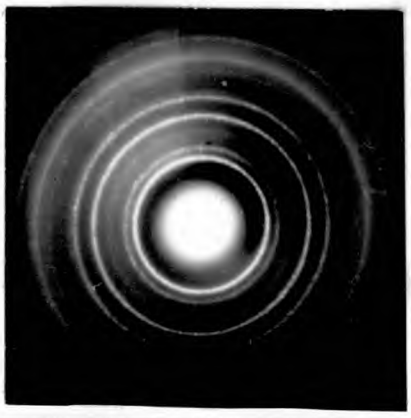

Fig. 59 Electron diffraction pattern from the aerosol formed by the Zr/carbon arc in CO_2 at 300 p.s.i.

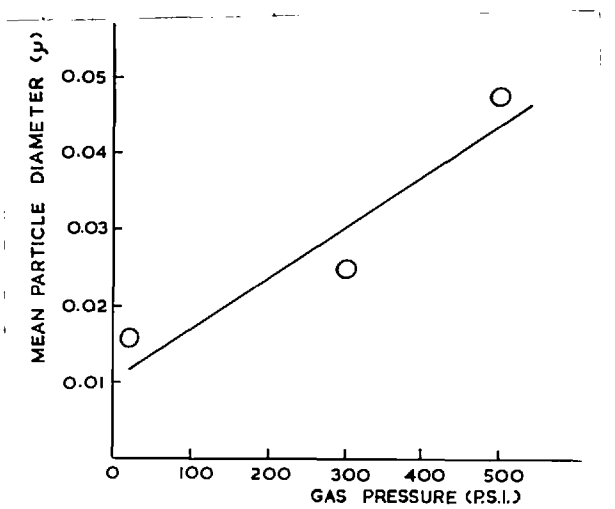

Fig. 60 Plot of the mean particles size against gas pressure for ZrO_2 aerosols formed in ~~air and~~ CO_2.

3.1.7. Aerosols from gold on a carbon arc.

(i) General observations.

A cored carbon arc was used for the generation of gold aerosols. Initially arcs between gold electrodes were tried, but they could not be maintained, due to melting of the electrodes.

The gold-cored carbon arc burnt strongly in both air and CO_2 at pressures from atmospheric to 500 p.s.i., the smoke deposits produced having the characteristic red-gold colour.

(ii) Aerosols from the gold/carbon arc in air.

(a) The composition and crystal structure of the aerosols.

Electron diffraction examination of the aerosols formed from the gold/carbon arc in air at pressures from atmospheric to 500 p.s.i. showed that they were composed of crystalline Au, as was expected. A typical diffraction pattern from the aerosol formed in air at 300 p.s.i. is shown in fig.64, and the ring radii and net plane spacings are given in Table 22.

(b) The particle shape.

Typical electron micrographs of the aerosols produced by the gold-cored carbon arc in air at atmospheric pressure and 500 p.s.i. are shown in figs.61 and 62. In all the aerosols, the particles were found to be perfect spheres. There was no evidence of any facet development,

Table 22. Electron diffraction data from the aerosol formed from the gold/carbon arc in air at 300 p.s.i., corresponding to gold, cubic, a = 4.0786.

Observed rings (cf. fig. 64)			Gold cubic ASTM card 4-0784		
Intensity*	Radius (cm)	d(A)≠	d(A)	I/I_1	hkl
VS	0.9826	2.356	2.355	100	111
S	1.1396	2.030	2.039	52	200
MS	1.5965	1.449	1.442	32	220
M	1.8816	1.229	1.230	36	311
VF	1.9593	1.179	1.1774	12	222
VVF	2.2602	1.024	1.0196	6	400
M	2.4580	0.940	0.9358	23	331
M	2.5260	0.917	0.9120	22	420
MF	2.7887	0.830	0.8325	23	422
MF	2.9414	0.787			

* S = strong, V = very, M = medium, F = faint.

≠ Relative to graphite d_{110} = 1.230 A.

and there was no effect of the air pressure on the particle shape.

The chain-like mode of aggregation was evident, as with metal oxide aerosols.

(c) The particle size distributions.

The frequency histograms for the aerosols formed from the gold/carbon arc in air at atmospheric pressure and 500 p.s.i. are shown in figs.61 and 62. The peaks at low particle diameters are again due to this value being the lower limit of the Zeiss particle size analyser.

The cumulative frequency curve for the aerosol formed in air at atmospheric pressure is shown in fig.63. The straight line graph indicates a Log-Normal distribution of particle size, as was found for the metal oxide aerosols. The gold aerosols formed in air at pressures from atmospheric to 500 p.s.i. were all found to have a Log-Normal distribution.

(d) The effect of the air pressure on the particle size.

The mean particle sizes and standard deviation of the gold aerosols formed in air at atmospheric pressure, 300 p.s.i. and 500 p.s.i. are given in Table 23.

Table 23. Mean particle sizes in aerosols formed from the gold/carbon arc in air.

Air pressure	Mean particle diameter (μ)	Standard deviation
Atmospheric	0.080	1.625
300 p.s.i.	0.075	1.613
500 p.s.i.	0.102	1.559

The results indicate that if there was any effect of the air pressure on the mean particle size, it was certainly very small. Since the reproducibility of the results was not better than about 0.01μ, a firm conclusion does not appear to be justified.

(iii) Aerosols from the gold/carbon arc in CO_2.

(a) The composition, crystal structure and size distributions.

The aerosols formed in CO_2 were found to be similar to those formed in air. Thus the aerosols were found to be composed of crystalline gold, (f.c. cubic, a = 4.0786 A), the individual particles were perfect spheres, and there was no evidence of any effect of the CO_2 pressure on the particle shape. The size distributions of the aerosols were again all found to be Log-Normal.

Electron micrographs from the aerosols formed in CO_2 at atmospheric pressure and 500 p.s.i., together with the associated frequency histograms, are shown in figs.65 and 66. A X100,000 enlargement of the aerosol formed at 300 p.s.i. is shown in fig.67.

(b) The effect of the CO_2 pressure on the particle size.

The mean particle sizes and standard deviations of the gold aerosols formed in CO_2 at atmospheric pressure and 500 p.s.i. are given in Table 24.

As for the aerosols formed in air from the gold/

carbon arc, the results are a little inconclusive. There is again a slight indication of a very small increase in mean particle size with increase in the CO_2 pressure.

Table 24. Mean particle sizes in aerosols formed from gold/carbon arc in CO_2.

CO_2 pressure	Mean particle diameter (μ)	Standard deviation (μ)
Atmospheric	0.051	2.00
	0.036	1.95
300 p.s.i.	0.094	1.734
	0.106	1.887
500 p.s.i.	0.088	1.932

(iv) Summary of results for aerosols from the Au/carbon arc.

(a) The aerosols were found to be composed of crystalline Au, (f.c. cubic, a = 4.0786 A).

(b) The particles were spherical in shape; there was no effect of gas pressure on shape.

(c) The size distributions of the aerosols were Log/Normal.

(d) There was possibly some small increase in particle size with increase in gas pressure, but the results were inconclusive.

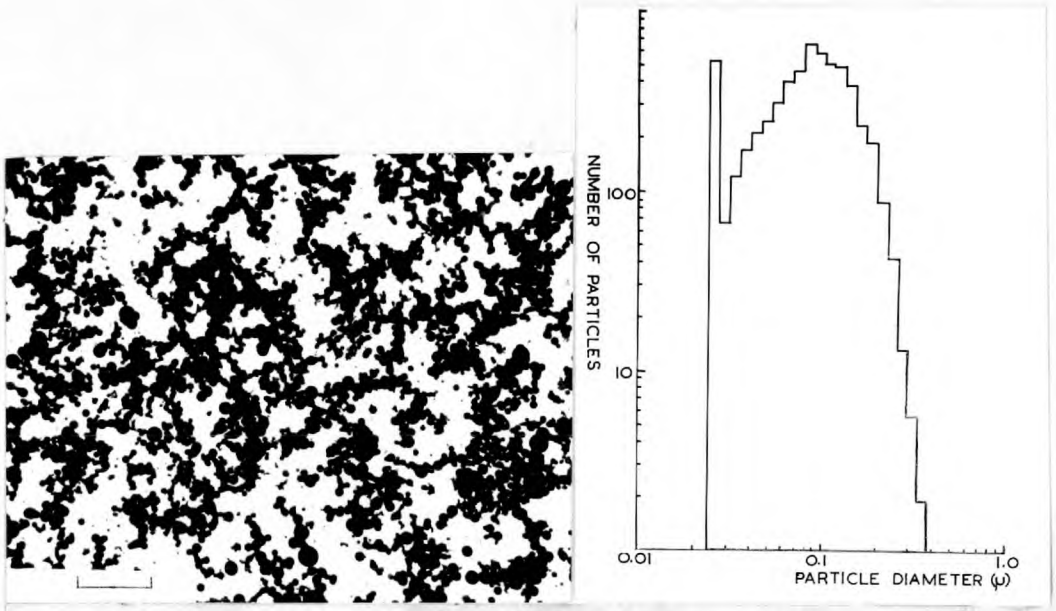

Fig. 61 Electron micrograph (X10,000 Scale =1μ) and frequency histogram of the aerosol formed by the gold/carbon arc in air at atmospheric pressure.

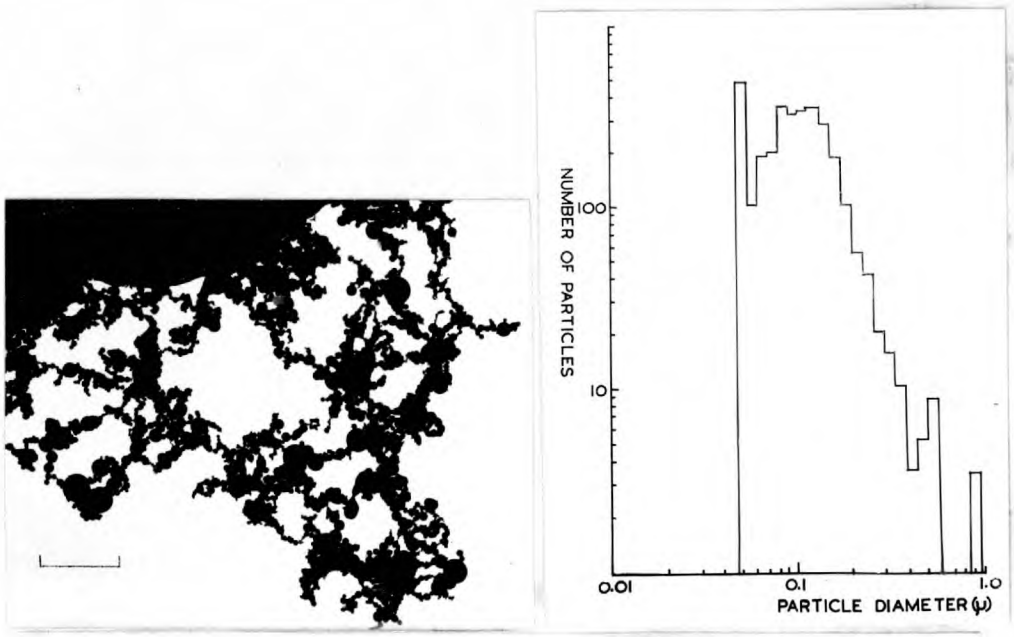

Fig. 62 Electron micrograph (X10,000 Scale = 1μ) and frequency histogram of the aerosol formed by the gold/carbon arc in air at 500 p.s.i.

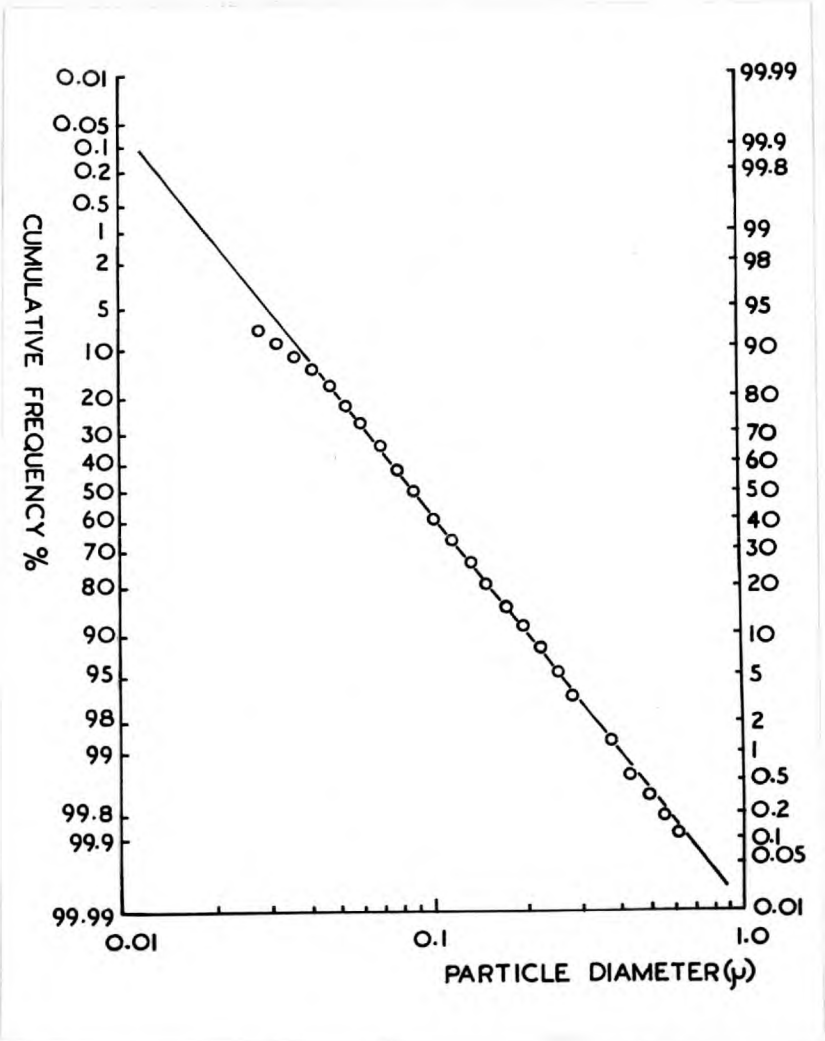

Fig. 63 Cumulative frequency curve for the gold aerosol formed in air at atmospheric pressure.

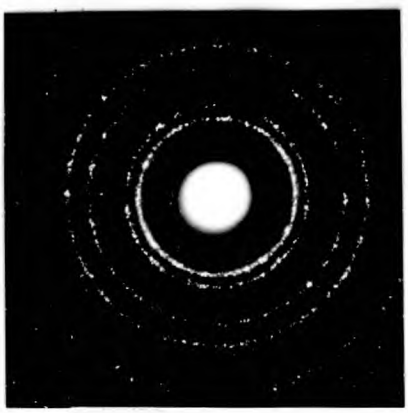

Fig. 64 Electron diffraction pattern from the aerosol formed by the gold/carbon arc in air at 300 p.s.i.

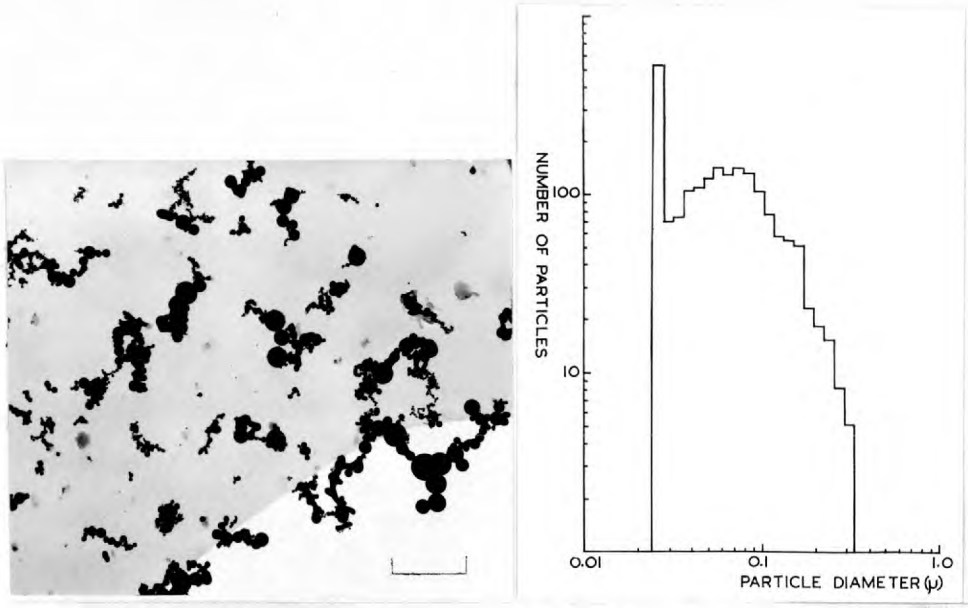

Fig. 65 Electron micrograph (X10,000 Scale = 1μ) and frequency histogram of the aerosol formed by the gold/carbon arc in CO_2 at atmospheric pressure.

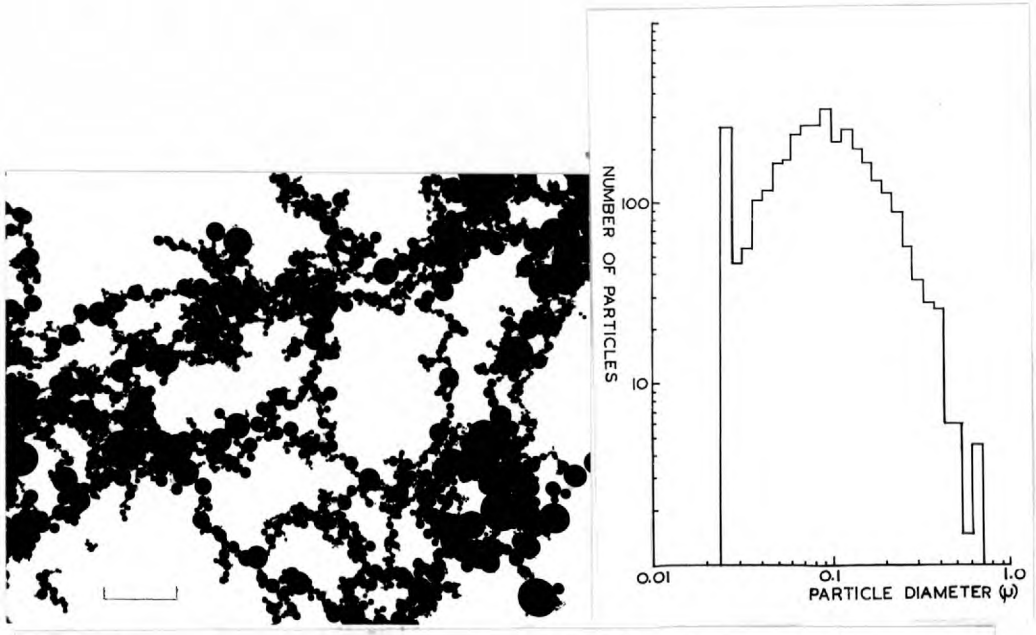

Fig. 66 Electron micrograph (X10,000 Scale = 1μ) and frequency histogram for the aerosol formed in CO_2 at 500 p.s.i.



Fig. 67 Electron micrograph of the gold aerosol formed in CO_2 at 300 p.s.i. X100,000 Scale = 0.1μ.

3.2 THE STRUCTURE OF THE ARC FLAMES

Photographs of the flames of the stainless steel arc and the gold-cored carbon arc are shown in figs. 68 and 69. The photographs were taken along the axis of the arc. The flames were also observed by projecting the flame image onto a ground-glass screen; more detail could be seen than is evident in the photographs, since differences in colour could be distinguished. Measurements of the flame dimensions were made from the screen.

The flames produced were approximately spherical in shape, but with the top drawn out due to convection. The most significant feature of the flames was a narrow, intensely bright zone observed at a small radial distance from the electrodes, this zone being separated from the electrodes by a dark region. This zone was first observed in the stainless steel arc flame, and it was thought that it might be due to oxidation of the metal vapour. However, it was also observed in the flame from the gold-cored carbon arc, and therefore could not be due to oxidation. It was also shown in this case that the zone was due solely to gold, since the carbon arc alone, without gold, showed no such zonal structure. It is well known that intense light is radiated by incandescent particles in flames (Wolfhard and Parker, 1949; see section 1.3.). The bright zone was therefore taken to be the zone in which aerosol particles were present, the particles having been formed from the vapour.

In addition, for both the stainless steel arc and the



Fig. 68 Photograph taken along arc axis of the flame produced by a stainless steel arc in air at atmospheric pressure.



Fig. 69 Photograph taken along arc axis of the flame produced by a gold/carbon arc in air at atmospheric pressure.

gold-cored carbon arc, blue scattered light could be seen at the immediate outside edge of the bright zone. This indicates the presence of aggregates of the order of the wavelength of light in size. Since the primary aerosol particles from both arcs were only a few hundred Angstroms in diameter, coagulation into larger units must have occurred even at this very small distance from the arc.

The dimensions of the flames of the stainless steel arc and the gold-cored carbon arc in air at atmospheric pressure are given in Table 25. The radial distance was measured in the horizontal plane.

Table 25. The dimensions of the stainless steel and gold/carbon arc flames.

Arc	Radial distance from centre of electrode to inner edge of bright zone. (cm)	Thickness of bright zone. (cm)
Stainless steel	0.2	0.013
Gold / carbon	0.4	0.03

3.3 THE TEMPERATURE DISTRIBUTION IN THE VICINITY OF THE ARC

The results for the temperature gradient around a gold-cored carbon arc in air at atmospheric pressure and at 500 p.s.i.,

and a stainless steel arc in air at atmospheric pressure are given in Table 26, and are shown graphically in fig. 70. The gas temperature at any point was found to increase over about the first 15 sec. of arcing. The temperature was measured after 5 and 10 sec., the average time of an evaporation.

3.4 THE RATE OF EVAPORATION OF MATERIAL FROM THE ARC

The rate of evaporation of material from the stainless arc in air at atmospheric pressure, measured as described in section 2.7, was of the order of 10^{-4} gms/sec. Sputtering of material also took place, however, giving an unknown, but probably considerable, error on this figure.

The rate of evaporation of gold from the gold/carbon arc in air at atmospheric pressure was found to be $0.0030 \pm .0005$ gms/sec, and in air at 500 p.s.i. the rate was $0.0032 \pm .0002$ gms/sec.

Table 26. The temperature distribution round the gold/carbon and stainless steel arcs in air.

Arc	Gas pressure	Thermocouple position, and radial distance from arc.	Temperature. °C. After 5 sec.	After 10 sec.
Gold/carbon	Atmospheric	Above arc		
		0.5 cm	650 ± 50	850 ± 50
		1.0 cm	420 ± 75	625 ± 100
		1.5 cm	200 ± 50	320 ± 100
		2.0 cm	190 ± 20	310 ± 20
Gold/carbon	Atmospheric	In horizontal plane of arc.		
		0.25 cm	675 ± 50	
		0.5 cm	400 ± 20	650 ± 70
		1.0 cm	160 ± 20	200 ± 20
Gold/carbon	500 p.s.i.	Above arc		
		0.5 cm	840 ± 80	
		1.0 cm	420 ± 50	780 ± 80
		1.5 cm	220 ± 50	380 ± 50
		2.0 cm	150 ± 20	210 ± 30
Gold/carbon	500 p.s.i.	In horizontal plane of arc.		
		0.25 cm	830 ± 75	
		0.5 cm	400 ± 50	450 ± 60
		1.0 cm	140 ± 20	200 ± 30
Stainless steel	Atmospheric	Above arc		
		0.25 cm	-	425 ± 40
		0.5 cm	-	230 ± 20
		1.0 cm	-	190 ± 30
		1.5 cm	-	80 ± 10
Stainless steel	Atmospheric	In horizontal plane of arc.		
		0.25 cm	-	400 ± 70
		0.5 cm	-	200 ± 50
		1.0 cm	-	50 ± 10

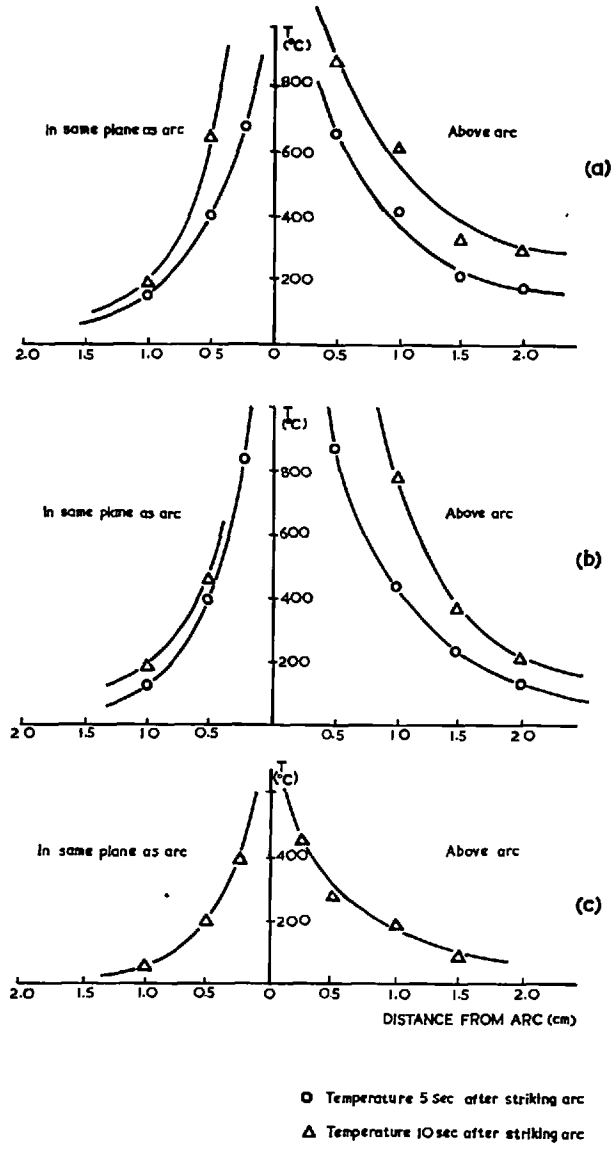

Fig. 70 The temperature gradients in the vicinity of a gold-cored carbon arc in (a) air at atmospheric pressure, (b) in air at 500 p.s.i.; and a stainless steel arc in air at atmospheric pressure (c).

4. DISCUSSION

4.1. THE GENERATION OF THE AEROSOLS

In order to explain the features of the aerosols observed on a submicroscopic scale, it is necessary to have some idea of the conditions existing at the time of their formation. The process of formation of metal and metal-oxide aerosols is an extremely complicated one, since there are a large number of variables, and two or more processes may be occurring simultaneously. This means that quantitative comparison of experiment with theory is only fully justified when a large body of accurate data on such quantities as vapour pressure, surface tension and volume and surface diffusion coefficients is available. Unfortunately the data relating to metal oxides is extremely sparse, and therefore at best only semi-quantitative estimates of behaviour can be made.

In this section the observed data on rates of evaporation, arc-flame structure, temperature distribution round the arc, and mean particle size will be used to obtain very approximate values of the particle growth rate, particle concentration, and the vapour pressure and supersaturation at the start of growth. This can only be done for aerosols formed at atmospheric pressure, since it was not possible to observe the arc-flame structure at higher pressures.

As a first approximation the arc will be considered as a point source emitting vapour uniformly in all directions. In

actual fact the radial symmetry of the flame is disturbed by convection, which draws out the top of the flame vertically. (see fig. 68). However, previous work on the combustion of fuel drops which support spherical diffusion flames has shown that convection can be ignored for low flow rates. Gaydon and Wolfhard (1955) give the equation: $m = m_o(1 - \sqrt{Re})$ where m = evaporation rate, m_o = rate in the absence of convection, and Re = Reynold's number.

It appears certain that the thin bright zone observed at a small distance from the arc (see fig. 68) is due to incandescent aerosol particles (cf. Wolfhard and Parker 1949, referred to in section 1.3). The inner edge of this bright zone presumably corresponds to the first appearance of nuclei which then move radially outwards, growing as they do so. Immediately beyond the outer edge of the zone scattered light was visible, indicating units of the order of the wavelength of light in size. These must have been formed by coagulation of the individual particles, and the electron micrographs indicate that there was no further growth after coagulation. Thus there can have been no further condensation beyond the outer edge of the bright zone. The bright zone will therefore be identified with the zone of condensation of vapour.

The most clearly defined zone was obtained for gold, and since some data such as surface tension at high temperature are available for gold, the growth rate, particle concentration etc. will be calculated for the gold aerosol. Presumably the

values for the oxide aerosols will be of a similar order of magnitude.

4.1.1. The time available for growth, and the average growth rate.

An upper limit to the growth time of an individual aerosol particle is given straight away by the total time of striking the arc. In a typical case this would be about 5 sec. For a particle of radius 500 A this gives a growth rate of $\sim$ 100A/sec, which is already a high rate. A more realistic value is obtained by calculating the time taken for a particle to cross the condensation zone, assuming that a nucleus is formed at the inner edge of the zone, and moves radially outwards. The condensation zone is taken to be at a uniform temperature T, this value being obtained from the measured temperature gradient. (see fig. 70).

Let the inner edge of the zone be at a radial distance x from the arc. At a time t = 0 a nucleus is formed here by condensation from the vapour, and starts to diffuse radially outwards.

The mean square displacement of the particle after time t is given by the three-dimensional case of Einstein equation:

$$\overline{\Delta x^2} = 6Dt. \qquad \ldots(24)$$

(see e.g. Jost 1961)

The diffusion coefficient D is given by:

$$D = k T B \qquad \ldots(25)$$

where B = mobility = $(1 + A1/r + Q1/r.\ e^{-br/1}) / 6\pi\eta r$.

r = particle radius, 1 = mean free path, η = viscosity of gas, A,Q,b = constants, T = absolute temperature, k = Boltzmann's constant.

Values of B in terms of r, calculated for oil droplets in air at 25°C and atmospheric pressure have been tabulated by Fuchs (1964). In order to obtain B we must assume a value of the particle radius r. This will not be constant, since the particle will be growing throughout the zone; it will vary from the radius of the nucleus ($\sim$20A) at the inner edge of the zone, to the final radius ($\sim$500A) at the outer edge.

Let us consider first an average particle size during growth, of 250 A, this being the mean of the initial and final particle size. For gold, the bright zone was found to occur at a radial distance of $\sim$ 0.4 cm. from the centre of the arc, and the measurements of the temperature gradient indicated a temperature of 1000 - 1500°C at this distance. For a particle of radius 250 A, Fuchs (1964) gives log B = 8.95. For T = 1000°C, this gives D = 1.57×10^{-4} cm^2/sec.

For gold, the thickness of the condensation zone was 0.03 cm. Substitution of these values in the Einstein equation (see above) gives the time taken to move through the zone, t $\sim$ 1 sec.

This is the time taken to produce a particle of final

radius 500 A, and thus the average growth rate is 500 A/sec, a high rate. The mean radial velocity of the particle through the growth zone is then 0.03/1 = 0.03 cm/sec.

Taking the upper estimate of the temperature in the growth zone, T = 1500°C, we get D = 2.2×10^{-4}. The time taken to traverse the growth zone comes out to be $\sim$ 0.7 sec, giving a slightly higher growth rate.

These values may still be conservative estimates of the growth rate, however, since the growth will certainly not be linear with time, but will more likely decay approximately exponentially. Thus the major part of growth may take place at an early stage; the initial radial velocity of the nucleus may be maintained over much of the growth. For comparison, therefore, we can calculate the radial velocity of a nucleus, and thus the growth time if this velocity is maintained.

For a particle of radius 20 A, Fuchs (1964) gives log B = 10.903. For T = 1000°C, D is 1.4×10^{-2} and from Einstein's equation, the time taken to traverse the growth zone is 1×10^{-2} sec. The observed thickness of the growth zone is $\sim$ 0.03 cm, and thus the mean radial velocity of a particle in this case is $\sim$ 3 cm/sec. Thus for the production of a particle of final radius 500 A, the growth rate would be about 50,000 A/sec. This extremely high rate is of course only an upper limit, based on the particle radius remaining constant throughout the growth zone.

4.1.2. The particle concentration in the growth zone.

In order to calculate the particle concentration in the case of gold we use the measured evaporation rate and assume that the vapour is entirely converted to particles of the mean radius, 500 A. For gold, the evaporation rate at atmospheric pressure was found to be 0.003 gms/sec, and if this is assumed to be converted to particles of radius 500 A and density 20 gm/cc, this gives a rate of production of particles of 3×10^{11} particles/sec.

The nucleation of particles takes place at the inner edge of the condensation zone, at a distance x from the arc.
Let the rate of production of particles = $\frac{dN}{dt}$.
In a time dt, $x \longrightarrow x + dx$, and thus for a spherical shell of thickness dx:

$$dN = n\, 4\pi x^2\, dx ,$$

where n = particle concentration, number/cc.
Now the radial velocity of the particles = $v = \frac{dx}{dt}$,

$$\therefore \quad dN = n\, 4\pi x^2\, v\, dt$$

$$\therefore \quad \frac{dN}{dt} = n\, 4\pi x^2\, v .$$

Thus $$n = \left(\frac{dN}{dt} \right) / 4\pi x^2 v. \qquad \ldots(26)$$

For gold, the radial distance x of the inner edge of the condensation zone from the centre of the arc was 0.4 cm. For a radial velocity of 0.03 cm/sec (see previous section), and

$dN/dt = 3 \times 10^{11}$, particles per second, we obtain the particle concentration:

$$n \sim 5.10^{12} \text{ particles/cc.}$$

For a radial velocity of 3 cm/sec we obtain:

$$n \sim 5.10^{10} \text{ particles/cc.}$$

The distance apart of the particles can be obtained by considering each particle to occupy a cube of side y cm. Then for a concentration of 5×10^{12} particles/cc the distance apart would be about 6000 A. For a concentration of 5.10^{10} particles/cc the distance apart is about 27,000 A.

4.1.3. Coagulation of the aerosol particles.

For both the extremes of estimated mean concentration considered above, the distance apart of the particles shows that conditions would obviously be favourable for coagulation, giving rise to the observed chain formation. Two observations are relevant here. Firstly it was observed that after coagulation there had apparently been no further growth. From this it is concluded that growth was completed in a time shorter than that necessary for coagulation to become appreciable. Secondly it was observed that coagulation had occurred immediately beyond the outer edge of the condensation zone, this being indicated by scattered light. Thus the time for appreciable coagulation cannot be very much greater than the growth time, and is probably

of a similar order of magnitude.

The equation which describes coagulation is:

$$1/n - 1/n_o = Kt \qquad \text{(see section 1.2.7.)}$$

where n_o = initial number of particles, n = number of particles after time t, K = coagulation constant.

The coagulation constants for various materials have been listed by Green and Lane (1957), and the variation of the coagulation constant with particle radius has been described by Fuchs (1964). The value of the coagulation constant is typically about 5.10^{-10} cm^3/sec.

To get some idea of the time taken for coagulation to become significant, we will consider the time taken to halve the number of particles, i.e. Each particle has coagulated with one other particle, thus $n = n_o/2$.

For $n_o = 5.10^{12}$ particles/cc, and $K = 5.10^{-10}$ cm^3/sec, we get:

$$t \sim 0.001 \text{ sec.}$$

For $n_o = 5.10^{-10}$ particles/cc, and $K = 5.10^{-10}$ cm^3/sec, we get:

$$t \sim 0.04 \text{ sec.}$$

To fit in with the observed coagulation behaviour, this time should be of a similar order to the growth time. For a particle concentration of 5.10^{12}/cc a growth time of $\sim$ 1 sec was inferred (section 4.1.1) which is much greater than the time to halve the number of particles, 0.001 sec. For the particle concentration 5.10^{10}/cc, however, the growth time came out as 0.01 sec. which is

of the same order as the time to halve the number of particles, 0.02 sec. Hence we may conclude that these latter values are the better estimates of the particle concentration and the growth time.

4.1.4. The nucleation rate, supersaturation and vapour pressure at the start of growth

The process of nucleation followed by growth has been discussed by Nielsen (1964). He states that, for a diffusion-controlled or polynuclear layer growth mechanism, the nucleation rate may be expressed as:

$$J = N/t \qquad \ldots(27)$$

where N = number of particles produced/cc and t = time during which the N particles/cc are produced.

In the case of gold the overall mean rate of production of particles was found to be $\sim 3.10^{11}$ particles/sec (section 4.1.2). To obtain N, this value must be divided by the volume of the condensation zone.

For gold, the volume of the condensation zone = $1.4\ 10^{-2}$cc.

$$\therefore \quad J = 2.10^{13}/\text{cc/sec.}$$

This value can now be inserted in the expression for the nucleation rate (Equation 4, section 1.2.1) in order to obtain the supersaturation. If a round estimate of 10^{30} is made for the pre-exponential factor (Nielsen 1964) the expression becomes:

$$\log J = 30 - A (\log S)^{-2} \qquad \ldots(28)$$

where S = supersaturation

$A = \beta \sigma^3 v^2 (kT \ln 10)^{-3}$

β = shape factor = 16.76 for a sphere

σ = surface tension

v = molecular volume, taken as $\frac{\text{molecular weight}}{\text{density x Avogadro No.}}$

Taking σ = 1000 dynes/cm for gold, we obtain $A \sim 100$, and thus

$$S \sim 300.$$

Thus for the gold aerosol a supersaturation of about 300 is indicated, confirming the supposition of previous workers that arc smokes are formed under conditions of very high supersaturation.

From the supersaturation the vapour pressure in the growth zone can now be calculated, since $S = p/p_\infty$.

For 1500°C the equilibrium vapour pressure of gold (p_∞) is 1.7×10^{-2} mm Hg. (Kubaschewski and Evans 1951). Hence the vapour pressure in the growth zone is:

$$p \sim 5 \text{ mm Hg}$$

This result gives us an alternative method for calculating the particle concentration. If we assume this vapour to be entirely converted to particles of radius 500 A and density 20 gm/cc, then we obtain: for the particle concentration:

$$n \sim 10^9 \text{ particles/cc}$$

Considering the approximations made, this agrees quite well with the value of n $\sim$ 10^{10} particles/cc previously calculated above.

4.1.5. Summary of the measured and calculated conditions for the formation of the gold aerosol in air at atmospheric pressure.

1) Temperature at which condensation occurs 1000 - 1500°C.
2) Growth rate 500 - 50,000 A/sec.
3) Particle concentration in growth zone 10^9 - 10^{10} particles/cc.
4) Supersaturation at start of growth $\sim$ 300.
5) Vapour pressure in growth zone $\sim$ 5 mm Hg.

Table 25 The recrystallisation temperatures of metal oxides.

Oxide	Recrystallisation Temperature °C.	Oxide	Recrystallisation Temperature °C
Al_2O_3	650	UO_2	< 20
Fe_2O_3	130	MoO_2	~200
NiO	150	MoO_3	~200
SnO	100	WO_3	~380
ZnO	< 20	ZrO_2	~420
CdO	< 20	Nb_2O_5	~590
MgO	< 20	Ta_2O_5	~700
Sb_2O_3	< 20	TiO_2	> 550
Bi_2O_3	250-300		

4.2. THE CRYSTAL STRUCTURE AND TEMPERATURE OF FORMATION OF THE AEROSOLS

Previous investigators into the structure of metal oxide aerosols (Walmsley, 1927; Yearian et al., 1935; Finch and Wilman, 1937; Erhardt and Lark-Horowitz, 1940; Harvey, Matthews and Wilman, 1960) found that the particles in smokes produced from electric arcs are crystalline in nature. In the present work also, for all the materials investigated, in both air and CO_2, the aerosol particles formed were found to be crystalline.

Harvey, Matthews and Wilman (1960) pointed out that this indicates that the smoke particles were formed at a temperature higher than the crystallisation temperature of the aerosol material. They state that this temperature is moderately well-defined, and is not much lower than the recrystallisation temperature of the particular material. Wilman (1956) has given a list of the recrystallisation temperatures of metal oxides observed by a number of workers; at these temperatures a deposit which was initially amorphous showed appreciable crystallisation, crystals of at least 30 A diameter being produced after 30 minutes heating. These temperatures are given in Table 25, p.149, together with the values for MoO_2, MoO_3, and WO_3 (Levin, 1956); ZrO_2, Nb_2O_5, and Ta_2O_5 (Harvey, 1960), and TiO_2 (Conjeaud, 1955).

Thus, of the materials investigated in the present work, the minimum temperatures of formation of the particles are: Al_2O_3 650°C, MgO < 20°C, and UO_2 < 20°C, and ZrO_2 420°C. There

do not appear to be any data in the literature for the recrystallisation temperature of $NiO.Fe_2O_3$. (A large number of substances have been included in Table 25 since the recrystallisation temperature appears to be of some significance in determining the shape and size of the aerosol particles. This will be discussed in a later section).

Of the materials investigated, only Al_2O_3 and ZrO_2 exhibit polymorphic forms. For the Al_2O_3 smoke, the particles were found to be composed of the γ-form, stable in the lower temperature range. This gives an upper limit of between 750 - 1000°C for the temperature of formation of the particles, since in this temperature range the transformation to the high-temperature α-form (corundum) takes place. It does not seem likely that the particles were formed at a temperature higher than this, because in that case α - Al_2O_3 would have been formed. Due to its great stability the α - Al_2O_3 would not have been transformed to the γ modification on cooling. A further relevant result of Harvey, Matthews and Wilman (1960) for the Sb_2O_3 aerosol is that smokes from an Sb arc in air at atmospheric pressure were composed of a mixture of the orthorhombic and cubic forms of Sb_2O_3. The orthorhombic form is normally only stable above 570°C, and therefore Harvey et al concluded that it had remained stable due to rapid quenching. In the Al_2O_3 case, if the α modification had been formed initially, it might be similarly expected that this modification would predominate in the final smoke deposit.

The smokes generated from the Zr arc in air and CO_2 were found to be composed entirely of the cubic form of ZrO_2, there being no evidence of the monoclinic form. Unfortunately this does not give any indication of the temperature of formation of the aerosols. As was pointed out in section 3.1.6, the cubic form is not normally a stable modification of ZrO_2, but it may be stabilised by the presence of particular substances. Runck (1956) has stated that if the cubic lattice is stabilised with CaO, it will remain stable at all temperatures up to the boiling point, whereas if it is stabilised with MgO, it may revert to the monoclinic form at low temperatures. This supports the previous assertion that the occurrence of the cubic form in the present case is probably due to the Ca impurity present in the Zr metal. To obtain information as to the temperature of formation from the particular polymorphic form occurring, it is clear that Zr metal of much higher purity must be used.

For the other aerosols investigated, MgO, $NiO.Fe_2O_3$, UO_2 and U_3O_8, and Au, there are similarly no indications as to the upper limit of the temperature of formation, apart from the fact that it must be below the boiling point of the particular material.

4.3. THE PARTICLE SHAPE.

4.3.1. Characteristic particle shapes observed in aerosols formed at atmospheric pressure.

For each arc material, in both air and CO_2, a characteristic particle shape was observed. The differences in particle shape between the different materials were most marked at atmospheric pressure. The results point towards a definite correlation between the observed particle shape and the crystallisation temperature of the particular material. It was found that the aerosols of MgO and UO_2 formed in air and in CO_2 were composed of well-defined polyhedral particles, each individual particle being a single crystal. Both of these materials crystallise readily at temperatures below 20°C. Aerosols of ZrO_2, with a crystallisation temperature of about 420°C, and $NiO.Fe_2O_3$, were composed of a mixture of polyhedral particles and more spherical particles. Aerosols of Al_2O_3, which has a crystallisation temperature of about 650°C, were found to consist of particles which were practically perfect spheres.

The only previous data on metal-oxide aerosols with which these results may be usefully compared appear to be those of Schechter (1946) and Harvey, Matthews and Wilman (1960). Schechter found that arc smokes formed in air from Au, Al, KCl and NaCl were comprised of spherical particles. Ag and Cu gave a mixture of spheres and cubes, and Mg and Zn gave regular

polyhedral particles. Harvey, Matthews and Wilman found that smokes from arcs in air at atmospheric pressure of Al, Zr, Ti and Ta gave oxide particles which were mainly spherical in shape. The recrystallisation temperatures of TiO_2 and Ta_2O5 are 550°C and 700°C respectively. On the other hand, oxide particles in smokes from Cu, Zn, Cd, Sn, W, Fe, Co and Ni arcs in air at atmospheric pressure were found to consist of well-developed polyhedra. The recrystallisation temperatures of all these oxides are low.

Clearly, the molecules of oxides with low crystallisation temperatures will have high mobility at high temperatures of formation and thus migration of molecules over the surfaces of the growing particles will be rapid, leading to plane faces and well defined polyhedral particles, such as those observed for MgO (see fig. 16). Molecules of oxides with high crystallisation temperatures will have lower mobility, and thus the formation of plane faces will be less favoured.

The occurrence of different particle shapes for different materials may also be discussed in relation to the ease with which nucleation can take place for a particular substance. This almost certainly has a strong connection with the mobility of the atoms or molecules and thus with the crystallisation temperature. The problem has been discussed by Egli and Zerfoss (1949), in relation to crystal growth from solution. They point out that in aqueous solution, compounds which grow readily are all quite soluble, whereas slightly soluble compounds are only grown

as crystals with great difficulty. For any substance a range of supersaturation must be considered, corresponding to (1) low supersaturations which will produce only perfect crystal growth, (2) higher supersaturations which will produce flawed growth, and (3) still higher supersaturations which will induce the spontaneous formation of 3-dimensional nuclei. The supersaturation necessary for perfect growth will be dependent on crystal configuration but will in general be lower than that required for nucleation. On this basis, compounds which are difficult to crystallise are those which form spontaneous nuclei at very small degrees of supersaturation, so that the range available for growth is very small. Easily grown crystals are those for which nuclei form only with considerable supersaturation so that there is a large range in which only perfect growth is obtained.

This dependence of the "ease of growth" on the supersaturation necessary to initiate nucleation will therefore affect simultaneously the crystal shape and the number and size attained. In the present work it was found that Al_2O_3 smokes formed in air at atmospheric pressure consisted of enormous numbers of very small spherical particles, while MgO smokes formed under the same conditions consisted of a smaller number of much larger particles which were mostly perfect cubes. The above argument of Egli and Zerfoss would therefore indicate that, at atmospheric pressure, the supersaturation necessary to initiate

nucleation of Al_2O_3 particles is low, whereas that for MgO particles is relatively high. Al_2O_3 and MgO represent extremes of the range for the substances investigated. UO_2, $NiO.Fe_2O_3$ and ZrO_2 might be expected to fall somewhere between Al_2O_3 and MgO in terms of the supersaturation necessary to initiate nucleation. Since this supersaturation clearly determines the nucleation and growth behaviour of the particles, it will be discussed further in the later section devoted to particle size.

Egli and Zerfoss also suggest that another criterion in determining the nucleation behaviour of a substance is its state of association. Thus NaCl, although soluble, is highly dissociated in solution, and it is found that NaCl is very hard to grow into a perfect crystal at any reasonable rate. It forms copious nuclei at very small degrees of supersaturation. On the other hand, HIO_3 is highly associated in solution; nuclei form only with considerable supersaturation, and large perfect crystals are easily grown.

An important point is whether the aerosol particles were formed initially as liquid drops which subsequently solidified or were formed by a direct vapour/solid transition. There has been some controversy on this point in the literature. At first sight the evidence in favour of the initial formation of liquid drops appears formidable. If the particles first form as liquid drops, and grow as such, then for the arriving molecules any site on the surface of the droplet is as good as any

other, and thus there is no limitation on the rate of growth due to the necessity for surface nucleation. For direct nucleation of a crystal from the vapour, the critical supersaturation necessary for surface nucleation must be maintained to allow continued growth. This supersaturation has a value of about 2/3 that necessary for the initial 3-dimensional nucleation to form the original nuclei from the vapour (Nielsen, 1964). This argument only holds good if we allow that the presence of dislocations is unlikely.

These facts would indicate that the initial formation of liquid drops should be highly favoured. The production of polyhedral particles for those oxides with low recrystallisation temperatures could again be explained in terms of the mobility of the oxide molecules; thus after solidification the particle shape would be determined by the time available for cooling to the recrystallisation temperature. For oxides with low recrystallisation temperatures this would be longer, and therefore particles of these oxides would be more likely to form plane faces. Also, the parallel orientation of polyhedral particles in chain-like aggregates (e.g. fig. 32) could be explained in terms of the initial formation of liquid drops. Thus after solidified drops had aggregated into chainlike groupings, a polyhedral particle present in a chain might be able to "seed" neighbouring particles, and thus transmit its own orientation along the chain. Another possible explanation of this corner-to-corner or edge-to-edge orientation of particles is that it is due to electric charge

on the particles (Whytlaw-Gray, 1922).

Stewart (1956), in his theoretical study of the condensation of metal oxides in the fireball of a nuclear explosion, assumed that liquid drops would be formed first, since the rate of cooling of the body of vapour would be relatively slow. Making a number of somewhat dubious assumptions, including the assumption that growth by the coagulation of drops would predominate over molecule-by-molecule growth, he showed that the condensation should result in a Log-Normal distribution in the final particle sizes. In the present work, all the aerosols were found to follow the Log-Normal distribution.

Thus, there are a number of reasons for supposing that liquid drops might be formed initially in the condensation of the oxide vapour generated by the arc. However, there is one fact which clearly contradicts this supposition for the case of Al_2O_3. The Al_2O_3 aerosols formed from the Al arc were found to consist of γ - Al_2O_3, the low-temperature form. This is only formed below 1000°C; above 1000°C it transforms to the α-modification, and this transformation is not reversible i.e. on cooling the α-form will not transform to the γ-form. If the Al_2O_3 vapour condensed initially as liquid drops, it must necessarily have been as the α-form which is the only modification stable above the melting point (2020°C). Since α-Al_2O_3 was not detected in the smoke, it appears probable that the aerosol particles were formed by a direct vapour/crystal transition, at a temperature below 1000°C.

Harvey, Matthews and Wilman (1960) found that particles from a Ti arc in air at atmospheric pressure consisted of the anatase modification of TiO_2. Conjeaud (1955) had previously shown that TiO_2 condensed on a substrate was amorphous below 550°C, anatase or rutile between 550°C and 800°C, and rutile alone above 800°C. Harvey et al therefore concluded that the TiO_2 arc smokes had been formed between 550°C and 800°C. This is well below the melting point of TiO_2 (1850°C) and therefore again suggests the formation of particles by a direct vapour/crystal transition.

In the condensation of water vapour to form ice crystals, a direct vapour/crystal transition at temperatures below -65°C has been suggested by a number of workers (Sander and Damkohler 1943, Pound et al 1955, Mason et al 1959). Buckle and Ubbelohde (1960) investigated the formation of NaCl aerosols using a diffusion cloud chamber. At low chamber temperatures (i.e. high supersaturations) they found evidence of direct nucleation of crystals from the vapour. With increasing supersaturation particle growth gave way to particle multiplication, the particles remaining small because the supersaturation necessary for surface nucleation was not maintained.

4.3.2. The change in particle shape with increase in gas pressure.

With the exception of Al_2O_3 and Au, the aerosol particles of all the materials investigated showed a trend towards more spherical shape with increase in the gas pressure at which they were formed. There is very little previous work with which these results may be compared. There have been a few isolated experiments at reduced pressures, but there appear to have been no previous investigations into aerosol formation at gas pressures above atmospheric.

Most of the useful relevant work on the variation of crystal habit with gas pressure has been concerned with the growth of ice crystals from water vapour. Marshall and Langleben (1954) suggested that the basic habit of ice crystals grown from the vapour in air was determined by the flux df vapour towards the growing particle (i.e. by $D(c - c_\infty)$), and therefore the habit might be expected to change if the crystals were grown in gases other than air, or at reduced pressures. Kobayashi (1958) investigated the effect of lowering the air pressure on the growth habit of ice crystals. He observed a change in habit below 70 mm Hg; hollow prisms gave way to solid prisms. The growth rate was much lower, suggesting that the increased value of the diffusion coefficient was more than offset by a reduction in the excess vapour concentration. However, Kobayashi's experimental arrangements caused the supply of water vapour to the crystals to be much reduced,

and this fact led Mason (1963) to conclude that in fact the basic habit was not altered by the nature and pressure of the gas. Van den Heuvel and Mason (1959) investigated the growth of ice crystals under various conditions, and found that the variation of habit with temperature was unchanged by reducing the air pressure to 20 mm, or by using air, CO_2, H_2 or He as the gas. However, the growth rate of the crystals was found to be affected. Mason (1963) has concluded that the principal factor controlling the basic habit of ice crystals grown from the vapour is the temperature, while secondary features are controlled by the supersaturation.

In the present work, the electric arc was used to generate the aerosols. Increasing the gas pressure in which an arc is operating causes both the electrode temperature and the vapour pressure at the electrode surface to increase. Thus the diffusion coefficient of the vapour, the temperature of formation of the particles and the excess vapour concentration might all be expected to change considerably with increase in the gas pressure. If we accept Mason's conclusions that crystal habit is independent of gas pressure, then the observed variations in habit must be due to variations in temperature and supersaturation, themselves functions of gas pressure in the present system. This leads to a discussion of the particle growth rate, which is obviously important in determining the ultimate particle size.

Besides the tendancy towards a more spherical shape, all the oxide aerosols showed an increase in particle size with increase in the gas pressure. It seems likely that these two

effects are intimately connected. A change in the growth rate with change in the gas pressure is the most obvious explanation for this behaviour. It is well known (Egli and Zerfoss 1949) that the difference in the growth rates of various crystal faces becomes smaller as the overall rate is increased. Thus the appearance of perfect cubes of MgO in the aerosol generated in air at atmospheric pressure could be due to a relatively low growth rate, so that high index faces grew out of the crystal, leaving only low index faces; if the growth rate increased with increase in the gas pressure the difference in the growth rate of various planes would decrease, and thus higher index facets might still be in evidence in the final crystal. This could give rise to the rounded corners seen in crystals of MgO formed in air at 500 p.s.i.

For diffusion-controlled growth, we have the expression for the growth rate:

$$\frac{dr^2}{dt} = 4\pi D(c - c_\infty) \qquad \text{(see section 1.2.5.)}$$

For an increase in the growth rate we must therefore have an increase in the diffusion coefficient D, or an increase in the excess vapour concentration $(c - c_\infty)$. The diffusion coefficient is directly proportional to the vapour concentration and inversely proportional to the gas pressure. Thus increase of the gas pressure to 500 p.s.i. should decrease the diffusion coefficient by a factor of ~ 30. A corresponding increase in the excess vapour concentration would be necessary to just maintain the growth

rate at its atmospheric pressure value. To produce a net increase in the growth rate at 500 p.s.i. a still higher vapour concentration would be required, and this does not seem likely. Even if the modification of Fuchs (1934) to the growth equation is taken into account, an increase in growth rate with increase in pressure seems improbable. Fuchs proposed that growth should take place at the rate it would have in complete absence of the gas up to a limiting particle radius, depending on the distance Δ, (see section 1.2.5.). Up to this limiting radius, growth is thus independent of diffusion. $\Delta \gg r$, where r is the particle radius, is normally taken as being a sufficient condition for growth to be independent of diffusion through the surrounding gas. (Bradley, Evans and Whytlaw-Gray 1946; Wright 1961). For metal-oxide particles a typical value is Δ = 4000 A in air at atmospheric pressure. At 500 p.s.i. this value will be reduced to $\sim$ 100 A. Thus diffusion can only be ignored when particles are very much smaller than this. Since particles with a mean radius of 500 A and greater were found in aerosols generated at 500 p.s.i., the above condition is not fulfilled, and therefore diffusion cannot be ignored in the present case. Thus the proposal that an increase in the growth rate is responsible for the change in crystal shape with increasing gas pressure does not seem too promising.

An alternative explanation arises out of a theoretical discussion made by Mullins and Sekerka (1963), who considered the morphological stability of a particle growing by diffusion or heat

flow. They investigated the diffusion-controlled growth of a nearly-spherical particle from a supersaturated matrix, and obtained an approximate solution of the time-dependent diffusion problem and the moving boundary problem taken together. The solution obtained approximates to:

$$R_c = \frac{1.4 \times 10^{-6}}{(c_\infty - c_o)/c_o} \qquad \ldots(29)$$

for the critical radius at which a sphere becomes unstable. This value is only seven times that which a sphere must have in order to be able to grow initially. Thus for 10% supersaturation, spheres bigger than 0.14μ are unstable. A diagrammatic plot of R_c against $(c_\infty - c_o)/c_o$ is shown in fig. 71.

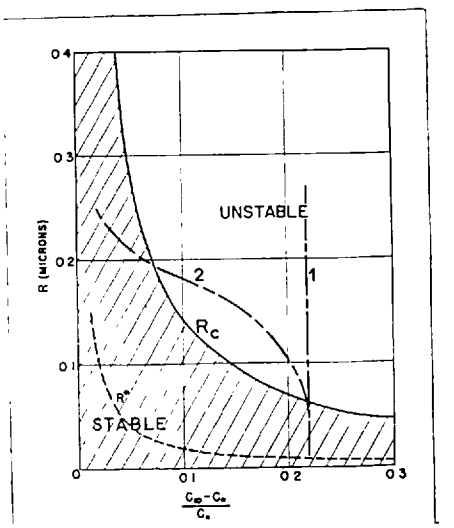

Fig. 71 Plot of the critical radius for a stable sphere against supersaturation. (Mullins and Sekerka, 1963).

An isolated sphere growing in a supersaturated vapour would eventually exceed R_c and become unstable. Its growth is represented by path 1 in fig. 71, starting from the R^* curve. (R^* is the critical nucleus size). The average growth of a number of spheres, on the other hand, would correspond to a path such as 2, which curves to the left as the overlapping diffusion fields of different spheres reduce the effective supersaturation. Mullins and Sekerka suggest that although the path could conceivably always remain in the stable zone, it is probable that it would penetrate far into the unstable zone during the early stages of growth, since at that time the particle size is expected to be several orders of magnitude greater than R^*. The fact that spheres are not seen in the early stages of precipitations is in accord with these theoretical expectations, although Mullins and Sekerka note that there are also undoubtedly strong crystallographic factors determining which faces are still coherent. They state that in the later stages of growth the interface usually becomes non-coherent, thereby minimizing crystallographic factors; at the same time there is a marked tendancy towards increased spheroidization and coarsening of the particles. Mullins and Sekerka conclude that the concomitance of coarsening and spheroidization is in significant accord with their calculations.

In the present work it is clear that the aerosol particles grow under conditions of very rapidly decling supersaturation, due to competition between large numbers of particles and consequent depletion of the vapour. A growing particle might

be expected to follow a path such as 2 in fig. 71. A spherical nucleus initially present would rapidly grow to a size at which the spherical shape was unstable and crystal faces would develop. It would continue to grow in a well-defined crystal habit until the supersaturation had fallen to such a value that a spherical shape was again stable. The final stage of growth would thus tend back towards a sphere, but at a very slow rate. The appearance of well-defined polyhedral particles or more spherical particles, depending on the gas pressure, may be explained in terms of the conditions of supersaturation during growth and the quenching rate.

With a very high supersaturation present in the vapour, a particle would start growing at some point to the far right of fig. 71 and would spend most of its time of growth in the unstable region i.e. the region of only polyhedral growth. The polyhedral particle would pass through the final region where the spherical form is again stable with probably only very little additional growth. In this way well-defined polyhedral particles may appear in the final aerosol. For lower supersaturations the amount of growth taking place in the unstable zone will be smaller; indeed in the limit of very low supersaturations (i.e. the extreme left of fig. 71) the growth path of a particle will not penetrate at all into the unstable zone, there will be no polyhedral growth, and perfect spheres will result. In this way the supersaturation present at the start of the

condensation could determine the particle shape in the final aerosol. The quenching rate may also affect the particle shape: at atmospheric pressure the vapour cloud will be moving relatively rapidly away from the arc, and thus we may expect initial rapid nucleation and growth to be followed by rapid quenching. It would be possible for most of the growth to take place in the region of polyhedral growth, and the final stage of stable spherical growth be passed through with little further condensation. At higher gas pressures the rate at which vapour can move away from the arc will be decreased, and the quenching rate will be correspondingly lower. Thus there is more possibility of spherical growth in the final stage.

A significant result of applying the theory of Mullins and Sekerka to the present work is the proposal that the supersaturation present in the vapour must decrease with increase in the gas pressure at which the aerosol is formed. This will be discussed further in the next section on particle size.

4.4. THE PARTICLE SIZE

In the formation of aerosol particles, three phenomena in general occur; nucleation, growth and coagulation. In the present work the evidence (no further sign of growth after chain formation) indicates that coagulation does not occur during formation of the individual particles. The nucleation and growth rates of the particular aerosol will thus determine its mean particle size and size distribution.

4.4.1. The mean particle size of aerosols formed at atmospheric pressure.

The particle sizes of aerosols formed at atmospheric pressure are of special interest since previous results on metal oxide aerosols have all been obtained at atmospheric pressure or below.

A factor of great importance in the nucleation of a vapour is the critical supersaturation which must be established to initiate nucleation. This is usually defined as the supersaturation for which J = 1. (J = nucleation rate; see section 1.2.). An expression for the critical supersaturation can be obtained by inserting this value in the equation for the nucleation rate (eqn. 4 , Section 1.2.1.) and combining this with the Gibbs-Kelvin equation (eqn. 1 , section 1.2.). The expression obtained for the critical supersaturation is:

$$\ln (p/p_\infty)_{crit} = K (\gamma/T) M/\rho \qquad \ldots(30)$$

where $(p/p_\infty)_{crit}$ is the critical supersaturation, γ is the surface tension at temperature T, M is the molecular weight, and ρ is the density of the material; K is a constant. In order to obtain the value of the critical supersaturation for any material it is thus necessary to know the surface tension. Only a very few determinations of the surface energies of metal oxides have been carried out. All the data available in the literature are given in Table 27. (Taken from Kingery, 1960).

Table 27: The surface energies of metal oxides.

	Material	Temperature °C	Surface Energy (γ) ergs/cm^2
SOLID	Al_2O_3	1800	905
	ZrO_2	1800	590
	MgO	25	1000
LIQUID	Al_2O_3	2050	690
	FeO	1420	585
	La_2O_3	2320	560
	ZnO	1300	455
	PbO	900	132

It can be seen that the values for MgO and Al_2O_3 are considerably

higher than those for any of the other oxides quoted. The figure for MgO is the value at 25°C; however, since the surface energy is relatively insensitive to temperature, this should not be too different from the value at 1800°C. The surface energy tends to decrease slightly with increase in temperature. For the purposes of comparison we can assume a lower limit of 500 ergs/cm^2 for MgO. The values of the critical supersaturation necessary to initiate condensation of Al_2O_3, MgO and ZrO_2, calculated from equation 30 , are given in Table 28 .

Table 28: Critical supersaturations for the condensation of metal oxides.

Oxide	$(p/p_\infty)_{crit}$	T°C	Mean particle diameter (Air, atmospheric pressure) (μ)
Al_2O_3	104.9	1800	0.029
ZrO_2	10.4	1800	0.016
MgO	8.7 (γ=1000)	1800	0.034
	2.1 (γ=500)		

In order to correlate these critical supersaturations with the observed particle size in aerosols formed at atmospheric pressure, we must consider the manner in which the supersaturation might be

expected to vary with distance away from the arc. A similar problem in the diffusion cloud chamber has been studied by Hallett and Mason (1958) for ice crystals, and by Price (1960) for the growth of cadmium and zinc crystals. In both cases the diffusion coefficient of the diffusing species was taken to be independent of temperature, and thermal diffusion was ignored. Hallett and Mason carried out a more detailed calculation accounting for the variation of diffusion coefficient with temperature and found only a few percent difference from the simplified treatment.

If we assume that the vapour concentration at the arc electrodes corresponds to the saturation vapour pressure at the arc temperature, and that vapour transport occurs solely by molecular diffusion, then the diffusion equation (equation 8, section 1.2.5) predicts a linear variation in vapour density with radial distance from the arc. Hallett and Mason showed that the supersaturation in the diffusion cloud chamber increased with distance from the vapour source, up to a maximum value, and then subsequently decreased. A similar variation of supersaturation with distance from the arc might be expected in the present case. Thus, for a given vapour pressure, vapours of metal oxides with low critical supersaturations would begin to condense relatively close to the arc, while those with higher critical supersaturations would have to move further away from the arc before the value necessary to initiate nucleation was reached. However, the further away from the arc nucleation commenced, the lower would be the vapour

concentration. There would be correspondingly less vapour per particle available for growth. Thus it might be expected qualitatively that vapours with higher critical supersaturations would exhibit a lower mean particle size in the final aerosol. Since the lack of surface energy data precluded the calculation of the critical supersaturation in all but three cases, it is not surprising that the values given in Table 28 do not show any convincing agreement with this proposal. Also, it may be that in practice any such variation would not be observable with any precision at the level of accuracy of the present experiment; due to the steepness of the temperature gradient, the supersaturation will increase rapidly over a very short distance with only a very small drop in total vapour concentration. Thus in the case of gold, calculation shows that over a radial distance of 1 mm the supersaturation increases by a factor of $\sim 10^2$, while the concentration falls to only about 4/5 of its initial value.

4.4.2. The correlation between mean particle size and shape in aerosols formed at atmospheric pressure.

In the aerosols generated in air and in CO_2 at atmospheric pressure, an apparent correlation between the mean particle size and particle shape for a given material was observed. In general, aerosols which were composed of regular polyhedral crystals were found to have a larger mean size than those which were spherical or nearly so. Thus, particles of aerosols from the Mg arc (mean

diameter 0.046 μ in air; 0.036 μ in CO_2), the magnox arc (0.046 μ in air; 0.018 μ in CO_2) and the UO_2 arc (0.042 μ in air, 0.027 μ in CO_2), all of which were largely composed of regular polyhedral crystals, were in general larger than those from the Al arc (0.029 μ in air; 0.027 μ in CO_2), the stainless steel arc (0.016 μ in air, 0.022 μ in CO_2) and the Zr arc (0.016 μ in CO_2), for which the particles were more spherical in shape.

Examination of the electron micrographs obtained by Harvey, Matthews and Wilman (1960) reveals a similar trend. They found more or less spherical particles in aerosols formed in air at atmospheric pressure of Ta_2O_5 (0.012 μ dia.), Al_2O_3 (0.03μ), ZrO_2 (0.03μ), TiO_2(0.03μ), and well-developed polyhedra of ZnO(0.4μ), Sb_2O_3(0.2μ), MoO_3(0.15μ), WO_3(0.05μ), NiO(0.05μ) and SnO_2(0.05μ). Their particle size measurements were only approximate.

This general correlation between shape and size would appear to indicate that the mobility of the vapour molecules on the surface of a growing crystal, and the nucleation and growth rates are all dependent to some extent on a common factor. This common factor may be the surface energy, which enters into the expression for the nucleation rate, and on which the mobility is presumably strongly dependent.

4.4.3. The effect of increased gas pressure on the mean particle size.

The effect of increasing the gas pressure on the mode of generation of the aerosol particles is undoubtedly complex, since the variables in the system will not be independent. A change in the gas pressure will give rise to a corresponding change (of unknown magnitude) in the arc temperature, and thus also to the rate of vaporization of material from the arc.

Approximate measurements of the vaporization rate of gold at 500 p.s.i. indicated a slight increase, of about 5%, over the mean rate at atmospheric pressure. The mean particle diameter of the aerosol formed at 500 p.s.i. was 0.102μ, while that of the aerosol formed at atmospheric pressure was 0.08μ. Thus there was an increase of approximately 20% in particle diameter in going from atmospheric pressure to 500 p.s.i.

The approximate mean rate of production of particles in air at 500 p.s.i. can be calculated using the measured evaporation rate of gold, and with the assumption that the vapour is entirely converted to particles of the mean radius, as was done previously for atmospheric pressure in section 4.1.2. This results in a value for the rate of production of particles in air at 500 p.s.i. of approximately 2×10^{11} particles/sec. Thus the overall rate of production of particles at 500 p.s.i. is approximately 2/3 of the rate at atmospheric pressure.

In order to calculate the nucleation rate at 500 p.s.i.

as was done for atmospheric pressure, the volume of the growth zone at 500 p.s.i. would be required. However, with the present apparatus it was unfortunately impossible to observe the arc at raised pressures, and thus measurements of the zone thickness and radial distance from the arc could not be measured. The volume of the condensation zone at 500 p.s.i. is therefore unknown. However, if the volume of the zone at 500 p.s.i. is not much different from that at atmospheric pressure, then a decrease in the nucleation rate is indicated. This would be in agreement with the proposition of Bradley (1960) that the nucleation rate should decrease with increase in the gas pressure (see section 1.1.2.), due to the effect of pressure on the saturated vapour pressure of the vapour. For a static system there would appear to be no simple alternative explanation for the increase in mean particle size with increase in gas pressure. The increase in vaporization rate obviously gives more vapour available for growth. The variation in vapour concentration of the metal or metal oxide with radial distance from the arc should be independent of the gas pressure (Fuchs 1959).

However, in the present case we have a dynamic system, since the vapour is moving rapidly outwards in a radial direction from the arc. In the case of the gold aerosol formed at atmospheric pressure, calculation showed that a supersaturation of the order of 300 existed in the vapour at the start of growth. The critical supersaturation for gold at 1000°C, calculated from equation 30 is about 5 (assuming γ = 1000 ergs/cm^2 and the constant K = 0.557).

The great difference between these two values is presumably explained by the rapid radial movement of vapour. It must be moving sufficiently rapidly that it can reach the zone of supersaturation 300 without previously condensing, although condensation would have been possible from the time when its supersaturation had reached a value of about 5.

Clearly, as the gas pressure in the system is increased the radial velocity of the vapour will decrease due to decrease in the value of the diffusion coefficient. It will not be able to move so far beyond the zone of critical supersaturation before condensing, and hence nucleation will begin at a lower supersaturation than in the case of atmospheric pressure. Since the supersaturation is lower, the nucleation rate will be lower; hence there will be more vapour per particle available for subsequent growth. Thus particles in the resultant aerosol will in the mean be larger than those formed at a lower pressure.

On this basis we would expect different materials to show a different pressure dependence of particle size, since the diffusion coefficient will vary from material to material. The diffusion coefficient of a vapour is proportional to $(1/m_1 + 1/m_2)^{\frac{1}{2}}$ where m_1 and m_2 are the molecular weights of the diffusing vapour and the gas. For a given surrounding gas, m_1 will be constant, and hence for aerosols generated in the same surrounding gas, those with lower molecular weights should show a greater increase in mean particle size with increase in pressure. This effect is

borne out by the results. For the oxide aerosols formed in air, MgO, with M.Wt. 40.32, showed the greatest increase in particle size with pressure, followed by Al_2O_3 (M.Wt. 101.94), followed by UO_2 (M.Wt. 270.07) and stainless steel (nickel ferrite, M.Wt. 234.39). Similar, although not quite so systematic, behaviour was observed for aerosols formed in CO_2. The rates of change of particle diameter with pressure for the different aerosol materials in air and CO_2 are given in Table 29 . These rates of increase of particle size with pressure were obtained from the measured particle sizes using the method of least squares.

This evidence for a decrease in the nucleation rate with increase in the gas pressure fits in with the possible interpretation of the change in particle shape with increase in pressure suggested in section 4.2. using the theory of Mullins and Sekerka (1963).

Table 29: The rate of variation of particle diameter with increase in gas pressure.

Aerosol material	$(1/m_1 + 1/m_2)^{\frac{1}{2}}$		Rate of increase of particle diameter with pressure (μ/p.s.i.)	
	Air	CO_2	Air	CO_2
MgO	0.2431	0.2179	4.01×10^{-4}	1.62×10^{-4}
Al_2O_3	0.2102	0.1803	2.70×10^{-4}	1.83×10^{-4}
ZrO_2	-	0.1755	-	0.66×10^{-4}
$NiO.Fe_2O_3$	0.1967	0.1643	0.72×10^{-4}	0.35×10^{-4}
UO_2	0.1949	0.1625	2.03×10^{-4}	0.85×10^{-4}

4.3.4. The particle size distributions

From the shape of the particle size distributions occurring in the aerosols it is possible to make some suggestions as to the nature of the nucleation and growth processes. There has been some previous speculation as to the factors determining the distribution function in disperse systems, as was described in section 1.5.1. Thus the Log-Normal distribution arising from the grinding of solids has been derived from consideration of the grinding process (Kolmogoroff 1941, Epstein 1948), and Kottler (1950) showed that a Log-Normal distribution of grain sizes in photographic emulsions could result from an exponential law of growth, if the growth times were Normally distributed.

In the present case it was felt that it might be possible to derive the distribution function from the equations for nucleation and growth; or alternatively, from the known distribution function, and assuming a nucleation law, to derive an expression for the growth rate. However, both these approaches resulted in expressions which could not be solved analytically, and thus no functional relationship between the fundamental parameters could be obtained.

The occurrence of a Log-Normal distribution as a result of a particular growth process has been previously discussed by Kottler (1950), Stewart (1960) and Brodynan (1960). (See section 1.5.2.). Stewart showed that a Log-Normal distribution might be expected in an aerosol formed by condensation from the vapour if

the growth process was the initial formation of liquid drops, followed by rapid coagulation. The assumption that coagulation would be significant, together with the assumption of an exponential fall in temperature gives, according to Stewart's treatment, an exponential growth law. With the proposition that the growth times should be Normally distributed (Kottler 1950), he obtained a Log-Normal distribution of particle sizes.

In the present work, the evidence appears to be slightly in favour of particles being formed by a direct vapour/crystal transition, rather than the initial formation of liquid drops. (See section 4.2.). If this is the case then coagulation cannot contribute significantly to the growth of an individual particle, and the growth will be controlled by the diffusion of vapour to the growing surface. In order to see how a particular size distribution might arise we must consider how the particle radius changes with time for this mode of growth. It has been established in section 4.1.4. that a very high supersaturation exists in the vapour at the start of condensation. Thus after initiation of condensation there will be continuous production of nuclei, and simultaneously growth on existing nuclei. Both these processes will deplete the vapour, continuing until the vapour is exhausted. These conditions are typically those for "non-stationary" growth. In particular, they seem to be exactly analogous to the conditions under which sulphur hydrosols were prepared by La Mer and Dinegar (1950), as described in section 1.2.6. La Mer and Dinegar pointed out that with

simultaneous nucleation and growth occurring, the final size of a particle depended on when it was formed; non-uniform growth and a polydisperse sol being the result. They obtained a differential equation for the change in particle radius with time under these conditions. The equation could not be solved analytically, but they obtained a solution by numerical methods. Their plot of the particle radius against time appears as if it could be fitted to a fairly good approximation by a curve of the general form $r = A(1 - \exp(-Bt))$, where r = particular radius after time t, and A, B = constants. Due to the close parallelism between the conditions of formation of aerosols in the present case, and hydrosols in the work of La Mer and Dinegar, it seems probable that an equation of this general form might describe the growth of aerosol particles generated by an electric arc. Thus where continued nucleation and growth lead to depletion of the vapour, an exponential growth law might be expected.

The growth time of a particle is the time between its nucleation and the total exhaustion of vapour. It seems likely that the times at which particles are nucleated will be Normally distributed (Kottler, 1950; Stewart, 1960), and thus the growth times will be Normally distributed. The combination of this Normal distribution of growth times and an exponential growth law could thus give rise to the Log-Normal distribution of particle sizes which has been found for all the aerosols investigated in the present work.

C O N C L U S I O N

The particle size distributions of metal-oxide aerosols formed by electric arcs have been determined for the first time by the above experiments, and from the Log-Normal distribution found to occur, an exponential law for the rate of growth of an aerosol particle has been inferred. From the measured particle sizes and other parameters, the approximate conditions of formation of these aerosols have been determined. Apart from the work of Harvey, Matthews and Wilman (1960), who estimated the temperature of formation of aerosols from electric arcs from their crystalline nature and observed crystal modification, these conditions of formation have been previously unknown.

The effect of the pressure of the surrounding gas on the crystal structure, mean particle size and shape of metal-oxide aerosols has been determined for air and CO_2. The observed increase in particle size with increase in pressure, and the change in particle shape with increase in pressure have been interpreted in terms of changes in the conditions of formation of the aerosols. The mean particle sizes and the change in particle size with change in gas pressure have been found to depend on the nature of the aerosol material.

Most of the previous work on the condensation of vapours to form aerosols has been concerned with vapours which condense at fairly low supersaturations, although some work has been done on aerosol formation by mixing vapours which react chemically

together, producing high supersaturations. In the mode of aerosol generation used in the present work, condensation has been shown to occur under conditions of very high supersaturation. The results obtained here provide a basis for further investigations into the largely unexplored field of combustion aerosols.

The theory of nucleation and growth is rather difficult, and accurate comparison of experiment with theory demands that the experimental parameters be closely specified. For the study of aerosols of metal oxides, their high melting points limit to some extent the possible experimental approach. Thus a technique such as the diffusion cloud chamber, which would probably allow fairly accurate determination of the conditions of aerosol formation, would undoubtedly pose great problems of apparatus design. One great advantage of using the electric arc as an aerosol generator is that the condensation is completed in a region far from the container walls, and thus all problems arising from loss of vapour by diffusion to the walls are avoided. It seems possible that more accurate determination of the conditions of formation of these aerosols could be obtained with a refinement of the present technique.

For the generation of aerosols under even higher supersaturations, exploding wires suggest possibilities, although determination of the conditions of formation might prove difficult or impossible.

Another possibility would be the use of metal-powder flames, or flames of metal compounds, burning in oxygen, e.g. aluminium chloride in an oxy-hydrogen flame. The rate of input of material could be very accurately measured, and with efficient collection it might be possible to obtain fairly accurate estimates of the nucleation rate. A treatment similar to that of Higuchi and O'Konski (1956) for the turbulent jet might prove feasible.

To sum up, the present experiments have provided much new detailed information from which it has been possible to derive a much closer estimate of the mean conditions of formation of arc smokes than has hitherto been available. The dependence of the mean particle size and shape upon the gas pressure (for air and CO_2) has been established and can be understood satisfactorily from the theoretical considerations, in the way described above.

A C K N O W L E D G E M E N T S

The author would like to thank Mr. R. Taylor of U.K.A.E.A. Windscale for the particle size analyses, Dr.K.E. Bett of Imperial College for assistance in the design of the pressure vessel, Mr.A.E.B.Presland of Imperial College for advice on electron microscopy and much useful discussion, and U.K.A.E.A. Windscale for the provision of a grant which made this work possible.

The author is particularly grateful to Dr.H.Wilman of Imperial College for his continued interest, advice and encouragement throughout the course of the work.

R E F E R E N C E S

Aloy J., 1900, Ann. Chem. et Phys., 24, 418.

Amelin A., 1948, Kholl. Zhur. USSR, 10, 169.

Arfvedson J.A., 1824, Pogg. Ann. 1, 269.

Becker R. and Doring W., 1935, Ann. Phys. Lpz. 24, 719.

Beeching R., 1936, Electron Diffraction, Methuen and Co., London.

Billington N.S. and Saunders D.W., 1947, J.Inst.Heat.Engrs. 15, 46.

Birks J. and Bradley R.S., 1949, Proc.Roy.Soc.London, 198A, 226.

Bradley R.S., Evans M.G. and Whytlaw-Gray R.W., 1946, Proc.Roy.Soc. 186A, 368.

Bradley R.S. and Shellard A.D., 1949, Proc.Roy.Soc. 198A, 239.

Bradley R.S., 1951, Quart.Revs. 5, 315.

Bradley R.S., 1955, J.Colloid Sci. 10, 571.

Bradley R.S., 1960, J.Colloid Sci. 15, 525.

Brodynan J.G., 1960, J. Colloid Sci. 15, 573.

Buckle E.R., and Ubbelhode A.R., 1960, Disc. Faraday Soc. 30, 50.

Cartwright J. et al, 1956, Quart. J. R. Met. Soc. 82, 82.

Cawood W. and Whytlaw-Gray R., 1936, Trans.Faraday Soc. 32, 1059.

Coffin K.P., 1945, 5th Symposium on Combustion, Academic Press, New York.

Conjeaud J., 1955, J.Rech. C.N.R.S. France, No.32, 273.

Conway J.B. et al, 1955, J.Amer.Chem.Soc. 77, 2026.

Cosslett V.E., 1951, Practical Electron Microscopy, Butterworth, London.

Davis H. and Hottel H.C., 1934, Ind.Chem.Eng. 26, 889.

Doeglas D.J., 1946, J.Sedim.Petrol. 16, 19.

Drinker P., 1925, J.Ind.Hyg. and Toxicol. 7, 305.

Egli P. and Zerfoss S., 1949, Disc.Faraday Soc. 5, 63.

Epstein B., 1948, Ind.Chem.Eng. 40, 2289.

Erhardt H. and Lark-Horowitz, 1940, Phys.Rev. 57, 603.

Fassel W.M., Gulbransen L.B. et al, 1951, J.Metals N.Y. 3, 522.

Finch G.I., Quarrel A.G., and Wilman H., 1935, Trans.Faraday Soc. 31, 1051.

Finch G.I., and Wilman H., 1937, Ergebn.der Exakt. Naturwiss, 16, 353.

Fordham S. and Finch G.I., 1935, Proc.Phys.Soc. 48, 85.

Frenkel J., 1946, Kinetic Theory of Liquids, Oxford: Clarendon Press.

Frisch H. and Collins F.C., 1953, J.Chem.Phys. 21, 2158.

Fuchs N.A., 1934, Phys.Z. Sowjet 6, 225.

Fuchs N.A., 1934b, Z.Phys. 89, 736.

Fuchs N.A., 1936, Trans.Faraday Soc. 32, 1067.

Fuchs N.A., 1959, Evaporation and Droplet Growth in Gaseous Media, Pergamon Press, London.

Fuchs N.A., 1964, The Mechanics of Aerosols, Pergamon Press, London.

Fuchs N.A. and Petrjanov I. 1935, Acta Physicochem. U.R.S.S. 3, 827.

Galton F. and Macalister D., 1879, Proc.Roy.Soc. 29, 365.

Gillespie T., 1953, Proc.Roy.Soc. A216, 569.

Green H., 1921, J.Franklin Inst. 192, 637.

Greene H.L., and Lane W.R., 1957, Particulate Clouds, Spon Ltd.London.

Grosse A.V. and Conway J.B., 1958, Ind.Eng.Chem. 50, 663.

Harvey J., Matthews H.I. and Wilman H., 1960, Disc.Faraday Soc. 29, 365.

Harvey J., 1960, Ph.D. thesis, University of London.

Hallett J. and Mason B.J., 1958, Proc.Roy.Soc. 247A, 440.

Harrison P.L., 1958, 7th Symposium on combustion, Academic Press, New York, p.913.

Herdan G., 1953, Small Particle Statistics, Elsevier, New York.

Higuchi W.I. and O'Konski C.T., 1960, J.Colloid Sci.,15, 14.

Hillebrand W.F., 1893, Z.Anorg.Chem. 3, 249.

Hillier J., 1948, J.App.Phys. 19, 226.

Hirth J.P. and Pound G.M., 1963, Progress in Material Science, 11, 15.

Hofmann K.A., 1915, Ber., 48, 21.

Houghton H.G., 1933, Physics 4, 419.

Isono K., 1957, J.Met.Soc. Japan, 75th Anniversary Volume.

Jost W., 1961, Diffusion, Academic Press, New York.

Katz J.K. and Rabinowitz E., 1951, The Chemistry of Uranium, Dover, New York.

Kimoto K., et al, 1963, Jap. J. Applied Physics 2, 702.

Kingery W.D., 1960, Introduction to Ceramics, Wiley, New York.

Knoll M. and Stark M., 1948, FIAT Review of German Science, Electronics 1 vol., p.57.

Kobayashi T., 1958, Phil.Mag. 6, 1363.

Kohlschutter V. and Ehlers C., 1912, Z.Electrochem. 18, 373.

Kohlschutter V., 1927, Kolloidzschr. 42, 209.

Kolmogoroff A.N., 1941, Doklady Akademii Nauk. SSSR, 31, 99.

Kottler F., 1950, J.Franklin Inst. 250, 339, 419.

Kubaschewski O. and Evans E.L.L., 1951, Metallurgical Thermochemistry, Butterworth, London.

La Mer V.K., Inn E.C.Y. and Wilson I.B., 1950, J.Colloid Sci.5, 471.

La Mer V.K. and Dinegar R.H., 1950, J.Amer.Chem.Soc. 72, 4874.

Langmuir I., 1918, Phys.Rev. 12, 368.

Langstroth G.O., Diehl C.H. and Winhold E.J., 1950, Canad.J.Research, 28A, 574.

Levin M.L., 1956, Ph.D.Thesis, University of London.

Loeb L.B. 1947, Fundamental processes of electrical discharges in gases, Wiley, New York.

Mahl H., 1945, Ergebn.Naturwiss. 21, 262.

Marshall J.S. and Langleben M.P., 1954, J.Meteor. 11, 104.

Martin J. et al, 1925, Trans.Brit.Ceram.Soc. 25, 240.

Mason B.J., and Maybank J., 1959, Proc.Phys.Soc. 74, 11.

Mason B.J., 1960, Disc. Faraday Soc. 30, 61.

Mason B.J., 1963, The Art and Science of Growing Crystals, Ed.Gilman, Wiley, New York, p.119.

Matusevich N., 1959, The growth of crystals, Ed.Shubnikov and Sheftal, Academy of Sciences USSR, 1956, p.168.

Maxwell C., 1877, Scientific Papers 2, 639, Cambridge University Press.

Meetham A.R., 1950, Quart.J.R.Met.Soc. 76, 366.

Monchik L. and Reiss H., 1954, J.Chem.Phys. 22, 831.

Morse L., 1910, Proc.Amer.Acad.Sci. 43, 463.

Mullins W.W. and Sekerka R.F. 1963, J.App.Phys. 34, 323.

Nelson J.B. and Riley D.P., 1945, Proc.Phys.Soc. 57, 477.

Nestle R., 1932, Z.Physik. 77, 174.

Nielsen A.E., 1964, Kinetics of precipitation, Pergamon, London.

O'Konski C.T., and Higuchi W., 1956, J.Phys.Chem. 60, 1598.

Olsen H.L. and Setze R., 1958, 7th Symposium on combustion, Academic Press, New York, p.883.

Parker W.G. and Wolfhard H.G., 1950, J.Chem.Soc., 150, 2038.

Peligot E., 1842, Ann.Chem. et Phys. 5, 24.

Pinsker Z., 1953, Electron Diffraction, Butterworth, London.

Pound G.M. et al, Airforce Cambridge Research Centre, Geophys. Res. Paper No. 37.

Powell C.F., 1928, Proc.Roy.Soc. A119, 553.

Price P.B., 1960, Phil.Mag. 5, 473.

Reiss H. and La Mer V.K., 1950, J.Chem.Phys., 18,1.

Runck R.J., 1956, High Temperature Technology, Ed. Campbell, Wiley and Son, New York.

Ruska E. and Von Borries B., 1938, Z.Tech.Physik. 19, 402.

Sander A. and Damkohler G., 1943, Naturwiss. 31, 460.

Schafer K., 1932, Z.Physik, 77, 198.

Schechter A., 1946, Acta Physicochem. U.R.S.S. 21, 463.

Shaler A.J., 1952, Structure and properties of solid surfaces, University of Chicago Press.

Shaw B. and Mason B.J., 1955, Phil.Mag. 46, 249.

Sheppard S.E., 1923, J.Phys.Chem. 27, 141, 466.

Smith R., 1940, Proc.Roy.Soc. 174, 110.

Smoluchowski M. von, 1916, Phys.Z. 17, 557, 585.

Smoluchowski M. von, 1918, Z.Physik.Chem. 92, 129.

Spalding D.P., 1950, Fuel, 29, 2.

Spalding D.P., 1951, Fuel, 30, 121.

Sreznevsky V., Zh.R.Ph.Kh.O. 14, 420, 483.

Stewart K., 1956, Trans.Faraday Soc. 52, 161.

Thomson G.P., 1930, Proc. Roy.Soc. A128, 649.

Thomson G.P., and Cochrane W., 1939, Theory and Practice of Electron Diffraction, Macmillan, London.

Thomson J.J. and Thomson G.P., 1928, Conduction of Electricity through Gases, vol.1, Cambridge Univ.Press, p.332.

Thomson W., 1870, Proc.Roy.Soc.Edin., 7, 63.

Tolman R.C., Vliet E.B., Pierce Mc.G. and Doherty R.H., 1919, J.Amer. Chem.Soc. 41, 297.

Topley B., and Whytlaw-Gray R., 1927, Phil.Mag. 4, 873.

Van den Heuvel B., and Mason B.J., 1959, Nature 184, 519.

Volmer M. and Flood H., 1934, Z.Phys.Chem. 170, 273.

Volmer M. and Weber A., 1926, Z.Phys.Chem. 119, 277.

Von Borries B., 1940, Z.Phys. 116, 370.

Von Borries B., and Kausche G.A., 1940, Koll.Z. 90, 132.

Von Borries B., 1949, Die Ubermikroskopie, Aulendorf, Wurttemburg.

Walmsley H.P., 1927, Proc.Phys.Soc. 40, 7.

Walmsley H.P., 1929, Phil.Mag. 7, 1097.

Watson J.H.L., 1947, J.App.Phys. 18, 153.

Wells P.V. and Gerke R.H., 1919, J.Amer.Chem.Soc. 41, 312.

Westermann I., 1930, Erzbergau 28, 613.

Whytlaw-Gray R. et al, 1922, Proc.Roy.Soc. 102A, 601.

Whytlaw-Gray R. et al, 1927, Proc.Roy.Soc. 116A, 547.

Whytlaw-Gray R. and Patterson H.S., 1932, Smoke, Edward Arnold, London.

Wiegner G., and Marshall C.E., 1929, Z.Phys.Chem. A140, 1.

Wilman H., 1948a, Proc.Roy.Soc. 60, 341.

Wilman H., 1948b, Proc.Phys.Soc. 61, 416.

Wilman H., 1950, Nature, 165, 321.

Wilman H., 1951, Proc.Phys.Soc. 64, 329.

Wilman H., 1952, Acta Cryst. 5, 782.

Wilman H., 1956, J.Chim.Physique, 607.

Wilson C.T.R., 1897, Phil.Trans. A189, 265.

Yearian, 1935, Phys.Rev. 48, 631.

Zaiser R. and La Mer V.K., 1948, J.Colloid Sci., 3, 571.